



universität
wien

DISSERTATION / DOCTORAL THESIS

Titel der Dissertation / Title of the Doctoral Thesis

“Preclinical pharmacokinetics of new bicycloheptyl-
anellated naphthoquinone derivatives”

verfasst von / submitted by

Mag. pharm. Nairi Baroian

angestrebter akademischer Grad / in partial fulfilment of the requirements for the degree of
Doktorin der Naturwissenschaften (Dr.rer.nat.)

Wien, 2016 / Vienna, 2016

Studienkennzahl lt. Studienblatt /
degree programme code as it appears on the student
record sheet:

A 796 610 449

Dissertationsgebiet lt. Studienblatt /
field of study as it appears on the student record sheet:

Pharmazie

Betreut von / Supervisor:

Univ.-Prof. Mag. pharm. Dr. Martin Czejka

Preface and Acknowledgment

The following work was conducted at the Division of Clinical Pharmacy and Diagnostics, Faculty of Life Sciences at the University of Vienna from the period from July 2013 to July 2016.

Firstly, I would like to express my sincere gratitude to my advisor Univ.-Prof. Dr. Martin Czejka for the continuous support of my Ph.D study, for his patience, motivation, and immense knowledge. His guidance helped me in all the time of research and writing of this thesis.

Besides my advisor, I would like to thank the team of SeaLife Pharma GmbH: Especially Dr. Alexander Pretsch, Dr. Michael Nagl and Dr. Chistoph Wieser. For providing me with all the compounds and samples and for their insightful comments and discussion, but also for their hard question which incented me to widen my research from various perspectives.

I would also like to thank my colleagues Mag. Marie Kitzmüller, Dr. Veronika Rachar, Dr. Philipp Buchner and Mag. Azra Sahmanovic-Hrgovic for their wonderful collaboration and for their moral support. My special thanks goes to Mag. Andrea Gruber, in course of her thesis work she provided me with the ADMET Predictor software data. You all supported me greatly and were always willing to help me.

I would also like to thank my parents and my brother for their wise counsel and sympathetic ear. You are always there for me. Finally, I also want to thank my cousin Emma Sahakian who always reminded me to not lose the sight of my goal and encouraged me never to give up.

Last but not least I want to thank my fiancé, Mag. Lukas Kuttner, for supporting me and always showing me what really is important in life.

Thank you everyone!

CONTENTS

1	Introduction.....	1
1.1	New Antibiotic Compounds	1
1.1.1	Antibiotic Resistance	1
1.1.2	New Class of Compounds	2
1.2	Drug Discovery and Development	5
1.2.1	Binding and Distribution	7
1.2.2	Metabolism	9
1.2.3	Animal Pharmacokinetics.....	10
1.2.4	Human Skin	12
2	Scope.....	14
3	Material and Methods	16
3.1	Laboratory Equipment.....	16
3.1.1	RP-HPLC Quantification.....	16
3.1.2	Reagents and Chemicals	18
3.2	Validation	19
3.2.1	Preparation of Standard Solutions	19
3.2.2	Sample Preparation.....	19
3.2.3	Method Validation.....	20
3.2.4	Comparison of CPD11 with seven other SeaLife Compounds	22
3.3	Binding and Distribution Experiments	23
3.3.1	TRANSIL ^{XL} Kit.....	23
3.3.2	ADMET Predictor	27
3.4	Hepatocytes.....	28
3.4.1	Certificates.....	28
3.4.2	Metabolic Stability	35
3.4.3	Data Analysis.....	37
3.5	Preliminary in vivo PK Studies of CPD3 and CPD11	39
3.5.1	Calibration Curves in Plasma	39
3.5.2	CPD3	40
3.5.3	CPD11	41

3.6	In vitro and in vivo Topic Studies of CPD11	43
3.6.1	Calibration Curves of CPD11 and Caffeine in PBS	43
3.6.2	LOQ & LOD	43
3.6.3	EpiDerm™ in vitro Model	43
3.6.4	In vivo Model	47
3.7	Software	48
4	Results	49
4.1	Validation	49
4.1.1	Optimization of Sample Preparation Method.....	49
4.1.2	Validation Results	51
4.1.3	Comparison of CPD11 with seven other SeaLife Compounds	57
4.2	Binding and Distribution Experiments	58
4.3	Cryopreserved Hepatocytes	65
4.3.1	CPD11	65
4.3.2	CPD22	85
4.3.3	Testosterone	97
4.4	Preliminary Pharmacokinetics of CPD3 and CPD11	104
4.4.1	Calibration curves	104
4.4.2	CPD3 in vivo Data	106
4.4.3	CPD11 in vivo Data	109
4.4.4	Pharmacokinetic Parameters	119
4.5	In vitro and in vivo Topic Studies of CPD11	122
4.5.1	Calibration curves	122
4.5.2	LOQ & LOD	125
4.5.3	In vitro EpiDerm™ Model	125
4.5.4	In vivo Model	130
5	Discussion.....	133
5.1	Validation	133
5.2	Binding and Distribution Experiments	134
5.3	Cryopreserved Hepatocytes	139
5.4	Preliminary Pharmacokinetics of CPD3 and CPD11	144
5.5	In vitro and in vivo Topic Studies of CPD11	149

6	Conclusion.....	150
7	Abstract.....	152
8	Zusammenfassung.....	153
9	List of Abbreviations	154
10	List of Tables	157
11	List of Figures.....	159
12	References	162
13	Curriculum Vitae	171

1 Introduction

1.1 New Antibiotic Compounds

1.1.1 Antibiotic Resistance

According to estimations from the World Health Organization (WHO), 25,000 people die each year in Europe due to nosocomial, i.e., hospital-acquired, infections with multi-resistant bacteria. The vast majority of these nosocomial infections are caused by *Staphylococcus aureus*, *Enterococcus faecium*, *Pseudomonas aeruginosa* and *Klebsiella pneumoniae*. [1, 2] The rapid progression of antibiotic resistance is influenced by several factors. First and foremost is the unnecessary and incorrect application of antibiotics, including the incorrect choice of antibiotic, an insufficient dose or treatment duration and the application of antibiotics during viral infections. Additionally, the use of antibiotics in commercially driven agriculture plays an essential role in the development of drug resistance in humans. The emergence of antibiotic resistance increases the demand for new anti-infective compounds. Targeted research activity in the field of antibacterial compounds is therefore of growing relevance. Nevertheless, for pharmaceutical companies, research in this sector appears to be less lucrative. On the one hand, newly developed drugs generally serve as reserve antibiotics when commercially used antibiotics do not show sufficient effect. On the other hand, there is the risk that after spending time and money in researching and developing a new drug, low income revenue may occur due to rapid resistance development. [3, 97, 75]

In summary, limited treatment options for existing multi-resistant pathogens, mainly arising in hospitals and similar environments, as well as the perpetual misuse of antibiotics, which have led to the emergence of antibiotic resistance, are causing ever-increasing problems in fighting bacterial infections. [4]

1.1.2 New Class of Compounds

The synthetic antibiotic compounds discussed within this study represent a new group of 5-O-alkylated bicycloheptyl-anellated naphthoquinones (synonymously 1,4-methano-1,4-dihydro-9,10-anthracenediones, for chemical structures see 1 Cyclohexenyl-anellated naphthoquinones exhibit pronounced antibacterial activities that are generally found in contrast to only moderate bioactivities of their aromatized congeners (viz. anthraquinones). Thirty-one new drug candidates showing pharmacological activity against gram-positive bacteria have been supplied by Sealife Pharma GmbH (Tulln, Austria), hereinafter referred to as CPD1-31. Eight out of this thirty-one drug candidates are shown in Figure 1.

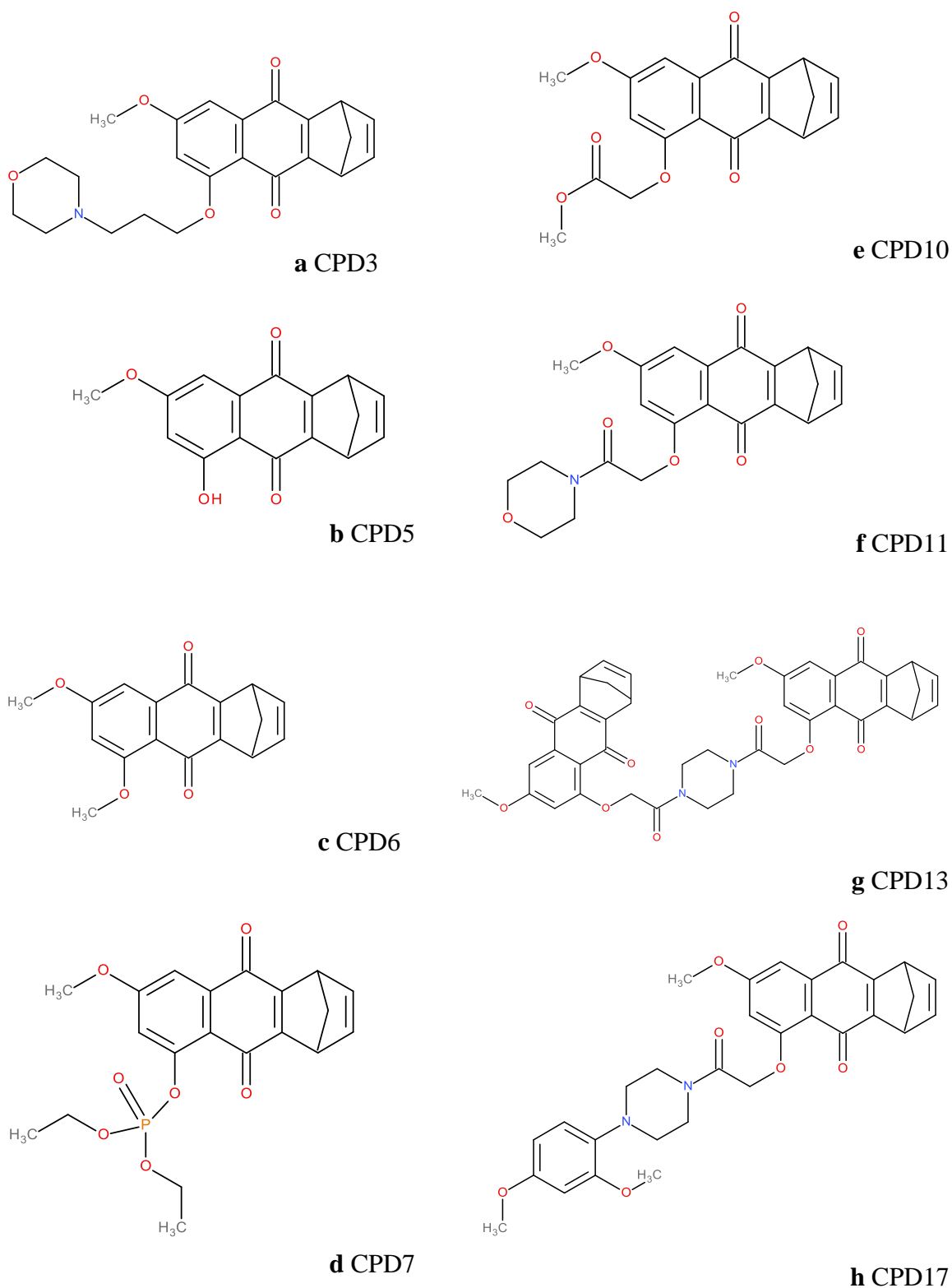


Figure 1: a-h Chemical structures of investigated test-compounds (CPD3, CPD5, CPD6, CPD7, CPD10, CPD11, CPD13 and CPD17)

The natural product group of altersolanols shares this common structural feature together along with other structurally related natural products, e.g. austrocortilutein and pleosporone. Altersolanols (A-E) – structurally representing polyhydroxy-methylcyclohexenyl anellated naphthoquinones (which might be coevally perceived as naphthoquinone anellated methyl -conduiritols) – and their metabolites are produced by several terrestrial and aquatic fungi, such as *Alternaria species*, *Dactylaria lutea*, *Phomopsis species*, *Stemphylium globuliferrum* or *Xylaria species*, as well as others not yet characterized. Some altersolanols are known to be toxic to plants and animals. In addition, altersolanols show antibacterial, antiviral, or cytotoxic activity. Thus, researchers have repeatedly focused on altersolanols during the last two decades and have demonstrated their potential for use in the development of new medications and elucidated the structures of increasing numbers of metabolites. Currently, research focus on the structural clarification of hitherto unknown derivatives and their mechanisms of action is still ongoing. In the past, various pharmacological studies have confirmed the antibacterial activity of altersolanols against *Escherichia coli*, *Pseudomonas aeruginosa* and gram-positive bacteria such as *Staphylococcus aureus*, *Bacillus subtilis* and *Micrococcus luteus*. [5, 6, 7, 8, 9, 10, 11, 12, 13, 14, 15, 16, 17, 18, 19]

Ring-C-oxa-analogues of the above mentioned structural group, such as the antibiotic benzo-isochromanquinones of the nanaomycine and kalamycine families, as well as the benzo-chromanquinones of the lapachone type, are also showing pronounced antibiotic activities. Nanaomycines (A-E) are isolated from *Streptomyces rosa subspecies notorensis* inhibiting the growth of gram-positive bacteria, fungi, mycoplasma and yeast. Nanaomycine A is approved for the treatment of ringworm for cattle in Japan. A previous study also showed the antiproliferative effects of nanaomycin A in three different human cancer cells by inhibiting DNMT3B (DNA methyltransferases) and reactivating the transcription of the RASSF1A tumor suppressor gene. Two new isolated nanaomycines F and G show no antimicrobial activity against various bacteria and fungi. [20, 21, 22]

Kalamycin, also known as kalafungin, is isolated from *Streptomyces tanashiensis* K. and inhibits the growth of gram-positive bacteria and fungi. Alpha-Lapachone is a naturally occurring lapachol derivative. Lapachol and its derivatives are widespread prenylated naphthoquinones isolated from the heartwood of *Paratecoma peroba* (Bignoniaceae) and teakwood of *Tectona grandis* (Verbenaceae). Alpha-Lapachone shows antibacterial activity against methicillin-resistant *Staphylococcus aureus*, *epidermidis* and *haemolyticus* strains. [20, 23]

1.2 Drug Discovery and Development

The search for new drugs comprises two main areas: drug discovery and drug development. Drug discovery consists of selecting a therapeutic area, choosing a target for a specific disease, setting up models for testing biological activities, screening the compounds for in vitro and in vivo biological activities, and determining early absorption, distribution, metabolism, excretion and toxicology (ADMET) outcomes. Drug development predominantly focuses on evaluating the efficacy and toxicity of drugs. [24, 25, 26]

The preclinical development of a lead compound candidate focuses on two major segments:

1. Pharmacological-toxicological investigations, to obtain detailed information about the efficacy, safety and toxicity of a drug candidate.
2. Pharmacokinetics (PK) investigations, to provide information related to the physicochemical properties of a compound, which are responsible for its in vitro fate. The physicochemical properties are determined by establishing the solubility, pH value, temperature, ionization, UV light, lipophilicity and other properties, which are responsible for plasma protein binding (PPB), membrane binding, distribution and metabolism.

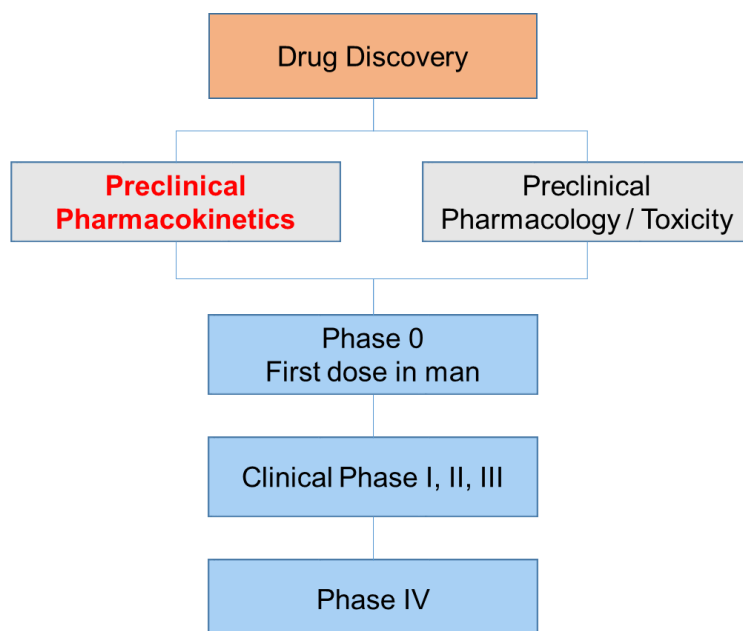


Figure 2: Drug discovery process

Data from Pharmaceutical Research Medical Association (2003) [27]

Figure 2 shows the processes in drug discovery and development. Phase 0 trials are not legally required but are strongly recommended. In this phase, a very low dose of a drug that lacks data on efficacy and safety is administered in humans. This phase serves primarily to evaluate the PK properties. [28]

Clinical phase I is designed to evaluate the safety and dosage in 20 to 30 healthy volunteers and patients. Clinical phase II is developed to assess the efficacy and side effects in 100 to 300 patients. Clinical phase III is needed to determine the effectiveness and side effects on a large group of patients, i.e., 1,000 to 1,500. Additionally, this phase compares the new drug with the standard drug and provides information on its safe usage. [27, 28, 29]

Clinical phase IV studies are performed after receiving the product license, to investigate very rare and/or long-term adverse drug reactions, to compare the drug with standard treatments and/or to enlarge the spectrum of applications. [27, 28, 29]

The focus of this thesis is on preclinical PK investigations, highlighted above in red in Figure 2.

Table 1 illustrates an overview of the most important parameters, which are usually recommended to perform during preclinical PK investigations according to the guidelines of the European Medicines Agency (EMA). [30]

Table 1: Overview of recommended PK parameters to investigate during drug development

Parameter	Value	References
Analytics	<ul style="list-style-type: none"> Isolation of compound from biological matrices Separation of compound from metabolites and/or degradation products 	31, 32
Stability	Solvent, pH, light, temperature, time, storage	33, 34
In vitro permeability	Caco2 and Parallel artificial membrane permeability assay (PAMPA)	35
Plasma proteins	<ul style="list-style-type: none"> Total binding Human serum albumin (HSA) – binding Alpha-1-acid glycoprotein (AGP) – binding 	36, 37, 38
Microsomal affinity	Metabolism	39, 40
Intestinal affinity	Intestinal absorption	41, 42
Metabolism	Hepatocytes: metabolic stability screening, metabolic profiling, drug-drug interactions, hepatotoxicity	43, 44, 45
Animal PK	PK and metabolism	46, 47
Tissue binding	E.g. liver, kidney, heart, brain, lipids	48
Skin	Penetration, permeation, resorption	

If the investigated compounds show antibacterial and antiviral activities, *in vitro* and *in vivo* skin models are additionally utilized in this initial phase of investigation. Since these compounds are often used for topical therapy and could provide an alternative to peroral or intravenous (iv) applications.

PK profiling and drug metabolism have become increasingly important even in early stages of drug development. *In vitro* screening of ADMET parameters, may provide a basis for the selection of new chemical entities. [99]

1.2.1 Binding and Distribution

One of the most important factors influencing the distribution of a compound is its protein binding (plasma and tissue) ability. Only the unbound fraction of a drug appears to have a pharmacological effect by penetrating through cell membranes and thereby becoming available for elimination. Generally, drugs with a low PPB have better tissue penetration but are consequently excreted much faster. Thus, these drugs have an accelerated elimination half-life ($t_{1/2el}$). By contrast, when a compound shows a PPB higher than 80–85%, its excretion is only modestly affected by PPB or is even unaffected. If the binding of a compound predominantly occurs to albumin, its *in vivo* $t_{1/2el}$ may be increased. Furthermore, PPB strongly affects the PK of a drug, specifically its clearance (CL) and volume of distribution (Vd). [36, 37, 38, 49, 50]

PPB ranges from 0 to 99%, depending on the physiochemical properties of the drug candidate, which can be based on electrostatic and/or hydrophobic mechanisms. High PPB represents an intravascular depot in equilibrium with the unbound and active fraction of a drug in plasma. Equilibrium occurs rapidly and reversibly within a few milliseconds, which can be advantageous for the pharmacological properties of a compound but might also lead to toxicological effects. [36, 38]

AGP and HSA are the most important plasma proteins, along with lipoproteins. Acidic and basic compounds can bind to HSA, whereas only basic compounds can bind to AGP. HSA is the protein with the highest concentration in human plasma. This protein is synthesized by polysomes in hepatocytes and has ligand-binding capacity and transport activity for various endogenous compounds, e.g., bilirubin. Additionally, HSA exhibits antioxidant

properties when binding to endogenous and exogenous compounds. AGP, also known as orosomucoid, is a glycoprotein synthesized in hepatic and non-hepatic cells, e.g., granulocytes and endothelial cells. [38, 51, 52, 53]

Along with PPB, the prediction of tissue binding has always been of great importance in drug development. Both parameters must be known in order to determine the free fraction of a compound that is available for pharmacological distribution and drug metabolism. Recent research has revealed that tissue binding may play an even larger role in the distribution and PK parameters of drug candidates than protein binding. Furthermore, the extent of binding to tissues and proteins in the central compartment can be related to the V_d of a compound. [54, 55]

Various methods have been described for predicting the PPB of compounds during drug discovery and development. The most commonly utilized methods for determining PPB are ultrafiltration, equilibrium dialysis and ultracentrifugation. To implement these methods, pooled plasma from healthy volunteers is usually needed, wherein the exact level of neither AGP nor HSA can be determined, which can lead to imprecise results. For tissue binding, several methods have been published and are available for implementation in *in vitro* and *in vivo* tissue binding studies, with various advantages but also disadvantages. This is especially true when analyzing lipophilic compounds. [41, 42, 56, 57, 58, 59]

In the current investigation, the novel *in vitro* TRANSIL^{XL} Kit was used to determine PPB, AGP binding, HSA binding, microsomal binding ($\log MA_{\text{micro}}$) and intestinal absorption ($\log MA_{\text{int}}$). A drug carrier molecule (plasma proteins, phosphatidylcholine or microsomes) is stabilized on silica beads at various concentrations in microwells. TRANSIL^{XL} investigations are able to predict the intestinal absorption rate of a test compound by determining its predicted intestinal permeability coefficient (P_{int}) together with its tissue binding ($\log MA$). Moreover, by using P_{int} and $\log MA_{\text{int}}$, it is possible to estimate an apparent V_d at steady state, which provides preliminary information on the affinity of the compound to tissue, representing a deep compartment. Generally, compounds with higher lipophilicity may have higher affinity for liver microsomes. Membrane affinity (MA) is expressed as the distribution coefficient of a drug between membrane and buffer. The microsomal kit enables the affinity of a drug for microsomal membranes to be determined, which can provide useful information on biotransformation processes. The main advantages of this assay are the following: it requires only a short incubation time, it is fully validated, and it allows a

compound to be quantitated without time-consuming sample preparation procedures. [60, 61]

To obtain additional information on preclinical PK, the ADMET-Predictor 7.2 computer software was used. This software is widely applied for the prediction of ADMET properties. The following parameters were calculated for our test compounds: f_u (unbound fraction %), logP (partition coefficient) and pKa/pKb (dissociation constant). Such in silico methods represent a very useful tool for predicting ADMET parameters without extensive laboratory investigations. Nevertheless, it is the synergy among in silico, in vitro and preclinical in vivo studies that facilitates finding, developing and refining a lead compound.

1.2.2 Metabolism

The term metabolism or biotransformation includes processes where exogenous substances, so-called xenobiotics, are chemically modified to more water-soluble compounds. These transformation products are referred to as metabolites. One of the main problems of not achieving therapeutic drug levels is the rapid metabolism of drugs. [33]

Drug metabolism can be divided into four phases (0-III), where enzymatic transformation processes take place in phases I and II. [44]

Phase 0: Describes the cellular uptake of the xenobiotic into hepatocytes. [44]

Phase I (*oxidation, reduction and hydrolysis*): Describes the addition of oxygen (primary epoxide or hydroxide) to the parent molecule. This phase is carried out through several enzyme pathways, e.g., numerous isoforms of the cytochrome P450 (CYP450) family, non-CYP450 biotransformation enzymes, flavin-containing monooxygenase and monoamine oxidase. [45]

Phase II (*conjugation*): Describes the addition of water-soluble molecules (phosphate, sulphate, β -D-glucuronic acid) to the drug that needs to be metabolized, allowing the chemical to be excreted efficiently. Enzymes involved in phase II metabolism are, for example, UDP-dependent glucuronosyl transferase, glutathione-S-transferase and sulfotransferase. [45]

Phase III: Defines the transport of metabolites out of hepatocytes. In contrast to phase I and II, no chemical modification of the compound is made. [44]

Evaluation of drug metabolism

Various test systems are available to evaluate in vitro drug metabolism, i.e., the liver S9 fraction, microsomes, cDND-expressed P450 isoforms and hepatocytes.

The liver S9 fraction is a post-mitochondrial supernatant that contains cytosolic and microsomal enzymes. The extraction is carried out through homogenization of the liver and subsequent centrifugation at 9,000 g. The liver S9 fraction enables the assessment of phase I and phase II metabolism, depending on the cofactor mixture. [62, 63]

Through ultracentrifugation of the liver S9 fraction at 100,000 g, liver microsomes can be obtained, which are widely used to evaluate in vitro drug metabolism. Microsomes contain endoplasmic reticuli, which allow for the determination of phase I metabolism and glucuronidation. [64, 62]

Furthermore, there are also cDND-expressed P450 isoforms serving for pathway identification.

Hepatocytes, in general, are very efficient in vitro experimental systems to determine the metabolism of substances in the human body. In particular, primary human hepatocytes are of growing importance, as they help to reflect drug properties and evaluate human metabolism. Hepatocytes consist of parenchymal cells of the liver and enable the evaluation of phase 0, I, II and III metabolism, as they contain all metabolizing enzymes and transporters. Through the development of cryopreserved hepatocytes, a commercial source for human hepatocytes became available. With the support of hepatocytes, the properties of a compound can be determined, e.g., metabolic stability, half-life ($t_{1/2}$) values and in vivo hepatic intrinsic clearance. Therefore, it was decided to use this system for the current study. [65, 66, 67, 68]

1.2.3 Animal Pharmacokinetics

In vitro models are essential in drug discovery and development, yet in vivo results can additionally provide valuable information on ADMET endpoints. In vivo models also

provide a significant set of PK parameters. Rats are usually the first animals used for in vivo testing as they only require a small amount of test drug and are inexpensive. Early PK screenings using different dose regimens and administration routes in different species (e.g., rat, mouse, guinea pig), even during the drug discovery process, help to identify ADMET problems, e.g., low absorption and high clearance, which could lead to undesirable PK. Non-compartmental and compartmental methods are used to evaluate the PK parameters of a compound, including the maximum plasma concentration (C_{\max}), time of maximum plasma concentration (T_{\max}), area under the curve (AUC), volume of distribution (V_d), clearance (CL), $t_{1/2el}$ and bioavailability (F). [46, 47]

1.2.4 Human Skin

Skin, with a total surface area of 2 m^2 , is functionally the most important human organ. In addition to its function as a heat conductor and sensory organ, the skin also builds a protective cover against harmful environmental factors. This effect is due to the fact that the skin is impermeable to most substances and pathogens, and the acidic protective layer of the skin prevents bacteria from settling. In the case of skin damage or injury, the skin defence system is compromised and pathogens or other harmful substances may penetrate the skin. [69]

As seen in Figure 3, human skin is divided into three layers: the epidermis, dermis and hypodermis (subcutaneous layer).

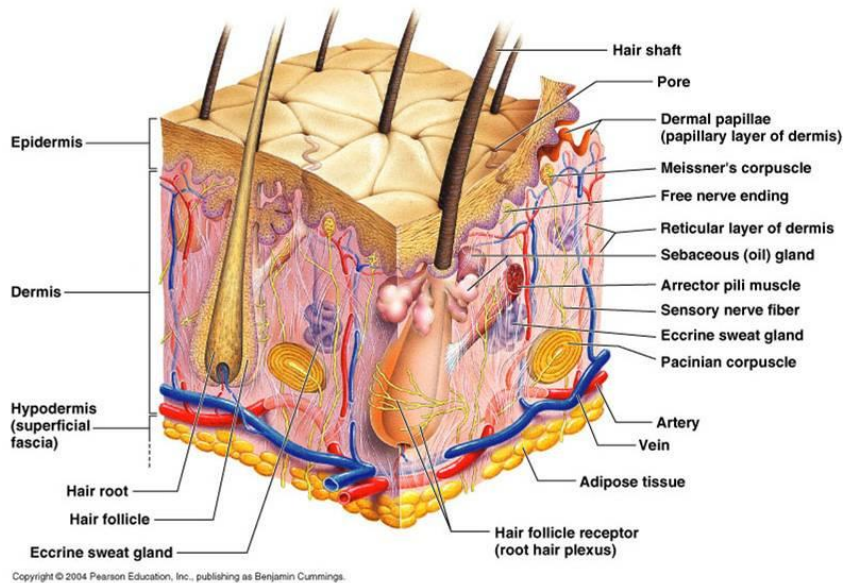


Figure 3: Skin structure [100]

The epidermis is the outer layer of the skin, with a thickness of approximately $70\text{-}150 \mu\text{m}$, containing living and dead cells. This layer sustains the skin's protective function through the thick corneal layer, which consists of dead keratinized cells. The epidermis itself can be divided into five layers: the stratum basale, stratum spinosum, stratum granulosum, stratum lucidum and stratum corneum (corneal layer). [70, 71, 72]

The dermis is much thicker than the epidermis and totals approximately 15-20% of the human body weight. It consists of collagen, elastin, nerves and blood vessels, among other components, which provide the skin with the necessary nutrients. [72]

The hypodermis is composed of loose fatty connective tissue, fatty cells, sweat glands and hair follicles. [72]

In general, a distinction must be made between penetration, permeation and resorption. Penetration describes the intrusion of the compound through the corneal skin into the epidermis. Permeation identifies the passage of the compound from the skin into the blood vessels. The permeation of a compound through the skin takes place by passive diffusion along a concentration gradient. The sum of permeation and penetration is called resorption. [73].

The properties of a compound also play a decisive role as they impact the resorption of the drug through the skin. In particular, the molecular weight, lipophilicity, PPB and polarity can influence the penetration depth. In particular, smaller molecules can surpass the transcutaneous layer more easily than large molecules. A limit of 500 Dalton molecular weight has been postulated for enhanced skin permeation. Generally, an increased molecular weight (> 500 Dalton) leads to a reduction of the physiological factors of the skin, such as the pH of the tissue, blood flow rate or oxygen consumption, which may also have an impact on the percutaneous resorption of a compound. [74]

2 Scope

The main purpose of these investigations was the evaluation of preclinical PK of a new class of highly antibacterial active synthetic bicycloheptyl anellated naphthoquinones.

In the last decade, the evaluation of in vitro preclinical PK has gained great importance in drug discovery and development. Assessing in vitro PK parameters early in drug discovery could save money and time by clarifying compound properties as early as possible. Furthermore, in early phases, animal experiments could be minimised by performing in vitro experiments rather than in vivo experiments. Nevertheless it is not possible to forego in vivo experiments entirely because in vitro assays still exhibit limitations (e.g., microsomal binding without consideration of blood flow).²⁸ Previous studies have shown the influence of the physicochemical properties of a drug on its absorption, distribution, metabolic conversion and elimination. [76, 77]

Therefore, the following aspects were particularly important in this thesis:

- The development and validation of a simple, robust and low-cost reverse phase-high performance liquid chromatography (RP-HPLC) method for the quantification of this group of compounds. The desired objective was to develop a single RP-HPLC method that could be used for the quantification of one class of compounds, which also show chemical inhomogeneity.
- The stability of the compounds, with a strong emphasis on the lead compound, (e.g., temperature, light, concentration and time).
- In vitro investigations of protein binding of the compounds to typical drug-transporters, e.g., AGP and HSA. In addition, we sought to evaluate the binding rates to intestinal tissue, Vd, microsomal binding and the meaning of membrane affinity. What significance do these in vitro parameters have for the PK, particularly for metabolism?
- Correlation of in vitro and in silico results.
- Evaluation of metabolism of the lead compounds using cryopreserved hepatocytes to distinguish metabolically stable from unstable compounds and

identify metabolites, as well as investigations of differences between species. Which species are similar to each other, and which are similar to humans?

- Determination of in vivo PK parameters in various species using different administration routes.

Furthermore, an in vitro skin model was utilized to evaluate the permeation properties of the lead compound, in case the compound would additionally be used for topical administration.

3 Material and Methods

3.1 Laboratory Equipment

3.1.1 RP-HPLC Quantification

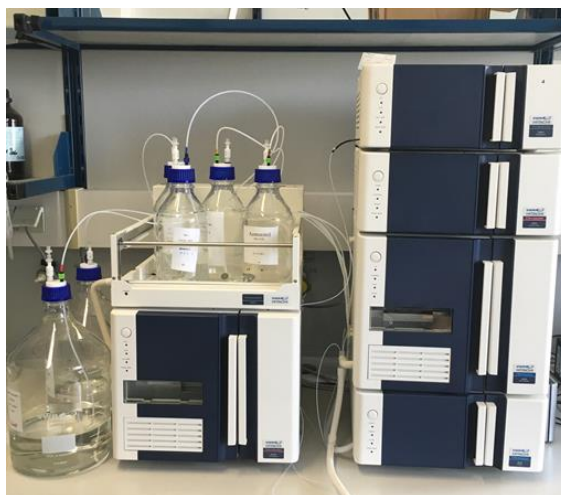


Figure 4: VWR® HITACHI Chromaster HPLC-System

HPLC is a chromatographic separation method where pumps pass a pressurized liquid solvent (mobile phase) containing the substance to be analysed through a column (stationary phase). The most commonly used method is RP-HPLC, in which a nonpolar stationary phase is utilized. This phase is usually a modified silica gel that is also mechanically stable at high pressure. The mobile phase, on the other hand, is a polar solution, which consists of, preferably, a mixture of water or buffer and acetonitrile (ACN) or methanol. Throughout the course of an isocratic separation, the composition of the mobile phase remains the same during the entire analysis period, while during gradient separation, the polarity of the solvent mixture is altered. [78, 79, 80]

HPLC analyses were performed on a VWR® Chromaster system (Figure 4) (all components Merck Hitachi, Germany), for detailed description see Table 2. The wavelength was detected to be between 270-290 nm and the retention time between 10-21 min, depending on the analysed compound.

To obtain the UV maximum wavelength (λ_{max}) for HPLC detection, the compounds have been dissolved in pure ACN in a concentration of 5.0 $\mu\text{g/mL}$ and analysed with a UV-1800 spectrophotometer.

Table 2: Data of HPLC-System

VWR® HITACHI Chromaster HPLC-System	
Precolumn	LiChroCART® 4-4 LiChrospher® 100 RP-18, 5-µm
Analytical column	Zorbax Eclipse XDB-C ₈ column 250 x 4.6 mm ID, 5 µm (Agilent Technologies)
Pump	Chromaster 5110
Autosampler	Chromaster 5210
Column oven	Chromaster 5310
UV/VIS-detector	Chromaster 5410
Degasser	Model 2003 VWR
Software	Chromaster HPLC System Manager
Flow rate	0.5 mL/min
Column temperature	37°C
Autosampler temperature	17°C
Injection volume	40µL
Analysis time	42 min
Wavelength	270-290 nm
Pressure	70-80 bar
Retention time	range from 10-21 min
Eluent	A: 99.9% Aqua bidest. / 0.1% acetic acid B: 99.9% acetonitrile / 0.1% acetic acid

The elution gradient time program is listed in Table 3. The mobile phase consisted of solvent A (99.9% aqua bidest. and 0.1% acetic acid) and solvent B (99.9% ACN and 0.1% acetic acid).

Table 3: Elution gradient profile

Time (min)	% Solvent	
	A	B
0	85	15
10	20	80
25	20	80
27	0	100
32	0	100
35	85	15
42	85	15

3.1.2 Reagents and Chemicals

Table 4 shows the laboratory equipment needed to conduct the required experiments.

Table 4: Materials and Equipment

Materials and Equipment	Name	Manufacturer
Heating block	DRI-BLOCK® DB 2A	Techne, (AUT)
Analytical balance	Sartorius handy H110	Sartorius Mechatronics Austria GmbH, (AUT)
Magnetic stirrer	MR 3001K	Heidolph Instruments, (GER)
Vortex	Star Lab Vortex Mixer	VELP® Scientifica, (AUT)
Centrifuge small	Galaxy 16DH	VWR® International, (AUT)
Centrifuge big	Labofuge 400 FUNCTION Line	Heraeus Instruments GmbH, (AUT)
Ultrasonic bath	BANDELIN SONOREX RK 510	BANDELIN electronic GmbH & Co. KG, (GER)
Freezer -80°C	Forma 900 Series	Forma Scientific, (AUT)
Freezer -20°C	Liebherr Premium GP 1476	Liebherr-International GmbH, (AUT)
Refrigerator	Liebherr profi line 7080 339-01	Liebherr-International GmbH, (AUT)
Liquid nitrogen	RS Series 750	Taylor-Wharton, (USA)
Laminar air flow	Biosafe 2	Ehret GmbH, (GER)
Plate shaker	MixMate	Eppendorf AG, (AUT)
CO ₂ -Incubator	Function Line	Heraeus Instruments GmbH, (AUT)
Water bath	Transonic Digital	Elma Schmidbauer GmbH, (AUT)
Microscope	Nicon Eclipse Te2000-S	Nicon GmbH, (AUT)
Counting chamber	Neubauer Improved (0.100 mm)	Assistent Germany, (GER)
Micropipettes	Eppendorf Research: 2-20 µL, 20-200 µL, 50-1000 µL	Eppendorf AG, (GER)
Pipette tips	Universal: yellow 2-200 µL, blue 50-1000 µL	VWR® International, (AUT)
Pipette tips	Disposable sterile pipette tips: yellow 200 µL, blue 1000 µL	VWR® International, (AUT)
Eppendorf tubes	Plastibrand 1.5 mL	BRAND GmbH, (GER)
Centrifuge tubes	SuperClear®, 15 mL	VWR® International, (AUT)
Test tubes	Plastibrand	BRAND GmbH, (GER)
HPLC Vials	2-SV (A)	Chromacol®, (AUT)
HPLC Septum	8-ST 15	Chromacol®, (AUT)
HPLC Caps	8-SC	Chromacol®, (AUT)
HPLC Microvials	02-MTV	Chromacol®, (AUT)
12-wells tissue culture plates	Multiwell, steril	VWR® International, (AUT)
6-wells tissue culture plates	Multiwell, steril	VWR® International, (AUT)
TRANSIL ^{XL} Kits		Sovicell GmbH, (GER)
Homogenizer	Minilys®	Peqlab, (GER)
Ceramic bead kit	Precellys® 2.8-mm	Peqlab, (GER)
EpiDerm™ skin model	EPI-100-FIX	MatTek Corporation, (USA)
Test tubes	thick-walled 100 x 16 mm	Assistent, (GER)
UV-VIS Spectrophotometer	UV-1800	Shimadzu, (AUT)

3.2 Validation

While the complete validation of the method was implemented with only the most active and non-toxic lead compound CPD11, a partial validation was performed for an extended set of seven test-compounds (CPD3, CPD5, CPD6, CPD7, CPD10, CPD13 and CPD17), to confirm the suitability of this method for this class of compound. .

3.2.1 Preparation of Standard Solutions

Stock solutions for the preparation of calibration curves and quality control (Q) samples in human plasma and phosphate-buffered saline (PBS) were obtained by dissolving CPD11 in dimethylsulfoxid (DMSO)/PBS 32:68 (v/v) in order to reach a final concentration of 1 mg/mL. To achieve suitable working concentrations for Q samples, further dilution with PBS was carried out at concentrations of 0.1, 1.0 and 10.0 µg/mL for pooled human plasma and PBS.

The PBS solution consisted of 10 mmol disodium hydrogen phosphate and 0.9% sodium chloride in water adjusted to a pH of 7.4 with phosphoric acid. All stock solutions were stored at +4°C until analysis.

For a sample chromatogram, all eight SeaLife compounds were dissolved in ACN in a final concentration of 10.0 µg/mL and afterwards analysed.

3.2.2 Sample Preparation

Human plasma samples were spiked with 5.0 µg/mL, from the stock solution, of the lead compound CPD11 and processed immediately as followed: 175 µL ice-cold ACN was added to 70 µL plasma for protein precipitation (dilution factor 1:2.5, v/v). After vortexing for 10 sec and centrifugation at 10,500 g for 5 min, 40 µL of the clear supernatant was injected into the HPLC system.

Liver tissue samples were chopped into pieces and PBS was added (1:3, v/v). The suspension was processed with a Minilys® homogenizer using a Precellys® 2.8-mm ceramic bead kit for more effective homogenization. The crude liver extract was spiked with 5.0 µg/mL of the stock solution of CPD11, homogenized 3 times for 30 sec, and centrifuged at 10,500 g for 5 min. The obtained clear supernatant was handled, as described above in the plasma section,

prior HPLC analysis. Sample preparation and analysis of samples obtained from metabolic stability screening with cryopreserved human male hepatocytes were carried out, as described in section 3.4, with an incubation concentration of 25 μ M.

3.2.3 Method Validation

Validation was performed in accordance with the ICH-GLP guidelines of the European Medicines Agency for the lead compound CPD11. That is, the mean values of the assayed concentrations must not exceed the range of $\pm 15\%$ deviation, and limit of quantification (LOQ) and limit of detection (LOD) must not exceed $\pm 20\%$.

Recovery, Precision, Accuracy, and Linearity

For quantification of analytes, an external standard method was used. The standard calibration curves were assayed from 0.1 to 10.0 μ g/mL in pooled human plasma and PBS. Their linearity was evaluated using linear regression analysis. To assess assay accuracy and precision, Q samples were prepared in triplicate at each concentration, that is 0.1, 1.0 and 10.0 μ g/mL for pooled human plasma and PBS, and analysed six times within the same day (intra-day) and six times after 7 days (inter-day).

To determine the accuracy, the deviation from the spiked concentration – in comparison to the concentration after sample analysis – was expressed as a percentage of the actual concentration ($\text{bias} = \frac{\text{conc}_{\text{spiked}} - \text{conc}_{\text{analysis}}}{\text{conc}_{\text{spiked}}} * 100$). To reflect the method's suitability for the compounds to be assayed, the percentage of recovery was calculated as follows: $\% \text{ recovery} = \text{bias} + 100$. The intra- and inter-day coefficients of variation (CVs) represent the observed imprecision of the method ($\text{CV} = \text{SD}/\text{mean} * 100$).

Sensitivity

LOQ is the lowest concentration at which an analyte can be quantitated. LOD describes the lowest detectable concentration of an analyte in the sample. These values can verify the interpretation of results and therefore are key parameters for validation of analytical methods. [81]

The LOQ and LOD were evaluated by diluting the stock solution of CPD11 (1 mg/mL DMSO/PBS 32:68, v/v) in PBS at concentrations of 0.03, 0.06, 0.12, 0.25, 0.50, 1.0 μ g/mL

with a minimum signal-to-noise ratio of 3:1. Likewise, these values were obtained in plasma at concentrations of 0.017, 0.035 and 0.070 $\mu\text{g/mL}$ with a signal-to-noise ratio of 10:1. To exclude possible interferences from matrix components, blank human plasma and liver tissue samples were prepared and processed equally, as samples, containing 5.0 $\mu\text{g/mL}$ CPD11.

Stability

For stability investigations stock solution (1 mg/mL DMSO/PBS 32:68, v/v) were diluted with PBS until reaching a concentration of 5.0 and 0.5 $\mu\text{g/mL}$. The short-term stabilities of CPD11 in plasma and PBS were tested considering a maximum analysis time of 24 h. Evaluation of long-term stabilities were investigated after three full cycles of freezing and thawing in both plasma and PBS. Samples were stored at -20°C for 24 h and then analysed and stored again until re-analysis.

In addition, the stability of 5.0 $\mu\text{g/mL}$ of CPD11 dissolved in DMSO/PBS (32:86, v/v) was evaluated at $+4^{\circ}\text{C}$ and repeated chromatographic analysis of 4 samples on day 0, 1, 7, 14, 20 and 34. Furthermore, 5.0 $\mu\text{g/mL}$ CPD11 was dissolved in DMSO/PBS (32:86, v/v) and was exposed to daylight at room temperature (24°C) for 1, 3, 7 and 21 days.

Calibration Curves

The calibration curves in this thesis were evaluated by using an external standard method. They were obtained by plotting the peak area of each concentration against the concentration of each standard sample using a linear regression method. For this purpose the equation $y = kx + d$, whereas variable y describes the peak area, k the slope of the regression line, variable x the concentration and constant d the intersection of the regression line with the y -axis. By the transformed calibration curve the exact concentration of an unknown sample can be calculated.

Calibration standards in plasma at concentrations of 0.625, 1.25, 2.5, 5.0, 10.0 and 20.0 $\mu\text{g/mL}$ were prepared, by diluting the stock solution (1.0 mg/mL DMSO/PBS 32:68, v/v) with PBS.

3.2.4 Comparison of CPD11 with seven other SeaLife Compounds

To obtain lambda maximum of seven SeaLife compounds, they were dissolved in pure ACN at a concentration of 5.0 µg/mL and scanned against blank ACN. For these investigations 1.0 mg of each compound was dissolved in 1.0 mL DMSO/PBS 32:68 (v/v), afterwards further diluted with PBS until reaching a final concentration of 5.0 µg/mL and chromatographed, as described in section 3.1.1.

For a chromatographic comparison of these compounds, HPLC analysis time was also set at 42 min. Following parameters were obtained: k' (capacity factor) = $(t_R/t_0)-1$ (according to the SST (System suitability testing) guidelines of the HSM software), N (number of theoretical plates), LOQ, LOD and recovery.

3.3 Binding and Distribution Experiments

3.3.1 TRANSIL^{XL} Kit

Special in vitro kits were used to determine the fraction of the test compounds f_u and bound (f) to the plasma proteins HSA and AGP and their affinity for phosphatidylcholine membranes and microsomal membranes. Additionally, V_d and P_{int} can be estimated by using the intestinal absorption kit. [61]

For validation purposes, four well-established drugs (erlotinib, capecitabine, doxorubicin, and linezolid) were included in our TRANSIL^{XL} investigations as a reference. These drugs show diverse physicochemical properties and pharmacological activity that differ significantly from the physicochemical properties of the SeaLife compounds.

The assay consists of a 96-well plate allowing twelve compounds to be analysed simultaneously (Figure 5).

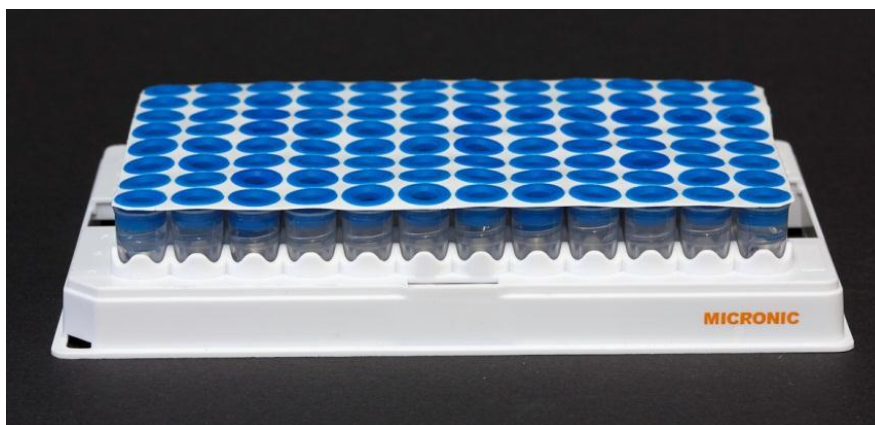


Figure 5: Illustration of the TRANSIL^{XL} Kits assay plate [61]

For the complete characterization of the affinity of a test compound, eight wells were needed: six samples containing increasing concentrations of the biological phase and two samples of standard PBS solutions (Figure 6). The PPB tubes were either filled with a suspension of plasma proteins containing a mixture of HSA and AGP at a physiological ratio of 24:1 or were solely incorporated with HSA or AGP immobilized on silica beads. For the intestinal and

microsomal absorption kits, phosphatidylcholine membrane vesicles (intestinal) or microsomal membranes were immobilized on silica beads.



Figure 6: Photograph of annotated tube units [61]

The compounds to be investigated were dissolved in DMSO/PBS 32:68 (v/v), yielding a stock solution concentration of 80 μM . The binding kits were stored at -20°C and were thawed at room temperature three hours before usage in order to reach a working temperature of approximately $20\text{-}25^{\circ}\text{C}$. After centrifugation of the plates for 5 sec at 750 g using a Labofuge 400 Function Line 15 μL of the stock solution was added to each of the eight wells, yielding a final compound concentration of 5 μM in the assay.

The next step was to incubate the plates at room temperature on a Mix Mate PCB-11 plate shaker for 12 min, except for the AGP binding kit, which required incubation for 30 sec on the plate shaker and thereafter 2 min of manual shaking. To separate the beads from the suspension containing the f_u compound, the plate was centrifuged for 10 min at 750 g. Sixty microliters of the clear supernatant in each well was pipetted into an autosampler microvial. For quantification, above mentioned RP-HPLC method was used, injecting 40 μL of the supernatant to quantify the amount of the compound in the supernatant. A summary of the workflow is shown in Figure 7.

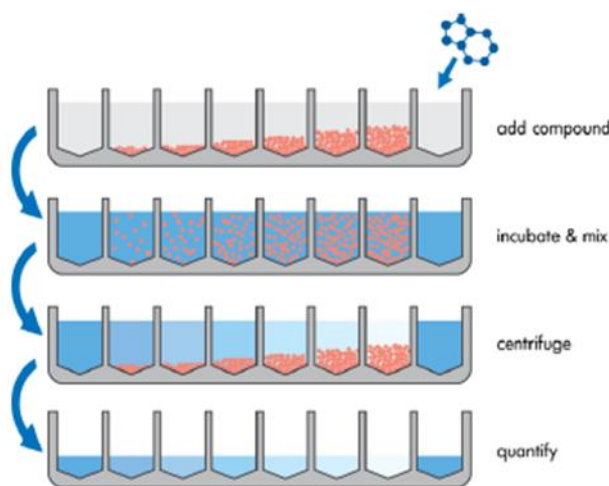


Figure 7: Workflow of TRANSIL^{XL} Kit [61]

After quantification of the reference and test samples, the above-mentioned parameters were calculated. The following calculations were performed according to the recommendations of the TRANSIL^{XL} user guide. The PPB, AGP and HSA parameters were measured through the dissociation constant (K_D): [61]

$$K_D = \frac{[A] * [P]}{[AP]} \quad (1)$$

where P is the free concentration of the protein and A is the free concentration of the drug. AP is the protein-drug complex. For the PPB kit only, a pseudo K_D was determined to evaluate the binding of a mixture of AGP and HSA. Another possibility for the expression of the free concentration of a compound is as follows:

$$[A] = f_u * ([A] + [AP]) \quad (2)$$

After combining (2) with (1), a linear model is created that can be transferred to either the AGP, HSA or PPB kit with $1/K_D$ and an intercept of 0:

$$\frac{f_b}{f_u} = \frac{1}{K_D} * P \quad (3)$$

Eventually, the f_u was predicted from the K_D s of AGP and HSA, wherein the physiological concentration of these proteins was also taken into consideration:

$$f_b = 1 - \frac{1}{1 + \frac{[AGP]}{K_D^{AGP}} + \frac{[HSA]}{K_D^{HSA}}} \quad (4)$$

The kits estimated the binding rates of the test compounds to AGP and HSA only, and plasma proteins at low concentration in blood (e.g., lipoproteins) were not included in the calculations.

The membrane affinity (MA) of a compound is defined as the coefficient of the concentration of the compound attached to the membrane (c_m) and the buffer (c_b):

$$MA = \frac{c_l}{c_m} \quad (5)$$

With the mass balance formula, membrane affinity can be calculated from data obtained from the assay:

$$n_t = c_b * V_b + c_m * V_m \quad (6)$$

where n_t is the amount of the drug, V_b is the volume of the buffer and V_m is the volume of the lipid membrane in each well. Rearranging (6) enables MA to be calculated from the slope of plotting the ratio of n_t over the c_b against V_m in each well:

$$\frac{n_t}{c_b} = \frac{c_l}{c_b} * V_m + V_b = MA * V_m + V_b \quad (7)$$

The P_{int} coefficient can be predicted from MA; it is the equilibrium partition coefficient between water, lipid bilayers and the effective molecular weight (MW_{eff}). The formula below is based on an equation first published in 1998, and its dimension is indicated as cm/s. [98]

$$P_{int} = A * \frac{MW_{eff}^{-\alpha-\beta} * MA}{MW_{eff}^{-\alpha} + B * MW_{eff}^{-\alpha} * MA} + C * \frac{MW_{eff}^{-\gamma}}{D^{-\gamma} + MW_{eff}^{-\gamma}} \quad (8)$$

On the right side of (8), the first term describes the transcellular and the second term the paracellular transport in the intestinal epithelium. $MW_{eff}^{-\alpha} + B * MW_{eff}^{-\alpha} * MA$ is defined as the diffusion process in the unstirred water layer. α (water) and β (membrane) are defined as the

diffusion coefficients in the two matrices. $\frac{MW_{eff}^{-\gamma}}{D^{-\gamma} + MW_{eff}^{-\gamma}}$ describes designated values between 0 and 1 (sigmoid function) and the slope γ . D represents diffusion via tight junctions, and C is the permeability coefficient, together (D and C) representing para-cellular transport.

Vd (L/kg) is estimated from measurements of PPB and MA. (9)

$$Vd = 10^{a \cdot \log(MA) + b \cdot \log(K_{b,f}) + c} \quad (9)$$

The term $K_{b,f}$ denotes the relation between the f and f_u fractions of a compound. a, b and c are determined from already known 42 drug Vds.

3.3.2 ADMET Predictor

The most important physicochemical factors calculated with the ADMET Predictor software are the pKa (dissociation constant dominated by acidic functional groups) / pKb (dissociation constant dominated by basic functional groups) value and logP. Both pKs and the logP calculations are based on atomic descriptors and artificial neural network ensembles (ANNEs), resulting in good performance and high accuracy in train/verify and test sets. In the prediction of pKa, the program is capable of showing ionized microspecies of multiprotic molecules and labelling the predicted pK value as either pKa or pKb. For the logP value, the S+logP model built by the integrated Simulations Plus ADMET Modeler (TM) module was applied.

3.4 Hepatocytes

3.4.1 Certificates

Certificates of amount of donors from monkey (cynomolgus), rat (sprague-dawley), human male and human female cryopreserved hepatocytes along with their properties and lot numbers are shown in Figure 8 to Figure 11.

MATERIAL AND METHODS



Quality Certificate

Primary Hepatocytes: Cryopreserved

Species: Human

Catalog Number: HMCS1S

Lot Number: Hu0885

Number of Donors: 1

Product Information Sheet

Shipping/Storage Temperature: Below -135 °C

Sample Information: Store using Vapor Phase Liquid Nitrogen

Certificate of Analysis

Volume: 1.5-2.0 mL Vial

FOR RESEARCH USE ONLY. CAUTION: Not intended for human or animal diagnostic or therapeutic uses. Users should treat all human and animal cells as potential pathogens. Wear protective clothing and eyewear. Practice appropriate disposal techniques for potentially pathogenic or biohazardous materials.

Contact the in-house Safety Officer for information on safe handling of human cell products, universal precautions, and for information on what to do in case of exposure. For recommended post exposure procedures, call the Centers for Disease Control (CDC) information line at +1 800 232 4635.

DONOR INFORMATION

Donor ID	Gender	Race	Age (yrs)	BMI	Smoker	Alcohol Use	Drug Use	Medications	Cause of Death
Hu0885	Male	Caucasian	45	18	Yes	Yes	Not Reported	Pericard - 6m Pharagran - 25mg po Lunesta - 3mg qd	N/A

SEROLOGY (PCR detection)

Hepatitis B:	Not Available	HTLV 1 & 2:	Not Available
Hepatitis C:	Not Available	CMV:	Not Available
HIV 1 & 2:	Not Available		

OTHER MEDICAL HISTORY:

History of Cancer diagnosed more than 1 year ago. Alcohol use stated as current, but occasional use. Smoking history described as 1/2 to 1 pack of cigarettes per day for 25 years, current use.

For technical questions about this product, contact Invitrogen's Hepatic Biology Support Team.
Email: hepaticproducts@invitrogen.com Phone: (USA) +1 866 952 3559 (Europe) +44(0)141 814 5900

Page 1 of 4

Form Human QC Rev 1d, 16MAR10



Quality Certificate

(Continued)

POST-THAW VIABILITY

Average Viability: 83%
Viable Cells/Vial: 7.0 x 10⁶

METABOLIC ACTIVITY

The cell suspension per 37°C incubation is 0.5 x 10⁶ cells/mL.
Metabolic activities are determined by HPLC or LC-MS/MS analysis and recorded as pmol/10⁶ cells/min.

Enzyme	Substrate	Concentration (μM)	Incubation Time (Min)	Marker Metabolite	Metabolic Activity
CYP1A2	Phenacetin	100	15	Acetaminophen	310
CYP2B6	Bupropion	500	15	Hydroxybupropion	44.2
CYP2C8	Paclitaxel	20	45	6α-Hydroxypaclitaxel	6.94
CYP2C9	Diclofenac	25	15	4'-Hydroxydiclofenac	136
CYP2C19	[S]-Mephenytoin	250	30	4'-Hydroxymephenytoin	16.6
CYP2D6	Dextromethorphan	15	15	Dextrophan	26.3
CYP2E1	Chloroazone	250	15	6-Hydroxychloroazone	117
CYP3A	Testosterone	250	15	6β-Hydroxytestosterone	471
CYP3A	Midazolam	10	10	1'-Hydroxymidazolam	164
FMO	Benzylamine	250	30	Benzylamine-N-oxide	541
Phase I	7-Ethoxycoumarin	100	30	(ECOC) 7-Hydroxycoumarin (7-HC)	51.3
Phase II	7-Hydroxycoumarin	100	30	7-Hydroxycoumarin Glucuronide (7-HCG)	384
Phase II	7-Hydroxycoumarin	100	30	7-Hydroxycoumarin Sulfate (7-HCS)	31.4

ENZYME INDUCTION

The number of plated cells per 37°C incubation is 0.375 x 10⁶ cells/well. Enzyme activities are determined after 72 hours in culture by LC-MS/MS analysis (vehicle-induced activity). Relative mRNA contents are determined after 48 hours by qRT-PCR analysis (TagMan®). Results are recorded as pmol/10⁶ cells/min.

Enzyme	Inducer *	Substrate	Conc. (μM)	Incubation Time (Min)	Marker Metabolite	Vehicle Activity	Induced Activity	Fold Induction	mRNA Relative-Fold
CYP1A2	3-MC (2 μM)	Phenacetin	100	15	Acetaminophen	N/A	N/A	N/A	N/A
CYP2B6	PB (1000 μM)	Bupropion	500	20	Hydroxybupropion	N/A	N/A	N/A	N/A
CYP3A	RF (10 μM)	Testosterone	200	14	6β-Hydroxytestosterone	N/A	N/A	N/A	N/A

* 3-MC = 3-Methylcholanthrene; PB = Phenobarbital; RF = Rifampicin

For technical questions about this product, contact Invitrogen's Hepatic Biology Support Team.
Email: hepaticproducts@invitrogen.com Phone: (USA) +1 866 952 3559 (Europe) +44(0)141 814 5900

Page 2 of 4

Form Human QC Rev 1d, 16MAR10

Received

In vitro screens donor tissues for thirteen different SNPs within four drug-metabolizing genes. These include the following: CYP2C9*2, CYP2C9*3, CYP2C9*4, CYP2C19*2, CYP2C19*3, CYP2C19*6, CYP2D6*3, CYP2D6*4, CYP2D6*6, CYP2D6*9, CYP3A5*3, CYP3A5*6, and CYP3A5*8. All SNPs were identified by qRT-PCR with Taqman® primer/probe sets.



GIBCO®
nutrison cell culture

(Continued)

Matthew Riggsbee 23 June 2010
Prepared By Date


 Quality Systems Department Date

Cryopreserved Human Hepatocytes were thawed in CHRM™ and plated. The concentrations and incubation times for prototypical CYP isozymes are included in the chart below. Incubations were conducted in duplicate in serum-free Williams' Medium E culture medium and reactions allowed to proceed in a humidified incubator at 37°C, 95% relative humidity, and 5% CO₂ on an orbital shaker. Reactors were stopped with the addition of ice-cold Acetonitrile. Well contents were stored at -70°C prior to analysis. The disappearance of parent was monitored by LC-MS/MS analysis and intrinsic clearance (CL_{int}) values determined by linear regression.

Cryopreserved hepatocytes were thawed in CHRM[®] and plated. The Transporter assay was performed on Day 5. Rates of substrate uptake were determined by the use of buffer with calcium. Hepatocyte cultures were incubated in triplicate with radio-labeled Tauracholic acid, Dexamethasone and Estradiol 17 β glucuronide [E2-17 β]. Substrate concentrations and incubation times are listed in the table below. To account for non-specific binding of the radio-labeled substrate, a negative control plate absent of cells was included. Cells were lysed following incubations and samples analyzed by use of a liquid scintillation counter.

For technical questions about this product, contact Invitrogen's Hepatic Biology Support Team.
Email: hepaticproducts@invitrogen.com Phone: (USA) +1 888 952 3559 (Europe) +44(0)141 814 5500



Quality Certificate

Primary Hepatocytes: Cryopreserved Suspension

Catalog Number: HMCS25

Species: Human

Lot Number: HU1464

Number of Donors: 1

Product Information Sheet

Shipping/Storage Temperature: Below -135 °C

Certificate of Analysis

Sample Information: Store using Vapor Phase Liquid Nitrogen

Volume: 1.5-2.0 mL/Vial

FOR RESEARCH USE ONLY. CAUTION: Not intended for human or animal diagnostic or therapeutic uses. Users should treat all human and animal cells as potential pathogens. Wear protective clothing and eyewear. Practice appropriate disposal techniques for potentially pathogenic or bio-hazardous materials.

Contact the in-house Safety Officer for information on safe handling of human cell products, universal precautions, and for information on what to do in case of exposure. For recommended post exposure procedures, call the Centers for Disease Control (CDC) Information line at +1 800 232 4636.

DONOR INFORMATION									
Donor ID	Gender	Race	Age (yrs)	BMI	Tobacco History ¹	Alcohol History ¹	Drug History ¹	Medications	Cause of Death
HU1464	Female	Caucasian	45	29	Yes	Yes	None Reported	Celene: 20mg poed Synthroid: 50mcg poed Karex XR: 1mg poed	N/A

¹Yes, see Tobacco, Alcohol and Drug History section below for additional information

POTENTIAL BIOLOGICAL CONTAMINANTS (P.L. & T. tested)			
Hepatitis B:	Non-Reactive	HTLV 1 & 2:	Non-Reactive
Hepatitis C:	Non-Reactive	CMV:	Non-Reactive
HIV 1 & 2:	Non-Reactive		

TOBACCO, ALCOHOL AND DRUG HISTORY:

Alcohol history stated as 1 glass of wine per day, current use. Tobacco history described as 1/2 to 1 pack of cigarettes per day, past use, quit years ago.

For technical questions about this product, contact the Hepatic Biology Support Team at Life Technologies.
Email: hepaticproducts@lifetech.com Phone: (USA) +1 866 952 3559



Quality Certificate

(Continued)

POST-THAW RESULTS

Average Viability: 81 % in Williams Medium E

Viable Cells/Vial: 11×10^6

METABOLIC ACTIVITY Assay Not Applicable

The cell suspension per 37°C incubation is 3.7×10^6 cells/mL.Metabolic activities are determined by HPLC or LC-MS/MS analysis and are reported as pmol/min/10⁶ cells.

Enzyme	Substrate	Concentration (μM)	Incubation Time (Min)	Marker Metabolite	Metabolic Activity
CYP1A2	Phenacetin	100	15	Acetaminophen	192
CYP2B6	Bupropion	500	15	Hydroxybupropion	11.5
CYP2C8	Paclitaxel	20	45	6α-Hydroxypaclitaxel	6.85
CYP2C9	Diclofenac	25	15	4'-Hydroxydiclofenac	114
CYP2C19	(S)-Mephasoin	250	30	4-Hydroxymephasoin	5.90
CYP2D6	Dextromethorphan	15	15	Dextrophan	31.5
CYP2E1	Chlorzoxazone	250	15	6-Hydroxychlorzoxazone	200
CYP3A	Testosterone	200	15	5β-Hydroxytestosterone	510
CYP3A	Midazolam	10	10	1'-Hydroxymidazolam	90.8
FMO	Benzylamine	250	30	Benzylamine-N-oxide	345
Phase I	7-Ethoxycoumarin	100	30	IECDE 7-Hydroxycoumarin (7-HC)	23.3
Phase II	7-Hydroxycoumarin	100	30	7-Hydroxycoumarin Glucuronide (7-G)	488
Phase II	7-Hydroxycoumarin	100	30	7-Hydroxycoumarin Sulfate (7-HS)	69.5

INTRINSIC CLEARANCE - SUSPENSION Assay Not Applicable

Cryopreserved human Hepatocytes were thawed in CHSETM and resuspended in 100 μL CHSE/2mL in serum free incubation medium. The final cell density was 0.5×10^6 cells/mL. Substrate concentrations and incubation times are included in the table below. Incubations were conducted in triplicate. Hepatic clearance values of substrate are reported. At the appropriate time point, an aliquot of sample was removed from the well and added to a polypropylene tube containing ice-cold acetonitrile. Well contents were stored at -80°C prior to analysis. The drug clearance of parent was determined by LC-MS/MS analysis and intrinsic clearance (CL_{int}) values calculated by linear regression.

SUBSTRATE	Concentration (μM)	Incubation Times (Min)	Intrinsic Clearance (CL _{int}) values (μL/min/10 ⁶ cells)
Dextromethorphan	1	0, 15, 30, 45, 90, 120	0
Midazolam	0.5	0, 15, 30, 45, 90, 120	N/A
Phenacetin	1	0, 15, 30, 45, 90, 120	N/A

For technical questions about this product, contact Invitrogen's Hepatic Biology Support Team.
Email: hepaticproducts@lifetech.com Phone: (USA) +1 866 952 3559



Quality Certificate

(Continued)

TRANSPORTER SUSPENSION UPTAKE RESULTS Assay Not Applicable					
Transporter active uptake was determined in suspensions of cryopreserved hepatocytes using pH-sens methodology. Cryopreserved hepatocytes were thawed, then re-suspended in a buffer. The hepatocytes and buffer were added to a 24-well plate and allowed to pre-incubate at 37°C. Reactions were initiated by the addition of pre-mixed radiolabeled substrate to the wells containing hepatocytes and incubated for time specified in the table. After termination, the cell pellet was placed into a scintillation vial and amounts of radiolabel determined with a liquid scintillation counter. Non-specific uptake was determined by performing the above experiment with cell samples were kept at 4°C. Facilitated active transport was determined using the following equation: uptake rate (DPC) = uptake rate (4°C) and expressed as pmol/min/mg protein.					
SUBSTRATE	Concentration (μM)	Incubation Time (min)	Accumulation Rate 37 °C (pmol/min/mg protein)	Accumulation Rate 4 °C (pmol/min/mg protein)	Facilitated Active Uptake (37 °C - 4 °C)
Tauracholate	1	1	N/A	N/A	N/A
Digoxin	1	1	N/A	N/A	N/A
Estradiol, 17β Glucuronide (E2-17G)	1	1	N/A	N/A	N/A
MEP+	1	5	N/A	N/A	N/A

GENOTYPING RESULTS															
Assay Not Applicable															
Sequencing across donor livers for the liver derived CNPs within four drug-metabolizing genes. These include the following: CYP2C9, CYP2C19, CYP2D6, CYP3A4, CYP3A5, CYP2C8, CYP2C18, CYP2C19, CYP2C19A, CYP2C19B, CYP2C19C, CYP2C19D, CYP2C19E, CYP2C19F, CYP2C19G, CYP2C19H, CYP2C19I, CYP2C19J, CYP2C19K, CYP2C19L, CYP2C19M, CYP2C19N, CYP2C19O, CYP2C19P, CYP2C19Q, CYP2C19R, CYP2C19S, CYP2C19T, CYP2C19U, CYP2C19V, CYP2C19W, CYP2C19X, CYP2C19Y, CYP2C19Z, CYP2C19AA, CYP2C19AB, CYP2C19AC, CYP2C19AD, CYP2C19AE, CYP2C19AF, CYP2C19AG, CYP2C19AH, CYP2C19AI, CYP2C19AJ, CYP2C19AK, CYP2C19AL, CYP2C19AM, CYP2C19AN, CYP2C19AO, CYP2C19AP, CYP2C19AQ, CYP2C19AR, CYP2C19AS, CYP2C19AT, CYP2C19AU, CYP2C19AV, CYP2C19AW, CYP2C19AX, CYP2C19AY, CYP2C19AZ, CYP2C19BA, CYP2C19BB, CYP2C19BC, CYP2C19BD, CYP2C19BE, CYP2C19BF, CYP2C19BG, CYP2C19BH, CYP2C19BI, CYP2C19BJ, CYP2C19BK, CYP2C19BL, CYP2C19BM, CYP2C19BN, CYP2C19BO, CYP2C19BP, CYP2C19BQ, CYP2C19BR, CYP2C19BS, CYP2C19BT, CYP2C19BU, CYP2C19BV, CYP2C19BW, CYP2C19BX, CYP2C19BY, CYP2C19BZ, CYP2C19CA, CYP2C19CB, CYP2C19CC, CYP2C19CD, CYP2C19CE, CYP2C19CF, CYP2C19CG, CYP2C19CH, CYP2C19CI, CYP2C19CJ, CYP2C19CK, CYP2C19CL, CYP2C19CM, CYP2C19CN, CYP2C19CO, CYP2C19CP, CYP2C19CQ, CYP2C19CR, CYP2C19CS, CYP2C19CT, CYP2C19CU, CYP2C19CV, CYP2C19CW, CYP2C19CX, CYP2C19CY, CYP2C19CZ, CYP2C19DA, CYP2C19DB, CYP2C19DC, CYP2C19DD, CYP2C19DE, CYP2C19DF, CYP2C19DG, CYP2C19DH, CYP2C19DI, CYP2C19DJ, CYP2C19DK, CYP2C19DL, CYP2C19DM, CYP2C19DN, CYP2C19DO, CYP2C19DP, CYP2C19DQ, CYP2C19DR, CYP2C19DS, CYP2C19DT, CYP2C19DU, CYP2C19DV, CYP2C19DW, CYP2C19DX, CYP2C19DY, CYP2C19DZ, CYP2C19EA, CYP2C19EB, CYP2C19EC, CYP2C19ED, CYP2C19EE, CYP2C19EF, CYP2C19EG, CYP2C19EH, CYP2C19EI, CYP2C19EJ, CYP2C19EK, CYP2C19EL, CYP2C19EM, CYP2C19EN, CYP2C19EO, CYP2C19EP, CYP2C19EQ, CYP2C19ER, CYP2C19ES, CYP2C19ET, CYP2C19EU, CYP2C19EV, CYP2C19EW, CYP2C19EX, CYP2C19EY, CYP2C19EZ, CYP2C19FA, CYP2C19FB, CYP2C19FC, CYP2C19FD, CYP2C19FE, CYP2C19FF, CYP2C19FG, CYP2C19FH, CYP2C19FI, CYP2C19FJ, CYP2C19FK, CYP2C19FL, CYP2C19FM, CYP2C19FN, CYP2C19FO, CYP2C19FP, CYP2C19FQ, CYP2C19FR, CYP2C19FS, CYP2C19FT, CYP2C19FU, CYP2C19FV, CYP2C19FW, CYP2C19FX, CYP2C19FY, CYP2C19FZ, CYP2C19GA, CYP2C19GB, CYP2C19GC, CYP2C19GD, CYP2C19GE, CYP2C19GF, CYP2C19GG, CYP2C19GH, CYP2C19GI, CYP2C19GJ, CYP2C19GK, CYP2C19GL, CYP2C19GM, CYP2C19GN, CYP2C19GO, CYP2C19GP, CYP2C19GQ, CYP2C19GR, CYP2C19GS, CYP2C19GT, CYP2C19GU, CYP2C19GV, CYP2C19GW, CYP2C19GX, CYP2C19GY, CYP2C19GZ, CYP2C19HA, CYP2C19HB, CYP2C19HC, CYP2C19HD, CYP2C19HE, CYP2C19HF, CYP2C19HG, CYP2C19HH, CYP2C19HI, CYP2C19HJ, CYP2C19HK, CYP2C19HL, CYP2C19HM, CYP2C19HN, CYP2C19HO, CYP2C19HP, CYP2C19HQ, CYP2C19HR, CYP2C19HS, CYP2C19HT, CYP2C19HU, CYP2C19HV, CYP2C19HW, CYP2C19HX, CYP2C19HY, CYP2C19HZ, CYP2C19IA, CYP2C19IB, CYP2C19IC, CYP2C19ID, CYP2C19IE, CYP2C19IF, CYP2C19IG, CYP2C19IH, CYP2C19II, CYP2C19IJ, CYP2C19IK, CYP2C19IL, CYP2C19IM, CYP2C19IN, CYP2C19IO, CYP2C19IP, CYP2C19IQ, CYP2C19IR, CYP2C19IS, CYP2C19IT, CYP2C19IU, CYP2C19IV, CYP2C19IW, CYP2C19IX, CYP2C19IY, CYP2C19IZ, CYP2C19JA, CYP2C19JB, CYP2C19JC, CYP2C19JD, CYP2C19JE, CYP2C19JF, CYP2C19JG, CYP2C19JH, CYP2C19JI, CYP2C19JJ, CYP2C19JK, CYP2C19JL, CYP2C19JM, CYP2C19JN, CYP2C19JO, CYP2C19JP, CYP2C19JQ, CYP2C19JR, CYP2C19JS, CYP2C19JT, CYP2C19JU, CYP2C19JV, CYP2C19JW, CYP2C19JX, CYP2C19JY, CYP2C19JZ, CYP2C19KA, CYP2C19KB, CYP2C19KC, CYP2C19KD, CYP2C19KE, CYP2C19KF, CYP2C19KG, CYP2C19KH, CYP2C19KI, CYP2C19KJ, CYP2C19KK, CYP2C19KL, CYP2C19KM, CYP2C19KN, CYP2C19KO, CYP2C19KP, CYP2C19KQ, CYP2C19KR, CYP2C19KS, CYP2C19KT, CYP2C19KU, CYP2C19KV, CYP2C19KW, CYP2C19KX, CYP2C19KY, CYP2C19KZ, CYP2C19LA, CYP2C19LB, CYP2C19LC, CYP2C19LD, CYP2C19LE, CYP2C19LF, CYP2C19LG, CYP2C19LH, CYP2C19LI, CYP2C19LJ, CYP2C19LK, CYP2C19LL, CYP2C19LM, CYP2C19LN, CYP2C19LO, CYP2C19LP, CYP2C19LQ, CYP2C19LR, CYP2C19LS, CYP2C19LT, CYP2C19LU, CYP2C19LV, CYP2C19LW, CYP2C19LX, CYP2C19LY, CYP2C19LZ, CYP2C19MA, CYP2C19MB, CYP2C19MC, CYP2C19MD, CYP2C19ME, CYP2C19MF, CYP2C19MG, CYP2C19MH, CYP2C19MI, CYP2C19MJ, CYP2C19MK, CYP2C19ML, CYP2C19MN, CYP2C19MO, CYP2C19MP, CYP2C19MQ, CYP2C19MR, CYP2C19MS, CYP2C19MT, CYP2C19MU, CYP2C19MV, CYP2C19MW, CYP2C19MX, CYP2C19MY, CYP2C19MZ, CYP2C19NA, CYP2C19NB, CYP2C19NC, CYP2C19ND, CYP2C19NE, CYP2C19NF, CYP2C19NG, CYP2C19NH, CYP2C19NI, CYP2C19NJ, CYP2C19NK, CYP2C19NL, CYP2C19NM, CYP2C19NN, CYP2C19NO, CYP2C19NP, CYP2C19NQ, CYP2C19NR, CYP2C19NS, CYP2C19NT, CYP2C19NU, CYP2C19NV, CYP2C19NW, CYP2C19NX, CYP2C19NY, CYP2C19NZ, CYP2C19OA, CYP2C19OB, CYP2C19OC, CYP2C19OD, CYP2C19OE, CYP2C19OF, CYP2C19OG, CYP2C19OH, CYP2C19OI, CYP2C19OJ, CYP2C19OK, CYP2C19OL, CYP2C19OM, CYP2C19ON, CYP2C19OO, CYP2C19OP, CYP2C19OQ, CYP2C19OR, CYP2C19OS, CYP2C19OT, CYP2C19OU, CYP2C19OV, CYP2C19OW, CYP2C19OX, CYP2C19OY, CYP2C19OZ, CYP2C19PA, CYP2C19PB, CYP2C19PC, CYP2C19PD, CYP2C19PE, CYP2C19PF, CYP2C19PG, CYP2C19PH, CYP2C19PI, CYP2C19PJ, CYP2C19PK, CYP2C19PL, CYP2C19PM, CYP2C19PN, CYP2C19PO, CYP2C19PP, CYP2C19PQ, CYP2C19PR, CYP2C19PS, CYP2C19PT, CYP2C19PU, CYP2C19PV, CYP2C19PW, CYP2C19PX, CYP2C19PY, CYP2C19PZ, CYP2C19QA, CYP2C19QB, CYP2C19QC, CYP2C19QD, CYP2C19QE, CYP2C19QF, CYP2C19QG, CYP2C19QH, CYP2C19QI, CYP2C19QJ, CYP2C19QK, CYP2C19QL, CYP2C19QM, CYP2C19QN, CYP2C19QO, CYP2C19QP, CYP2C19QQ, CYP2C19QR, CYP2C19QS, CYP2C19QT, CYP2C19QU, CYP2C19QV, CYP2C19QW, CYP2C19QX, CYP2C19QY, CYP2C19QZ, CYP2C19RA, CYP2C19RB, CYP2C19RC, CYP2C19RD, CYP2C19RE, CYP2C19RF, CYP2C19RG, CYP2C19RH, CYP2C19RI, CYP2C19RJ, CYP2C19RK, CYP2C19RL, CYP2C19RM, CYP2C19RN, CYP2C19RO, CYP2C19RP, CYP2C19RQ, CYP2C19RR, CYP2C19RS, CYP2C19RT, CYP2C19RU, CYP2C19RV, CYP2C19RW, CYP2C19RX, CYP2C19RY, CYP2C19RZ, CYP2C19SA, CYP2C19SB, CYP2C19SC, CYP2C19SD, CYP2C19SE, CYP2C19SF, CYP2C19SG, CYP2C19SH, CYP2C19SI, CYP2C19SJ, CYP2C19SK, CYP2C19SL, CYP2C19SM, CYP2C19SN, CYP2C19SO, CYP2C19SP, CYP2C19SQ, CYP2C19SR, CYP2C19SS, CYP2C19ST, CYP2C19SU, CYP2C19SV, CYP2C19SW, CYP2C19SX, CYP2C19SY, CYP2C19SZ, CYP2C19TA, CYP2C19TB, CYP2C19TC, CYP2C19TD, CYP2C19TE, CYP2C19TF, CYP2C19TG, CYP2C19TH, CYP2C19TI, CYP2C19TJ, CYP2C19TK, CYP2C19TL, CYP2C19TM, CYP2C19TN, CYP2C19TO, CYP2C19TP, CYP2C19TQ, CYP2C19TR, CYP2C19TS, CYP2C19TT, CYP2C19TU, CYP2C19TV, CYP2C19TW, CYP2C19TX, CYP2C19TY, CYP2C19TZ, CYP2C19UA, CYP2C19UB, CYP2C19UC, CYP2C19UD, CYP2C19UE, CYP2C19UF, CYP2C19UG, CYP2C19UH, CYP2C19UI, CYP2C19UJ, CYP2C19UK, CYP2C19UL, CYP2C19UM, CYP2C19UN, CYP2C19UO, CYP2C19UP, CYP2C19UQ, CYP2C19UR, CYP2C19US, CYP2C19UT, CYP2C19UU, CYP2C19UV, CYP2C19UW, CYP2C19UX, CYP2C19UY, CYP2C19UZ, CYP2C19VA, CYP2C19VB, CYP2C19VC, CYP2C19VD, CYP2C19VE, CYP2C19VF, CYP2C19VG, CYP2C19VH, CYP2C19VI, CYP2C19VJ, CYP2C19VK, CYP2C19VL, CYP2C19VM, CYP2C19VN, CYP2C19VO, CYP2C19VP, CYP2C19VQ, CYP2C19VR, CYP2C19VS, CYP2C19VT, CYP2C19VU, CYP2C19VV, CYP2C19VW, CYP2C19VX, CYP2C19VY, CYP2C19VZ, CYP2C19WA, CYP2C19WB, CYP2C19WC, CYP2C19WD, CYP2C19WE, CYP2C19WF, CYP2C19WG, CYP2C19WH, CYP2C19WI, CYP2C19WJ, CYP2C19WK, CYP2C19WL, CYP2C19WM, CYP2C19WN, CYP2C19WO, CYP2C19WP, CYP2C19WQ, CYP2C19WR, CYP2C19WS, CYP2C19WT, CYP2C19WU, CYP2C19WV, CYP2C19WW, CYP2C19WX, CYP2C19WY, CYP2C19WZ, CYP2C19XA, CYP2C19XB, CYP2C19XC, CYP2C19XD, CYP2C19XE, CYP2C19XF, CYP2C19XG, CYP2C19XH, CYP2C19XI, CYP2C19XJ, CYP2C19XK, CYP2C19XL, CYP2C19XM, CYP2C19XN, CYP2C19XO, CYP2C19XP, CYP2C19XQ, CYP2C19XR, CYP2C19XS, CYP2C19XT, CYP2C19XU, CYP2C19XV, CYP2C19XW, CYP2C19XX, CYP2C19XY, CYP2C19XZ, CYP2C19YA, CYP2C19YB, CYP2C19YC, CYP2C19YD, CYP2C19YE, CYP2C19YF, CYP2C19YG, CYP2C19YH, CYP2C19YI, CYP2C19YJ, CYP2C19YK, CYP2C19YL, CYP2C19YM, CYP2C19YN, CYP2C19YO, CYP2C19YP, CYP2C19YQ, CYP2C19YR, CYP2C19YS, CYP2C19YT, CYP2C19YU, CYP2C19YV, CYP2C19YW, CYP2C19YX, CYP2C19YZ, CYP2C19ZA, CYP2C19ZB, CYP2C19ZC, CYP2C19ZD, CYP2C19ZE, CYP2C19ZF, CYP2C19ZG, CYP2C19ZH, CYP2C19ZI, CYP2C19ZJ, CYP2C19ZK, CYP2C19ZL, CYP2C19ZM, CYP2C19ZN, CYP2C19ZO, CYP2C19ZP, CYP2C19ZQ, CYP2C19ZR, CYP2C19ZS, CYP2C19ZT, CYP2C19ZU, CYP2C19ZV, CYP2C19ZW, CYP2C19ZX, CYP2C19ZY, CYP2C19ZZ															
DONOR	DONOR ID	CYP2C9				CYP2C19				CYP2D6				CYP3A5	
		*2	*3	*6	*8	*2	*3	*6	*8	*2	*3	*6	*8	*2	*8
1		N/A	N/A	N/A	N/A	N/A	N/A	N/A	N/A	N/A	N/A	N/A	N/A	N/A	N/A

The Liver Cells from Lot H1U1464 were derived from tissue obtained from accredited institutions. Consent was obtained by these institutions from the donor or the donor's legal next of kin, for use of the tissue and its derivatives for research purposes.

[Signature]
Quality Systems Department Date

For technical questions about this product, contact Invitrogen's Hepatic Biology Support Team.
Email: hepaticproducts@lifetech.com Phone: (USA) +1 855 952 3559

Page 3 of 3

Form Human QC Rev 3a, Draft

Figure 9: Certificate of cryopreserved human female hepatocytes

GIBCO® Quality Certificate

Primary Hepatocytes: Cryopreserved Suspension Catalog Number: RTC310
 Species: Rat (Sprague-Dawley) Lot Number: Rs702
 Number of Donors: 3

Shipping/Storage Temperature: Below -135 °C
 Sample Information: Store using Vapor Phase Liquid Nitrogen
 Volume: 1.5-2.0 mL Vial

☐ Product Information Sheet
☒ Certificate of Analysis

FOR RESEARCH USE ONLY. CAUTION: Not intended for human or animal diagnostic or therapeutic uses. Users should treat all human and animal cells as potential pathogens. Wear protective clothing and eyewear. Practice appropriate disposal techniques for potentially pathogenic or bio-hazardous materials.

Contact the in-house Safety Officer for information on safe handling of human cell products, universal precautions, and for information on what to do in case of exposure. For recommended post exposure procedures, call the Centers for Disease Control (CDC) Information line at +1 800 232 4636.

ANIMAL DONOR INFORMATION
 These Hepatocytes were obtained from non-infectious, non-contagious, healthy animal

Sex	Age
Male	8 Weeks

POST-THAW RESULTS
 Average Viability: 75% in Williams Medium E media
 Viable Cells/Vial: 7.1×10^6

METABOLIC ACTIVITY ☐ Assay Not Applicable
 The cell suspension per 37 °C incubation is 0.5×10^6 cells/mL.
 Metabolic activities are determined by HPLC or LC-MS/MS analysis and recorded as pmol/10⁶ cells/min.

Enzyme	Substrate	Concentration (µM)	Incubation Time (Min)	Marker Metabolite	Metabolic Activity					
Phase I	7-Ethoxycoumarin	100	30	(ECOC) 7-Hydroxycoumarin (7-HC)	69.3					
Phase II	7-Hydroxycoumarin	100	7-Hydroxycoumarin Glucuronide (7-HCG)	914	Phase II	7-Hydroxycoumarin	100	30	7-Hydroxycoumarin Sulfate (7-HCS)	306
Phase II	7-Hydroxycoumarin	100	30	7-Hydroxycoumarin Sulfate (7-HCS)	306					

For technical questions about this product, contact Invitrogen's Hepatic Biology Support Team.
 Email: hepaticproducts@invitrogen.com Phone: (USA) +1 866 962 3559 (Europe) +44(0)141 814 5000

Page 1 of 2 Form HANON QC Rev 2a, 15JUN11

GIBCO® Quality Certificate
 (Continued)

The Liver Cells from Lot Rs702 were derived from tissue obtained from accredited institutions. Consent was obtained by these institutions from the donor or the donor's legal next of kin, for use of the tissue and its derivatives for research purposes.

Prepared By: *[Signature]* Date: 10 Aug 2011
 Quality Systems Department Date: 10 Aug 2011

For technical questions about this product, contact Invitrogen's Hepatic Biology Support Team.
 Email: hepaticproducts@invitrogen.com Phone: (USA) +1 866 962 3559 (Europe) +44(0)141 814 5000

Page 2 of 2 Form HANON QC Rev 2a, 15JUN11

Figure 10: Certificate of cryopreserved rat (sprague-dawley) hepatocytes



Quality Certificate

Primary Hepatocytes: Cryopreserved

Catalog Number: MKCS10

Species: Monkey (Cynomolgus)

Lot Number: Cy292

Number of Donors: 1

☐ Product Information Sheet

Shipping/Storage Temperature: Below -135 °C

☒ Certificate of Analysis

Sample Information: Store using Vapor Phase Liquid Nitrogen

Volume: 1.5-2.0 mL Vial

FOR RESEARCH USE ONLY. CAUTION: Not intended for human or animal diagnostic or therapeutic uses. Users should treat all human and animal cells as potential pathogens. Wear protective clothing and eyewear. Practice appropriate disposal techniques for potentially pathogenic or biohazardous materials.

Contact the in-house Safety Officer for information on safe handling of human cell products, universal precautions, and for information on what to do in case of exposure. For recommended post exposure procedures, call the Centers for Disease Control (CDC) information line at +1 800 232 4636.

ANIMAL DONOR INFORMATION

These Hepatocytes were obtained from non-infectious, non-contagious, healthy animal

Sex	Age
Male	3 Years

POST-THAW VIABILITY

Average Viability: 82%
Viable Cells/Vial: 6.7×10^6

METABOLIC ACTIVITY

The cell suspension per 37°C incubation is 0.5×10^6 cells/mL.
Metabolic activities are determined by HPLC or LC-MS/MS analysis and recorded as pmol/10⁶ cells/min.

Enzyme	Substrate	Concentration (μM)	Incubation Time (Min)	Marker Metabolite	Metabolic Activity
Phase I	7-Ethoxycoumarin	100	30	(ECOD) 7-Hydroxycoumarin (7-HC)	253
Phase II	7-Hydroxycoumarin	100	30	7-Hydroxycoumarin Glucuronide (7-HCG)	331
Phase II	7-Hydroxycoumarin	100	30	7-Hydroxycoumarin Sulfate (7-HCS)	94.3

For technical questions about this product, contact Invitrogen's Hepatic Biology Support Team.
Email: hepaticproducts@invitrogen.com Phone: (USA) +1 866 952 3559 (Europe) +44(0)141 814 5000

Page 1 of 2

Form Animal QC Rev 1c, 14DEC09



Quality Certificate

(Continued)

ENZYME INDUCTION

The number of plated cells per 37°C incubation is 0.375×10^6 cells/well. Enzyme activities are determined after 72 hours in culture by LC-MS/MS analysis (vehicle-induced activity). Relative mRNA contents are determined after 48 hours by qRT-PCR analysis (TopGene®). Results are recorded as pmol/10⁶ cells/min.

Enzyme	Inducer *	Substrate	Conc. (μM)	Incubation Time (Min)	Marker Metabolite	Vehicle Activity	Induced Activity	Fold Induction	mRNA Relative-Fold
CYP1A2	3-MC (2 μM)	Phenacetyl	100	15	Acetaminophen	N/A	N/A	N/A	N/A
CYP2B6	PB (1000 μM)	Bupropion	500	20	Hydroxybupropion	N/A	N/A	N/A	N/A
CYP3A	RF (10 μM)	Testosterone	200	14	6β-Hydroxytestosterone	N/A	N/A	N/A	N/A

* 3-MC = 3-Methylcholanthrene; PB = Phenobarbital; RF = Rifampin

The Liver Cells from Lot Cy292 were derived from tissue obtained from accredited institutions. These hepatocytes were obtained from non-infectious, non-contagious, healthy animals.

Prepared By: *Matthew Lingg* Date: 11 FEB 2010

Quality Systems Department: *J. K. R. f.* Date: 11 Feb 2010

For technical questions about this product, contact Invitrogen's Hepatic Biology Support Team.
Email: hepaticproducts@invitrogen.com Phone: (USA) +1 866 952 3559 (Europe) +44(0)141 814 5000
Page 2 of 2 Form Animal QC Rev 1c, 30NOV08

Figure 11: Certificate of cryopreserved monkey (cynomolgus) hepatocytes

3.4.2 Metabolic Stability

The metabolic stability of CPD11 was evaluated using cryopreserved human male, human female, cynomolgus monkey and rat hepatocytes. Upon delivery, the cryopreserved hepatocytes were stored in liquid nitrogen at -195°C until use.

Incubation medium was prepared by mixing 20 mL hepatocyte maintenance medium (serum-free) with 5 μL dexamethasone and then adding the mixture to 500 mL Williams Medium E. Prior to usage, freshly prepared incubation medium was warmed in a water bath to 37°C .

After thawing, cryopreserved hepatocytes were gently suspended in cryopreserved hepatocytes recovery medium and centrifuged at room temperature. The following centrifugal forces and durations were used for each species: human, 100 g/12 min; monkey, 76 g/9 min; and rat, 55 g/10 min. Subsequently, the supernatant was re-suspended in the incubation medium. Cell counting was performed using trypan blue so that dead cells could be differentiated from live cells, and cell viability was determined. The cell viabilities, calculated by trypan blue exclusion, of the cryopreserved hepatocytes were at least 80%. [82]

The incubation of CPD11 in different concentrations and species was conducted in duplicate, if permitted by the number of cells; otherwise, only single determinations were implemented (1×10^6 cells/mL).

Incubation concentrations of CPD11 in hepatocytes:

- Human male hepatocytes: 5 μM , 10 μM , 25 μM , 50 μM , 100 μM
- Human female hepatocytes: 10 μM , 20 μM
- Rat hepatocytes: 5 μM , 10 μM , 25 μM , 50 μM , 100 μM
- Monkey hepatocytes: 10 μM , 20 μM

Concentrations of 25 μM , 50 μM and 100 μM CPD11 for rat and human male hepatocytes were performed separately from the 5 μM and 10 μM test series.

For validation purposes, 50 μM testosterone (reference substance) was included in each test series. CPD11 and testosterone were dissolved in 1% (v/v) DMSO and 99% (v/v) medium and further diluted with medium until reaching the desired concentration. As DMSO has P450 inhibitory effects, its concentration never exceeded 1% (v/v) in our experiments.

0.5 mL of incubation medium containing CPD11 or testosterone were pipetted into a 12-well plate (non-coated). The reaction started by adding 0.5 mL of 1×10^6 cells/mL in each well. Thus, a final concentration of 0.5×10^6 cells/mL was obtained. Incubations were conducted at 37°C in a 95% humidified incubator and 5% CO₂ for 24 h. Aliquots of 70 µL were taken from each well at different time points, i.e., at 1, 15, 30, 60, 120, 180, 240, 300 and 1,440 min. For testosterone, aliquots were only taken after 1, 15, 30, 60, 120 and 180 min. The reactions were terminated by adding 70 µL ACN. Samples were centrifuged at 10,500 g for 5 min at room temperature, and 40 µL of the supernatants were analysed by RP-HPLC as described in chapter 3.1.1.

In addition, to compare the instability of CPD11 itself at 37°C in a 95% humidified incubator and 5% CO₂, CPD11 was incubated in incubation medium without the addition of hepatocytes at concentrations of 25 µM, 50 µM and 100 µM for a period of 24 h. These samples were also analysed by RP-HPLC.

CPD22 was incubated with rat, monkey and human female cryopreserved hepatocytes at concentrations of 12.5 µM and 25.0 µM and then processed as described previously for CPD11. Samples were taken at time points of 1, 15, 30, 60, 120, 180, 240, 300 and 1,440 min.

Calibration Curves

The concentrations in incubation medium were evaluated by using an external standard method.

CPD11: Calibration standards in incubation medium at concentrations of 6.25, 12.5, 25, 50 and 100 µM were prepared. CPD11 was therefore dissolved in 1% (v/v) DMSO and 99% (v/v) incubation medium and further diluted in medium until reaching the desired concentration.

CPD22: Calibration standards in incubation medium at concentrations of 5, 10, 20 and 40 µM were prepared, by diluting CPD22 in 1% (v/v) DMSO and 99% (v/v) and further dilution in medium until reaching the required concentration.

Testosterone: Calibration standards in incubation medium at concentrations of 12.5, 25, 50, 100 and 200 µM were prepared. As the other compounds, also testosterone was also diluted in 1% (v/v) DMSO and 99% (v/v) and further dilution in medium until reaching the desired concentration.

3.4.3 Data Analysis

The metabolic stability of CPD11 and testosterone was determined over an incubation period of 24 h. The results were expressed in percentage [%] of the test compound remaining after incubation.

$$\% \text{ Remaining} = \frac{\text{Concentration after incubation}}{\text{Concentration before incubation}} \times 100$$

Time point 1440 were excluded in the following calculations. The slope of the linear regression from ln (CPD11 and/or testosterone) vs time curve (= elimination constant - k) was determined and thus in vitro half-life ($t_{1/2}$) could be calculated by following equation.

$$t_{\frac{1}{2}}(\text{min}) = \frac{0.693}{k_{el}}$$

The intrinsic clearance of CPD11 and/or testosterone in various cryopreserved hepatocytes species (CL_{int}) was determined by following equation, expressed in $\mu\text{L}/\text{min}/10^6$ cells.

$$CL_{int} = \frac{V \times k_{el}}{N}$$

V = incubation volume, in this case 1000 μL

k_{el} = elimination constant

N = number of hepatocytes per well (0.5×10^6 cells)

CL_{int} was scaled to in vivo prediction of the intrinsic clearance (scaled CL_{int}) according to Houston et al., 1997: [83]

$$Scaled\ CL_{int}\ (mL/min/kg) = CL_{int} \times \frac{120 \times 10^6\ cells}{g\ liver} \times \frac{v\ g\ liver}{kg\ body\ weight}$$

$v = 40$ for rat, 32 for monkey, 21 for human (g liver/kg body weight). [84]

Prediction of in-vivo hepatic clearance was calculated by using the “well-stirred” model by Houston, 1994: [85]

$$Scaled\ CL_{met}\ (mL/min/kg) = \frac{Scaled\ CL_{int} \times Q_h}{Scaled\ CL_{int} + Q_h}$$

where Q_h is the hepatic blood flow, which is 55, 44 and 21 mL/min/kg for rat, monkey and human, respectively.

Analysis of CPD22 and its metabolite were calculated for time points 0-300 min. 1440 min values were excluded in the calculations. For non-compartmental PK data analysis (NCA), PK Solutions 2.0 was used.

3.5 Preliminary in vivo PK Studies of CPD3 and CPD11

All the animal experiments were approved by the Austrian Animal Welfare Committee (Vote: BMWF-66.009(0263-II/3b/2013)). The administration and blood sampling of CPD3 and CPD11 for mice and rats PK studies were performed at Medical University Vienna, Division of Infectious Diseases and Tropical Medicine at the Department of Medicine I (Vienna, Austria).

3.5.1 Calibration Curves in Plasma

The calibration curve is obtained by plotting the peak area of each concentration against the concentration in the standard stock solutions using a linear regression method, as already described above.

The concentrations in plasma samples were evaluated by using an external standard method. Preparation and analytical assay of calibration samples were performed under identical conditions as plasma sample preparation and analysis of CPD3 and CPD11 of animal samples.

CPD3

Calibration standards in plasma at concentrations of 1.563, 3.125, 6.25, 12.0, 25.0, 50.0 and 100.0 µg/mL were prepared, by diluting the stock solution (1 mg/mL DMSO/PBS 32:68, v/v) with PBS.

CPD11

Refer to section 3.2.3.

3.5.2 CPD3

Male Wistar rats ($n = 3$, mean body weight 650 g) received CPD3, dissolved in 1 mL glycerofomal/PBS 70:30 (v/v), intravenous (iv). Rat 1 received 12.5 mg, rat 2 and rat 3 received 20 mg. Exact blood sampling time points are listed in Table 5.

Table 5: Blood sampling time points of rats after iv CPD3 administration

Rat intravenous CPD3		
rat 1 iv	rat 2 iv	rat 3 iv
time [min]		
3	2	2
7	30	30
42	40	39
43	60	60
156	159	157
171		

Male Wistar rats ($n=3$, mean body weight 650 g) received 20 mg CPD3, dissolved in 1 mL glycerofomal/PBS 70:30 (v/v), intraperitoneal (ip). Exact blood sampling time points are listed in Table 6.

Table 6: Blood sampling time points of rats after ip CPD3 administration

Rat intraperitoneal CPD3		
rat 1 ip	rat 2 ip	rat 3 ip
time [min]		
0	0	0
18	17	20
37	37	39
55	54	55
160	160	161

3.5.3 CPD11

Male Wistar rats (n=3, mean body weight 600 g) received 20 mg CPD11, dissolved in 1 mL glycerofomal/PBS 70:30 (v/v), via iv bolus injection into the caudal vein. Whole blood samples were collected in heparinized tubes. Exact blood sampling time points are listed in Table 7.

Table 7: Blood sampling time points of rats after iv CPD11 administration

Rat intravenous CPD11		
rat 1 iv	rat 2 iv	rat 3 iv
time [min]		
0	0	3
2	2	8
13	11	18
28	25	42
46	45	61
145	143	194

Male Wistar rats (n=3, mean body weight 650 g) also received 20 mg CPD11, dissolved in 1 mL glycerofomal/PBS 70:30 (v/v), ip. Exact blood sampling time points are listed in Table 8.

Table 8: Blood sampling time points of rats after ip CPD11 administration

Rat intraperitoneal CPD11		
rat 1 ip	rat 2 ip	rat 3 ip
time [min]		
16	17	17
33	34	34
52	53	53
159	159	159

Female NMRI Charles River mice (n=24, mean body weight 29 g) received 580 µg (20 mg/kg) CPD11 dissolved in 0.3 mL, 30% Cremophor EL/DMSO and 70% ringer-lactat solution, as iv bolus injection into the caudal vein. At each blood sampling time point three mice were anesthetized with a ketamine-xylazine solution and 500 µL whole blood was drawn by cardiac puncture. Blood samples were collected in heparinized tubes pre dose, 5, 10, 15, 30, 60, 180, 360 min after administration.

Two female NMRI Charles River mice (body weight 27 g) received 750 μ g CPD11 dissolved in 100 μ L 30% dimethylisobutyl alcohol (DMIB) and 70% PBS. Mouse 0 was given CPD11 ip and mouse 1 subcutaneous (sc). Additional two female NMRI Charles River mice (body weight 27 g) received a solution of 750 μ g CPD11 dissolved in 100 μ L 70% polyethylenglycol (PEG400) and 30% PBS. Mouse 2 received CPD11 ip and mouse 3 sc. Exact blood sampling time points are listed in Table 9.

Table 9: Blood sampling time points of mouse after ip and sc CPD11 administration

Mouse intraperitoneal & subcutaneous CPD11			
mouse 0 ip	mouse 2 ip	mouse 1 sc	mouse 3 sc
time [min]			
6	6	26	17
34	26	46	25
61	59	59	60
120	90		

Whole blood samples for all in vivo experiments were collected in heparinized tubes. Plasma samples for PK studies were obtained by centrifuging blood samples for 10 min at 2,500 g and stored frozen at approximately -80°C until HPLC analysis. Sample preparation for PK studies was performed as described previously: 70 μ L plasma was mixed with the 2.5 fold volume of ice-cold ACN (= 175 μ L) and after vortexing for 10 sec and centrifugation at 10,500 g for 5 min, 40 μ L of the clear supernatant was injected into the HPLC.

3.6 In vitro and in vivo Topic Studies of CPD11

Before CPD11 was tested in vivo, in vitro experiments were performed to predict the permeability of CPD11 through the skin, using the patented EpiDerm™ system of MatTek. In addition, to obtain relevant data regarding the different formulations for the in vivo model, same formulations were used for the in vitro model. Furthermore, caffeine was used for validation purposes in this in vitro model.

3.6.1 Calibration Curves of CPD11 and Caffeine in PBS

The concentrations of CPD11 and caffeine were evaluated by using an external standard method. Calibration standards in PBS at concentrations of 1.25, 2.5, 5, 10 and 20 µg/mL were prepared, by diluting the stock solution (1.0 mg/mL DMSO/PBS 32:68, v/v) with PBS until reaching the required concentration. CPD11 was assayed as described above.

For caffeine an isocratic HPLC method was utilized. HPLC analyses were also performed on the same VWR® Chromaster system (Figure 4). The mobile phase consisted of aqua bidest. and ACN 75:25 (v/v). Detection was performed at 272 nm and flow rate was set on 0.75 mL/min. Analysis time was 10 min and the retention time of caffeine was 3.2 min.

3.6.2 LOQ & LOD

Refer to section 3.2.3.

3.6.3 EpiDerm™ in vitro Model

Table 10 shows the quantity of compound, solvent and ultrabase used for the preparation of the different formulations.

The mixing of the solved compound with ultrabase for 10 min was performed on 48°C water bath. After cooling down to room temperature, the formulations were stored, protecting from light, until further usage.

Table 10: Preparation set up of different formulations for the EpiDerm™ in vitro model

Description	Compound	Solvent 1	Solvent 2	Ultrabase
Myristyl alcohol 15 % ultrabase	————	750 mg myristyl alcohol	————	4250 mg
DMSO 5 % ultrabase	————	50 mg DMSO	————	950 mg
CPD11 1 % myristyl alcohol 15 % ultrabase	CPD11 49.7 mg	759 mg myristyl alcohol	————	4200 mg
CPD11 1 % DMSO 2.5 % ultrabase	CPD11 49.9 mg	126 mg DMSO	————	4800 mg
CPD11 1 % DMSO 5.0 % ultrabase	CPD11 49.8 mg	254 mg DMSO	————	4700 mg
CPD11 0.01 % DMSO 0.5 % PBS	CPD11 1 mg	9 mL PBS	1 mL DMSO	————
Caffeine 0.6 % PBS DMSO 5 % ultrabase	Caffeine 50 mg	2.5 mL PBS	250 mg DMSO	4700 mg
Caffeine 0.6 % PBS myristyl alcohol 5 % ultrabase	Caffeine 50 mg	2.5 mL PBS	750 mg myristyl alcohol	4200 mg
Caffeine 1 % PBS DMSO 2.5 %	Caffeine 50 mg	4826 µL PBS	124 µL DMSO	————
Caffeine 1 % PBS DMSO 0.5 %	Caffeine 25 mg	2463 µL PBS	12 µL DMSO	————

The specific name of the model used for this in vitro skin model investigations, is EPI 100 FIX. The device itself consists of two teflon rings which are fixed together by screws. The cultivated skin layer is inserted between the two teflon rings (Figure 12). In the inner annulus of the EPI 100 FIX, the respective donor formulation is applied on the cultivated skin.



Figure 12: EpiDerm™ skin model devices [86]

To create sterile conditions all the procedures were conducted under the laminar air flow. Solely, the donor formulation preparation could not be performed under the laminar air flow.

Workflow [86]

1. Remove the skin from the agarose medium by placing it into 2 mL assay medium.
2. Incubate for 24 h (37°C, \pm 1% CO₂, 95% room humidity).
3. Fix incubated skin into the EPI 100 FIX and transfer into the receiver medium (= 5 mL PBS in each six well culture plate).

4. Apply the 0.5 mL of the donor formulations into the inner annulus of the EPI 100 FIX. The concentration ratio of donor/receiver amounts usually 1:1000.
5. At time point X (X = 1 h, 2 h, 3 h, 4 h, 6 h) the apparatus with the skin is removed into the next well of the six well culture plate. The plate should be kept in the incubator and should only be taken out during sampling.
6. At different time points 2.5 mL of the receiver medium is taken and the volume is minimized by Vac-speed to 300 μ L.

40 μ L of the minimized receiver medium was injected into the HPLC. Solely for the CPD11 0.01% solution 100 μ L was injected, in order to compare the permeation results with the other CPD11 investigations, the peak was divided by factor of 2.5.

Figure 13 illustrates the permeability configuration utilizing the EpiDerm™ skin model in the well.

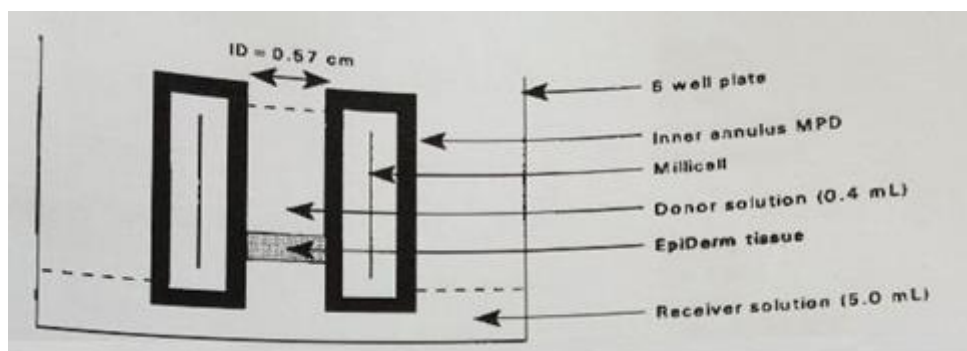


Figure 13: Permeability configuration utilizing EpiDerm™ tissue model [86]

Table 11 shows the experimental setup of the EpiDerm™ model for CPD11 and caffeine in different compound concentrations and solvents. The compounds occur either in form of a solution or in a solid form in ultrabase. 30 pieces of skin were processed. Skin number 1 and 2 are blank samples, whereas no compound was applied. R1 to R5 indicate the number of replicates. LT (long term) refers to 5 samples taken 1 h, 2 h, 3 h, 4 h, 6 h and if possible also 24 h after incubation from the same sample. 6 h means that only one sample was taken 6 h after the incubation.

To stimulate the permeability of CPD11 on lesions, skin number 28, 29 and 30 were pierced with a needle and afterwards CPD11 (0.01%) was applied on the perforated skin; samples

were taken after 1 h, 2 h, 3 h, 4 h and 6 h. To depict the permeation of CPD11 in ointment formulations, skin number 3 and 7 were perforated after the first test run and later the same formulation which was applied in the first test run was reapplied once again and samples were taken after 1 h, 2 h, 3 h, 4 h and 6 h.

Table 11: Experimental setup of in vitro EpiDerm™ model

Skin No.	Compound	Solvent	Base	Comments
1	blank sample	Myristyl alcohol (15 %)	Ultrabase	LT
2	blank sample	DMSO (5 %)	Ultrabase	LT
3	CPD11 (1 %)	DMSO (2.5 %)	Ultrabase	LT, R1
4	CPD11 (1 %)	DMSO (2.5 %)	Ultrabase	LT, R2
5	CPD11 (1 %)	DMSO (2.5 %)	Ultrabase	LT, R3
6	CPD11 (1 %)	DMSO (2.5 %)	Ultrabase	6 h
7	CPD11 (1 %)	DMSO (5 %)	Ultrabase	LT, R1
8	CPD11 (1 %)	DMSO (5 %)	Ultrabase	LT, R2
9	CPD11 (1 %)	DMSO (5 %)	Ultrabase	LT, R3
10	CPD11 (1 %)	DMSO (5 %)	Ultrabase	6 h
11	CPD11 (1 %)	Myristyl alcohol (15 %)	Ultrabase	LT, R1
12	CPD11 (1 %)	Myristyl alcohol (15 %)	Ultrabase	LT, R2
13	CPD11 (1 %)	Myristyl alcohol (15 %)	Ultrabase	LT, R3
14	CPD11 (1 %)	Myristyl alcohol (15 %)	Ultrabase	6 h
15	CPD11 (0.01 %)	PBS & DMSO (0.5 %)	Solution	LT, R1
16	CPD11 (0.01 %)	PBS & DMSO (0.5 %)	Solution	LT, R2
17	CPD11 (0.01 %)	PBS & DMSO (0.5 %)	Solution	LT, R3
18	CPD11 (0.01 %)	PBS & DMSO (0.5 %)	Solution	LT, R4
19	CPD11 (0.01 %)	PBS & DMSO (0.5 %)	Solution	LT, R5
20	Caffeine (1 %)	PBS & DMSO (2.5 %)	Solution	LT, R1
21	Caffeine (1 %)	PBS & DMSO (2.5 %)	Solution	LT, R2
22	Caffeine (0.6 %)	PBS & DMSO (5 %)	Ultrabase	LT, R1
23	Caffeine (0.6 %)	PBS & DMSO (5 %)	Ultrabase	LT, R2
24	Caffeine (0.6 %)	PBS & Myristyl alcohol (15 %)	Ultrabase	LT, R1
25	Caffeine (0.6 %)	PBS & Myristyl alcohol (15 %)	Ultrabase	LT, R2
26	Caffeine (1 %)	PBS & DMSO (0.5 %)	Solution	LT
27	Caffeine (3 %)	PBS & DMSO (0.5 %)	Solution	LT
28	CPD11 (0.01 %)	PBS & DMSO (0.5 %)	Solution	LT, injured skin R1
29	CPD11 (0.01 %)	PBS & DMSO (0.5 %)	Solution	LT, injured skin R2
30	CPD11 (0.01 %)	PBS & DMSO (0.5 %)	Solution	LT, injured skin R3

3.6.4 In vivo Model

The topical applications were performed in the General Hospital of Vienna (AKH Wien) and the experiments were carried out on guinea pigs. The hair of the animals was removed over an area of 8 x 5 cm² and different topical formulations were extensively applied. Details of the formulations are listed in Table 12.

Table 12: Experimental setup of in vivo guinea pigs model with CPD11

Animal No.	Preperation	Solvent	Base	volume [mL]
1	1 % CPD11 cream	15 % myristyl alcohol	Vaseline	50
2	1 % CPD11 cream	15 % palmityl alcohol	Vaseline	50
3	1 % CPD11 cream	2% DMSO	Ultrabase	50
4	negative control cream	15 % myristyl alcohol	Vaseline	50
5	negative control cream	15 % palmityl alcohol	Vaseline	50
6	negative control	na	na	na

na = not applicable

Guinea pigs 1-3 were treated with CPD11 and guinea pigs 4 and 5 with placebo, whereas guinea pig 6 served as negative control receiving neither CPD11 cream nor a placebo cream. After 2 h exposure time, whole blood samples were collected in heparinized tubes. During this procedure the animals were narcotized with a combination of midazolam, fentanyl, medetomidine and ketamine. Plasma samples were obtained by centrifuging blood samples for 10 min at 2,500 g and stored frozen at approximately -80°C until HPLC analysis. For HPLC-analysis the samples were sent to the Division of Clinical Pharmacy and Diagnostics.

For sample preparation 70 µL plasma was mixed with the 2.5 fold volume of ice-cold ACN (= 175 µL) and after vortexing for 10 sec and centrifugation at 10,500 g for 5 min, 40 µL of the clear supernatant was injected into the HPLC.

3.7 Software

For the data evaluation and preparation of this thesis, following software programs were utilized:

- Microsoft® Office Word 2010
- Microsoft® Office Excel 2010
- Microsoft® Office Power Point 2010
- Microsoft® Office Paint 2010
- GraphPad Prism® 6.0, GraphPad Software, La Jolla California, USA
- Phoenix WinNonlin® 6.1, Certara Inc., Princeton, USA
- Kinetica Software Version 5.1, Alfasoft Limited, Luton, UK
- PK Solutions 2.0, (Summit Research Services) Ashland, Ohio, USA
- ADMET-Predictor 7.2 computer software, Simulations Plus Inc., California, USA

4 Results

4.1 Validation

4.1.1 Optimization of Sample Preparation Method

After performing a UV/VIS scan of CPD11 (5.0 µg/mL in ACN) the optimum detection wavelength of 270 nm (λ_{max}) was verified.

Due to the chemical inhomogeneity, the CPD compounds were partly water soluble (CPD3 and CPD4) but mostly water insoluble and showed basic, acid and neutral properties. Especially lead compound CPD11 was poorly water-soluble. Therefore, the use of a gradient elution on a Zorbax Eclipse XDB-C8 column, 250 x 4.6 mm, 5 µm (Agilent) was the method of choice. This column shows optimum separation of such acidic, basic and neutral molecules. Peak of interests showed high sharpness and symmetry (using peak width parameters obtained 10% from baseline according to the guidelines of the European Pharmacopeia). Other tested HPLC analytical columns were Symmetry C8 column, 100 x 4.6 mm, 3.5 µm (Waters) and a C8 column, 150 x 4.6 mm (ACE), but the separation results were unsatisfactory (data not shown).

The optimum HPLC conditions were achieved by using a mobile phase consisting of solvent A (99.9% aqua bidest. and 0.1% acetic acid) and solvent B (99.9% ACN and 0.1 % acetic acid) on a Zorbax Eclipse XDB-C8 column, 250 x 4.6 mm ID, 5 µm, in elution gradient mode.

The chromatographic profiles of all eight compounds in a concentration of 10.0 µg/mL diluted in ACN are shown in Figure 14. Differences in peak areas may be based on the measurement wavelength and the individual extinction coefficient.

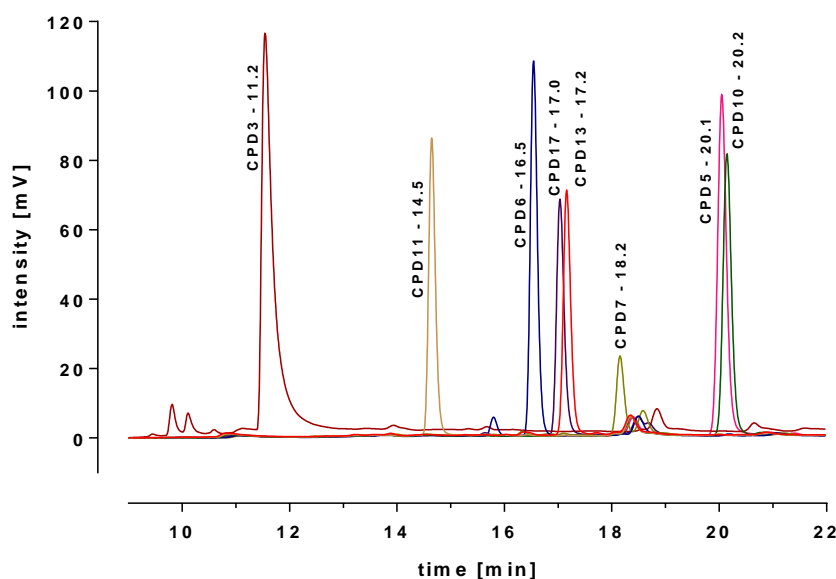


Figure 14: HPLC chromatograms of some CPD compounds diluted in ACN with a concentration of 10 $\mu\text{g/mL}$

As seen in Figure 15, CPD11 eluted after 14.5 min as a sharp and uniform peak, almost independent of the type of the biological matrix. Comparison of blank human plasma, bovine liver tissue samples and hepatocytes incubations of the same matrix spiked with CPD11 revealed no peak interferences from matrix components within the elution time frame of the analyte (Figure 15). For better resolution, the chromatograms were truncated after 17 min; the gradient profile is not visible.

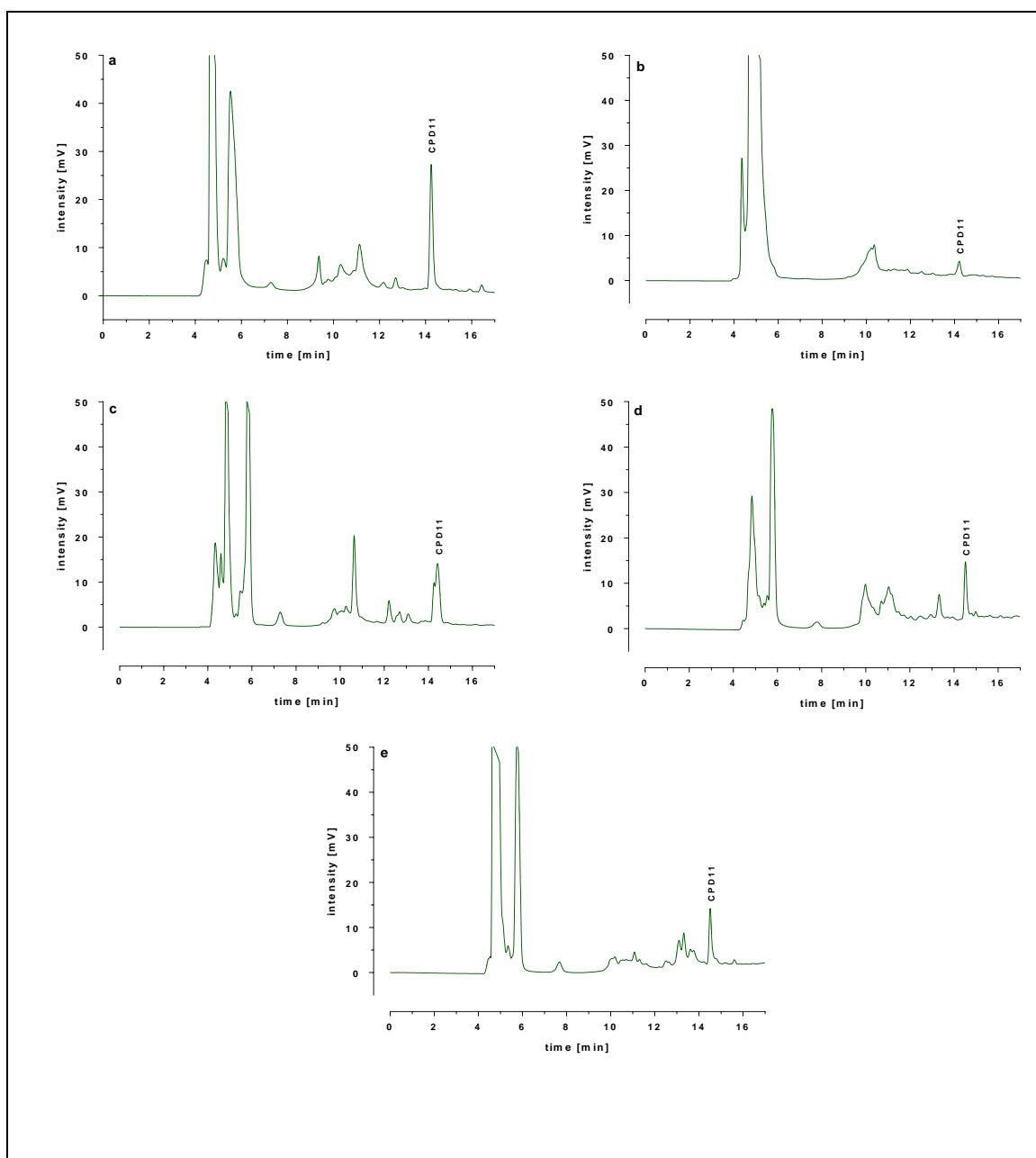


Figure 15: a-e Representative HPLC chromatograms of CPD11 in, human pooled plasma 5.0 µg/mL (a), bovine liver tissue 5.0 µg/mL (b), cryopreserved human hepatocytes 25µM (c), PK mouse plasma 10 min after iv bolus injection (d) and PK rat plasma 10 min after iv bolus injection (e).

4.1.2 Validation Results

Linearity and Sensitivity

Linear regression analysis were performed by plotting the peak area against the concentration of CPD11, revealing the linearity of the assay over the range from 0.1 to 10.0 µg/mL (correlation quality (r^2) plasma = 0.996; r^2_{buffer} = 0.998). The LOQ was found to be

0.06 $\mu\text{g/mL}$ in PBS (Figure 16) and 0.07 $\mu\text{g/mL}$ in pooled human plasma. LOD was found to be 0.03 $\mu\text{g/mL}$ in PBS (Figure 16), and 0.035 $\mu\text{g/mL}$ in pooled human plasma.

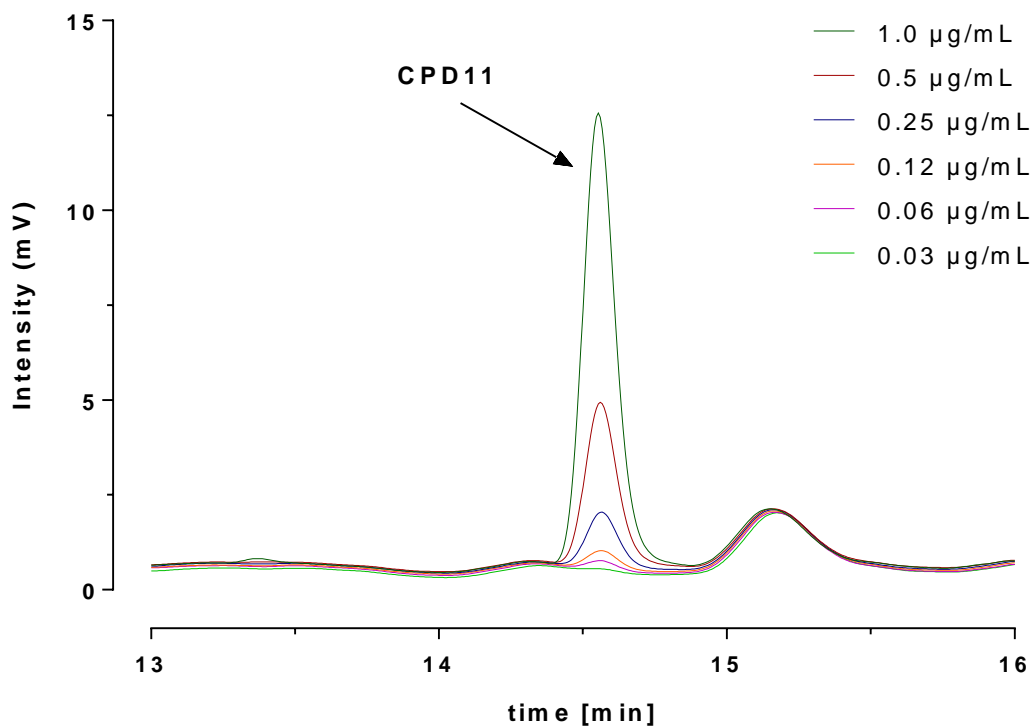


Figure 16: LOQ and LOD of CPD11 in PBS

The accuracy and precision in both PBS and plasma were assessed by analysing Q (Q 1, Q 2 and Q 3) samples at low, medium and high concentrations. With regard to the PBS, the CV ranged from 3.2 to 8.7% and the bias from -4.0 to +4.1%, as seen in Table 13.

Table 13: Intra- and inter-day coefficients of variation (% CV), bias [%] and recovery [%] for the determination of CPD11 in PBS (n = 6)

	Conc. (µg/mL)		± SD	% Recovery	% Bias	% CV
	Spiked	Found mean				
Day 1						
1 st run						
Q 1	0.1	0.096	0.008	96.0	-4.0	8.3
Q 2	1.0	0.964	0.073	96.4	-3.6	7.6
Q 3	10	10.04	0.317	100.4	0.4	3.2
2 nd run						
Q 1	0.1	0.101	0.006	101.0	1.0	5.9
Q 2	1.0	0.972	0.085	97.2	-2.8	8.7
Q 3	10	10.063	0.561	100.6	0.6	5.6
Day 7						
Q 1	0.1	0.097	0.004	97.0	-3.0	4.1
Q 2	1.0	1.039	0.054	103.9	3.9	5.2
Q 3	10	10.408	0.567	104.1	4.1	5.4

Accuracy and Precision

An assessment of accuracy and precision in plasma yielded a CV ranging from 2.0 to 9.1% and bias values within $\pm 7\%$, as summarized in Table 14.

Table 14: Intra- and inter-day coefficients of variation (% CV), bias [%] and recovery [%] for the determination of CPD11 in pooled human plasma (n = 6)

	Conc. (µg/mL)		± SD	% Recovery	% Bias	% CV
	Spiked	Found mean				
Day 1						
1 st run						
Q 1	0.1	0.104	0.005	104.0	4.0	4.8
Q 2	1.0	0.94	0.051	94.0	-6.0	5.4
Q 3	10	9.35	0.599	93.5	-6.5	6.4
2 nd run						
Q 1	0.1	0.095	0.006	95.0	-5.0	6.3
Q 2	1.0	1.031	0.049	103.1	3.1	4.8
Q 3	10	9.732	0.368	97.3	6.7	3.8
Day 7						
Q 1	0.1	0.101	0.003	101.0	1.0	3.0
Q 2	1.0	1.008	0.020	100.8	0.8	2.0
Q 3	10	9.895	0.904	99.0	-1.0	9.1

Recovery

Excellent recoveries in plasma were obtained; the recovery values ranged from 93.5 to 104%. By contrast, CPD11 extracted from crude liver yielded recoveries between 30 and 34%.

Stability

As stated above, freshly prepared solutions were used for all experiments; the short-term stability was anticipated to be 24 h and the long-term stability to be 72 h. Nonetheless, the long-term stability of the standard stock solution was evaluated.

After evaluation of the short-term stability in PBS and plasma, CPD11 was found to be stable in PBS. Whereas storage in human plasma led to a loss of approximately 40% within 72 h (see Table 15). Thus, plasma samples should be analysed within one day to avoid compound degradation, which would lead to inaccurate results.

Table 15: Short-term (24 h) and long-term (72 h) stability of CPD11 in PBS and plasma

Medium	Time [h]	Conc. ($\mu\text{g/mL}$)		% Recovery
		Spiked	Found	
PBS	24	5.00	5.05	101.0
	72	0.50	0.50	100.0
	72	5.00	5.16	103.2
Plasma	24	5.00	3.03	60.0
	72	0.50	0.19	38.0
	72	5.00	1.88	37.6

Investigations of long-term stability, stability on ice and stability after several freeze-thaw cycles in PBS showed identical results, as listed in Table 15.

By contrast, stability on ice and freeze-thaw cycle stability tests carried out at two different concentration levels in plasma yielded a significant decrease of approximately 63%. Thus, long-term stability experiments in plasma exceeding 72 h were not performed due to the substantial loss of CPD11 within one week.

The solution of CPD11 (5.0 $\mu\text{g/mL}$ dissolved in DMSO/PBS 32:68, v/v) remained stable for 34 days when stored at +4°C. When the same CPD11 solution was exposed to daylight at room temperature (24°C), the compound degraded with a half-life of 15 days.

Calibration Curve

The calibration curve of CPD 11 in plasma was linear over the range of 0.625-20.0 $\mu\text{g/mL}$ (Figure 17), prepared by plotting peak area against sample concentration, with a correlation coefficient >0.999. The slope was 7.417 ± 0.1096 , as shown in Table 16.

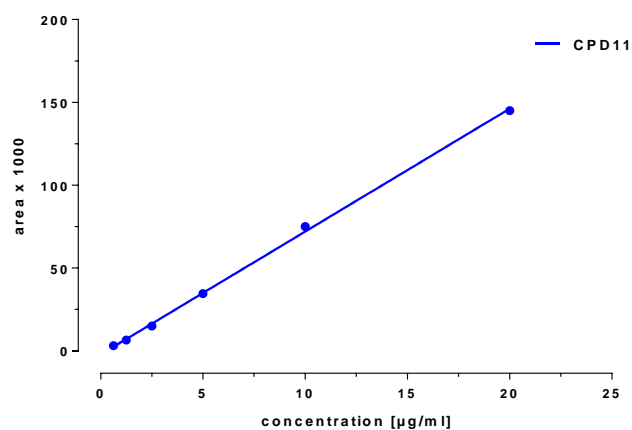


Figure 17: Calibration curve of CPD11 in plasma

Table 16: Rgression parameters of the calibration curve of CPD11 in plasma

CPD11	
Best-fit values	
Slope	7.417 ± 0.1096
Y-intercept when X=0.0	-2.154 ± 1.033
X-intercept when Y=0.0	0.2904
1/slope	0.1348
95% Confidence Intervals	
Slope	7.113 to 7.721
Y-intercept when X=0.0	-5.022 to 0.7137
X-intercept when Y=0.0	-0.09906 to 0.6588
Goodness of Fit	
R square	0.9991
Sy.x	1.817
Is slope significantly non-zero?	
F	4581
DFn, DFd	1.000, 4.000
P value	< 0.0001
Deviation from zero?	Significant
Data	
Number of X values	6
Maximum number of Y replicates	1
Total number of values	6
Number of missing values	0
Equation	$Y = 7.417 * X - 2.154$

4.1.3 Comparison of CPD11 with seven other SeaLife Compounds

As already mentioned seven other SeaLife compounds were partially validated in these investigations. For in vitro studies the current method can be used for each of these SeaLife and compounds (see in Figure 1) and also for related compounds. Detailed information regarding LOQ, LOD, recovery and HPLC parameters are listed in Table 17.

Table 17: Summary of the characteristics of CPD11 related test-compounds and HPLC parameters

	CPD 3	CPD5	CPD6	CPD7	CPD10	CPD13	CPD17
Molecular weight	395	268	282	404	382	703	531
k'	1.02	2.63	1.98	2.34	2.80	2.30	2.22
N	39490	66810	28926	40341	33172	76456	80319
LOQ (µg/mL)	0.608	0.878	0.180	0.182	0.206	0.429	0.377
LOD (µg/mL)	0.304	0.434	0.090	0.092	0.103	0.211	0.197
Recovery (%)	71	89	74	48	52	46	62

k' capacity factor, calculated by $k' = (t_R/t_0) - 1$, *N* number of theoretical plate

4.2 Binding and Distribution Experiments

Thirty-one SeaLife compounds with antibacterial activity and four established drugs (erlotinib, capecitabine, doxorubicin, linezolid) with different physicochemical and pharmacological properties were investigated using the TRANSIL test system. Table 18 shows these 35 compounds along with their molecular mass and pKa, pKb and logP values predicted by the ADMET Predictor software. Furthermore, the fPPB [%] parameters using the TRANSIL system and the ADMET Predictor were compared (Table 18). The SeaLife drugs showed a wide range of physicochemical characteristics, with molecular mass ranging from 240.3 to 702.7 g/mol and lipophilicity, calculated as logP, ranging from 1.0 to 4.2. Nine SeaLife compounds were calculated to have neither a pKa nor a pKb. These neutral compounds have neither acidic nor basic centres and therefore lack ionizable groups.

Table 18: List of SeaLife compounds and marketed drugs. Physiochemical parameters and f_u were predicted using the ADMET Predictor. fPPB parameters determined from TRANSIL^{XL} results (n = 6) are shown as the means with the SD.

Drug	Molecular Mass g/mol	ADMET Predictor					TRANSIL fPPB±SD %
		pKa	pKb	logP	f_u PPB %	fPPB * %	
CPD1	240.3	8.47	None	3.1	9.8	90.2	93.9 ± 0.968
CPD2	242.3	8.50	None	3.3	8.0	92.0	96.4 ± 0.246
CPD3	395.5	None	6.92	3.3	6.4	93.6	95.2 ± 0.537
CPD4	271.4	2.22	8.06	1.0	24.7	75.3	99.1 ± 0.041
CPD5	268.3	7.77	None	3.3	5.5	94.5	88.2 ± 1.646
CPD6	282.3	None	None	3.0	11.1	88.9	96.1 ± 0.292
CPD7	404.4	None	None	3.4	3.6	96.4	98.1 ± 0.056
CPD8	390.3	None	None	3.3	4.5	95.6	94.0 ± 0.196
CPD9	420.4	None	None	3.4	3.9	96.1	94.6 ± 0.367
CPD10	382.4	None	None	3.8	4.5	95.5	98.4 ± 0.138
CPD11	395.4	None	None	1.9	16.6	83.4	88.2 ± 0.876
CPD12	270.3	7.80	None	3.3	4.8	95.2	99.1 ± 0.061
CPD13	702.7	None	None	3.4	7.1	92.9	99.0 ± 0.080
CPD14	418.4	None	None	3.3	4.3	95.7	97.2 ± 0.191
CPD15	521.6	None	5.76	1.3	23.2	76.9	87.2 ± 3.024
CPD16	507.6	None	7.44; 4.14	2.2	17.8	82.2	59.2 ± 4.074
CPD17	530.6	None	4.50	3.3	5.2	94.8	97.5 ± 0.169
CPD18	500.6	None	4.12	3.3	4.9	95.1	96.3 ± 0.425
CPD19	552.6	None	6.14	4.2	1.4	98.6	95.2 ± 0.225
CPD20	502.5	None	6.46	3.8	3.3	96.7	99.2 ± 0.041
CPD21	514.6	None	6.56	3.6	4.2	95.8	98.7 ± 0.099
CPD22	439.5	10.09	None	2.8	5.1	94.9	95.9 ± 0.186
CPD23	274.3	7.99	None	2.4	11.6	88.4	99.8 ± 0.040
CPD24	290.3	8.09; 4.21	None	1.8	11.1	88.9	99.8 ± 0.058
CPD25	401.4	None	None	1.4	22.8	77.2	97.1 ± 0.128
CPD26	558.6	None	6.18	3.5	2.4	97.6	84.3 ± 1.800
CPD27	nc	nc	nc	nc	nc	nc	97.5 ± 0.354
CPD28	nc	nc	nc	nc	nc	nc	96.6 ± 0.196
CPD29	nc	nc	nc	nc	nc	nc	99.5 ± 0.049
CPD30	nc	nc	nc	nc	nc	nc	95.9 ± 0.413
CPD31	nc	nc	nc	nc	nc	nc	92.3 ± 0.895
Capecitabine	359.4	9.73	0.11	1.3	23.9	76.1	66.1 ± 9.527
Doxorubicin	543.5	9.50; 6.77	8.43	0.5	22.1	77.9	66.3 ± 3.978
Erlotinib	393.4	None	4.46; -0.18; -1.60	3.1	4.6	95.4	93.9 ± 0.885
Linezolid	337.4	None	4.1	0.9	30.0	70.0	44.9 ± 3.239

*calculated from f_u PPB parameters of ADMET Predictor; not calculated (nc)

Due to pending patent matters, data calculated for CPD27 to CPD31 with the ADMET Predictor could not be approved for publication. The design of the TRANSIL^{XL} fPPB [%] method was such that one drug was incubated in six wells, with an increasing amount of plasma protein immobilized on silica beads, enabling a 6-fold determination of PPB. The values of fPPB [%] from both methods are shown in Table 18 and range from 59.2 to 99.8% for the TRANSIL^{XL} system and 75.3 to 98.6% for the ADMET Predictor. Because the ADMET Predictor was only able to predict the f_u PPB [%] parameter, the values for fPPB [%] were calculated by deducting the f_u PPB [%] from 100%. Generally, the SeaLife compounds showed high PPB values. Uncharacteristically, CPD16 in the TRANSIL^{XL} system and CPD4, CPD15 and CPD25 in the ADMET Predictor showed lower PPB values. Overall, both methods yielded more or less the same PPB results, with variation from 1 to 15%, but only when excluding compounds CPD4, CPD16 and CPD25. The SD of fPPB [%], as predicted with the TRANSIL^{XL} system, is also presented in Table 18.

Table 19 shows the mean values of fAGP [%] and fHSA [%] together with SD values and the f_u AGP [%] and f_u HSA [%] parameters. The fHSA [%] values ranged from 82.5 to 99.8% and the fAGP [%] values from < 1.4 to 96.5%. This finding confirms the results characterized above, which showed an overall high fPPB [%]. Although the fHSA [%] parameters for the 31 SeaLife compounds showed more or less the same range, the fAGP [%] values covered a wide range and were up to 68-fold higher than the obtained values. When comparing the fHSA [%] and fAGP [%] results, a higher binding affinity of the compounds for HSA than AGP can be predicted. This phenomenon can be seen quite clearly for the compounds CPD1, CPD4, CPD15, CPD24, CPD26 and CPD30. The f_u HSA [%] values ranged from 0.2 to 12.0% and the f_u AGP [%] values from 0.2 to 9.9%, showing very similar and partly identical results (CPD5, CPD6, CPD8, CPD9, CPD11-CPD14, CPD16-CPD18, CPD20-CPD25 and CPD28). When comparing fPPB [%] in Table 18 with the fHSA [%] parameters in Table 19, almost equal results can be seen. Moreover, if the fraction bound [%] parameters obtained from CPD5 and CPD16 are neglected, the difference seems not to exceed 6.9% because the PPB kit consists of HSA and AGP in a physiological ratio of 24:1.

Table 19: List of SeaLife compounds and marketed drugs with the f and f_u parameters for HSA and AGP predicted with the TRANSIL^{XL} assay ($n = 6$). TRANSIL^{XL} results are shown as the means with the SD.

Drug	TRANSIL			
	$f_{\text{HSA}} \pm \text{SD}$ %	$f_u \text{HSA}$ %	$f_{\text{AGP}} \pm \text{SD}$ %	$f_u \text{AGP}$ %
CPD1	92.8 \pm 9.758	7.2	4.1 \pm 2.717	9.9
CPD2	93.5 \pm 0.781	6.4	28.7 \pm 5.281	7.6
CPD3	89.0 \pm 2.824	10.3	44.4 \pm 6.728	9.3
CPD4	97.5 \pm 0.279	2.4	< 1.4 \pm 5.203	3.0
CPD5	99.7 \pm 0.124	0.3	16.3 \pm 6.906	0.3
CPD6	97.1 \pm 0.495	3.0	22.8 \pm 2.768	3.0
CPD7	98.5 \pm 0.230	1.4	75.2 \pm 0.623	1.4
CPD8	91.7 \pm 0.539	8.1	21.5 \pm 2.656	8.1
CPD9	88.8 \pm 1.005	6.9	84.6 \pm 2.017	6.9
CPD10	97.5 \pm 0.327	2.2	83.1 \pm 12.707	0.7
CPD11	90.6 \pm 1.964	9.2	18.6 \pm 9.092	9.2
CPD12	98.5 \pm 4.531	1.5	44.9 \pm 1.686	1.5
CPD13	99.8 \pm 0.139	0.2	38.8 \pm 4.961	0.2
CPD14	94.4 \pm 0.206	3.9	86.2 \pm 18.197	3.9
CPD15	94.2 \pm 3.875	5.6	7.2 \pm 15.675	5.8
CPD16	95.7 \pm 1.589	4.3	23.9 \pm 5.535	4.3
CPD17	97.9 \pm 0.119	2.0	59.6 \pm 3.597	2.0
CPD18	92.0 \pm 0.861	7.4	50.4 \pm 5.165	7.4
CPD19	93.2 \pm 0.158	5.7	49.2 \pm 4.859	8.5
CPD20	98.8 \pm 0.379	0.9	96.5 \pm 0.711	0.9
CPD21	96.8 \pm 0.263	2.7	84.5 \pm 0.749	2.7
CPD22	92.8 \pm 0.265	5.9	75.0 \pm 1.324	5.9
CPD23	99.5 \pm 0.022	0.5	29.2 \pm 5.319	0.5
CPD24	99.0 \pm 0.166	1.0	7.8 \pm 4.621	1.0
CPD25	96.2 \pm 0.251	3.8	13.3 \pm 2.838	3.8
CPD26	82.5 \pm 0.189	12.0	< 1.4 \pm 10.182	5.1
CPD27	94.3 \pm 0.726	3.0	13.3 \pm 2.838	3.8
CPD28	89.7 \pm 0.624	4.2	93.5 \pm 1.137	4.2
CPD29	99.5 \pm 0.356	0.5	84.1 \pm 3.401	5.9
CPD30	91.5 \pm 0.908	5.9	7.0 \pm 0.909	0.5
CPD31	97.0 \pm 0.354	2.9	36.7 \pm 2.977	2.8
Capecitabine	42.0 \pm 4.490	< 57.6	< 1.4 \pm 4.871	57.6
Doxorubicin	61.2 \pm 3.673	38.1	4.5 \pm 9.172	38.2
Erlotinib	91.5 \pm 0.215	8.1	40.2 \pm 2.208	8.5
Linezolid	12.9 \pm 1.575	< 86.1	< 1.4 \pm 2.920	86.1

Furthermore, as seen in Table 20, the Vd parameters of the SeaLife compounds with the TRANSIL^{XL} method predicted and compared the collected data with the calculations obtained from the ADMET Predictor software.

Overall, the tested drugs showed Vd values ranging from 0.203 to 6.698 L/kg when analysed with the TRANSIL^{XL} assay and values ranging from 0.129 to 6.052 L/kg when calculated with ADMET Predictor. It was not possible to obtain intestinal or microsomal results for CPD26 due to the chemical instability of the compound. The mean value of Vd was predicted by TRANSIL^{XL} to be 1.866 L/kg and by the ADMET Predictor to be 1.999 L/kg. Although the two methods show similar Vds, the values vary between the systems for some drugs, e.g., for CPD13, approximately an 8-fold higher Vd is predicted by the TRANSIL^{XL} method when compared with the ADMET Predictor (0.601 vs. 4.745).

P_{int} values ranged widely from 1.6 to 23.2*10⁻⁶ cm/sec, with a mean value of 11.0*10⁻⁶ cm/sec. This value would imply that the SeaLife compounds have a high permeability coefficient because the majority of the compounds possess a P_{int} over 10.0*10⁻⁶ cm/sec. Moreover, because many SeaLife compounds show lipophilic properties, a high P_{int} value might also reflect good bioavailability of the drug when given orally. The logMA_{int} ranged from 1.58 to 4.27, with a mean rate of 2.85, which implies an overall high affinity of the drugs to phosphatidylcholine membranes.

CPD17, CPD19 and CPD28 showed the highest affinity to intestinal membranes, whereas CPD24, CPD25 and CPD29 showed the lowest affinity. The f_u [%] parameter in the intestinal assay was predicted to be between 0.3 and 12.2%.

The logMA_{micro} parameter ranged from 1.46 to 3.90, with a mean value rate of 2.88. The majority of the compounds showed a low logMA_{micro} rate, which not only could reduce the concentration of free drug available to be metabolized by CYP (cytochrome P450) enzymes but could also decrease the amount available to inhibit these enzymes. Only the unbound fraction is available for metabolic conversion. For instance, as shown in Table 3, CPD24 shows a logMA_{micro} of 1.46, which is clearly lower than the logMA_{micro} of 3.90 predicted for CPD13. Therefore, it can be assumed that CPD13 will be metabolized to a greater extent than CPD24. In addition to the logMA_{micro} parameter, microsomal f_u [%] values were predicted with the microsomal absorption kit. The f_u [%] results ranged from 30.2 to 99.2%, with a mean value of 73.8%. The majority of the SeaLife compounds were predicted to have

high f_u [%] properties; only CPD13, CPD23, CPD27, CPD28 and CPD31 appeared to have f_u [%] values below 36%.

Table 20: List of SeaLife compounds and marketed drugs with their Vd (L/kg), logMA, f_u [%] and P_{int} [cm/sec] parameters predicted with the ADMET Predictor and in TRANSIL^{XL} assays. TRANSIL^{XL} results (n = 6) are shown as the means with the SD.

Drug	ADMET Predictor	TRANSIL Intestinal				TRANSIL Microsomal	
	Vd L/kg	Vd L/kg	logMA \pm SD	P_{int} [10 ⁻⁶ cm/sec]	f_u %	logMA \pm SD	f_u %
CPD1	1.418	1.554	2.69 \pm 0.21	22.8	7.2	2.41 \pm 0.20	93.1
CPD2	2.872	0.849	2.22 \pm 0.14	16.6	6.4	2.13 \pm 0.08	92.1
CPD3	2.602	3.235	3.18 \pm 0.27	14.0	10.3	3.16 \pm 0.05	70.3
CPD4	0.794	1.748	3.24 \pm 0.07	16.9	1.5	2.51 \pm 0.07	91.4
CPD5	0.832	0.260	2.12 \pm 0.08	11.6	0.3	2.60 \pm 0.08	89.7
CPD6	1.334	1.363	2.84 \pm 0.10	19.6	3.0	2.81 \pm 0.03	84.4
CPD7	1.054	0.675	2.50 \pm 0.18	5.6	1.4	3.02 \pm 0.06	76.6
CPD8	0.906	1.371	2.55 \pm 0.07	7.9	8.1	2.88 \pm 0.04	81.9
CPD9	1.848	1.846	2.84 \pm 0.07	8.6	6.9	2.72 \pm 0.07	86.8
CPD10	1.698	1.543	3.03 \pm 0.03	13.2	2.2	3.03 \pm 0.08	76.5
CPD11	1.090	0.976	2.23 \pm 0.15	4.0	9.2	2.29 \pm 0.06	94.7
CPD12	1.438	3.355	3.16 \pm 0.08	23.2	12.2	3.14 \pm 0.05	71.3
CPD13	4.745	0.601	2.96 \pm 0.15	1.8	0.2	3.90 \pm 0.13	30.2
CPD14	1.201	1.563	2.87 \pm 0.03	9.1	3.9	2.54 \pm 0.07	90.8
CPD15	1.688	1.105	2.53 \pm 0.11	7.8	5.8	2.78 \pm 0.15	85.1
CPD16	3.439	1.174	2.61 \pm 0.56	3.1	4.3	1.49 \pm 0.13	94.0
CPD17	2.029	6.698	4.27 \pm 0.14	15.4	2.0	3.29 \pm 0.07	63.8
CPD18	2.093	1.836	2.82 \pm 0.05	4.9	7.4	3.10 \pm 0.03	73.3
CPD19	2.636	4.235	3.53 \pm 0.03	16.2	6.0	2.41 \pm 0.04	81.3
CPD20	2.633	1.729	3.38 \pm 0.04	10.3	0.9	3.32 \pm 0.05	62.3
CPD21	2.413	2.846	3.50 \pm 0.04	10.1	2.7	2.91 \pm 0.02	80.9
CPD22	0.533	2.626	3.18 \pm 0.02	11.3	5.9	3.13 \pm 0.04	71.7
CPD23	2.310	0.919	3.04 \pm 0.04	22.1	0.5	3.85 \pm 0.16	32.9
CPD24	0.129	0.203	1.58 \pm 0.04	3.7	1.0	1.46 \pm 0.10	99.2
CPD25	2.186	0.396	1.76 \pm 0.06	1.6	3.8	2.30 \pm 0.02	94.5
CPD26	6.052	nc	nc	nc	nc	nc	nc
CPD27	nc	1.937	3.16 \pm 0.10	11.9	2.7	3.85 \pm 0.04	32.5
CPD28	nc	4.363	3.70 \pm 0.06	17.9	4.2	3.88 \pm 0.08	31.1
CPD29	nc	0.241	1.90 \pm 0.09	2.6	0.5	1.98 \pm 0.09	97.3
CPD30	nc	2.142	3.01 \pm 0.21	6.1	5.9	3.58 \pm 0.01	47.8
CPD31	nc	2.600	3.38 \pm 0.08	10.3	2.9	3.79 \pm 0.23	35.9
Capecitabine	0.675	1.416	1.80 \pm 0.22	3.0	57.6	2.21 \pm 0.28	95.5
Doxorubicin	8.780	3.577	2.83 \pm 0.04	3.4	35.3	2.63 \pm 0.05	88.9
Erlotinib	1.036	1.797	2.77 \pm 0.02	8.6	8.1	2.68 \pm 0.10	87.8
Linezolid	0.827	2.991	2.00 \pm 0.20	5.5	86.1	1.36 \pm 0.10	99.3

Moreover, the TRANSIL^{XL} system determines a quality index (QI), which is derived from five independent measurements of data analysis, and a r^2 value is determined from the predicted parameters (data not shown). For all the compounds investigated, in all 5 TRANSIL^{XL} systems, the QI ranged from 7.6 to 9.7 on a scale of 0 to 10 (7 to 10: good data quality; 5 to 7: compromised data quality; and below 5: poor data quality). The r^2 values were approximately 0.99, suggesting a close correlation and excellent assay quality. For the ADMET Predictor, the RMSE (root mean squared error) obtained was 0.33 and the MAE (mean absolute error) was 0.25 for all calculations.

4.3 Cryopreserved Hepatocytes

4.3.1 CPD11

Calibration Curve

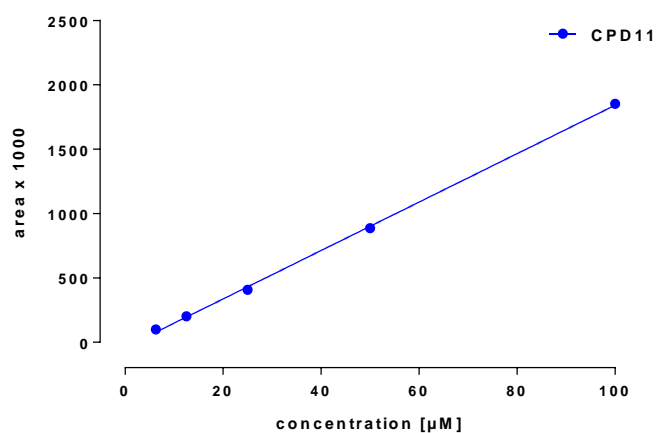


Figure 18: Calibration curve of CPD11 in incubation medium

The calibration curve of CPD11 in incubation medium was linear over the range of 6.25 and 100 μM, prepared by plotting peak area against sample concentration (Figure 18). Detailed information about the regression parameters are listed in Table 21. For calculation of CPD11 concentrations in hepatocytes the formula $x = y/18.81$ was used, whereby 18.81 represents the slope regression line.

Table 21: Regression parameters of the calibration curve of CPD11 in incubation medium

CPD11	
Best-fit values	
Slope	$18,81 \pm 0,2844$
Y-intercept when X=0.0	$-39,49 \pm 14,68$
X-intercept when Y=0.0	2.099
1/slope	0.05317
95% Confidence Intervals	
Slope	17,90 to 19,71
Y-intercept when X=0.0	-86,19 to 7,217
X-intercept when Y=0.0	-0,3981 to 4,427
Goodness of Fit	
R square	0.9993
Sy.x	21.68
Is slope significantly non-zero?	
F	4375
DFn, DFd	1,000, 3,000
P value	< 0,0001
Deviation from zero?	Significant
Data	
Number of X values	5
Maximum number of Y replicates	1
Total number of values	5
Number of missing values	0

Instability of CPD11 in Incubation Medium

To identify the stability of CPD11 in the incubator during a period of 24 h, 25 μM , 50 μM and 100 μM doses were incubated in medium without adding cryopreserved hepatocytes to the experiments. The results [μM] of these negative control experiments in incubation medium are depicted in Table 22. As can be seen in, already 180 min after incubation only 50% of CPD11 was quantifiable in the samples at concentrations of 50 μM and 100 μM . In general, CPD11 was degraded solely in incubation medium and under incubation conditions.

Table 22: Stability of CPD11 in incubation medium

Medium CPD11			
time [min]	Concentration [μM]		
	25 μM	50 μM	100 μM
1	22.65	42.02	89.77
	23.64	42.12	97.53
mean	23.15	42.08	93.65
15	24.94	40.15	80.30
	24.43	40.29	84.62
mean	24.69	40.22	82.46
30	23.73	41.75	72.20
	24.06	43.65	57.62
mean	23.90	42.70	64.91
60	24.46	41.27	89.28
	23.29	38.97	66.51
mean	23.88	40.12	77.90
120	21.46	36.61	60.87
	23.53	39.80	58.79
mean	22.50	38.20	59.83
180	21.74	16.60	41.19
	7.63	26.23	44.22
mean	14.69	21.42	42.70
240	22.75	15.63	53.76
	7.30	27.67	55.50
mean	15.03	21.65	54.63
300	13.90	10.75	50.23
	19.64	30.47	49.62
mean	16.77	20.61	49.92
1440	10.81	24.09	37.84
	na	na	na
mean	10.81	24.09	37.84

na: not applicable (not done)

Metabolic Stability

The results of metabolic stability studies of cryopreserved human male hepatocytes, cryopreserved human female hepatocytes, cryopreserved rat hepatocytes and cryopreserved monkey hepatocytes are shown in the following tables and figures. The metabolic stability assay helps to differentiate metabolic stable compounds from less stable compounds.

- Cryopreserved Human Male Hepatocytes

CPD11 was incubated in cryopreserved human male hepatocytes in incubation medium at concentrations of 5 μ M, 10 μ M, 25 μ M, 50 μ M and 100 μ M. Duplicate incubations were conducted at concentrations of 25 μ M, 50 μ M and 100 μ M. Samples were taken at time points, as listed in Table 23 and Table 24.

Table 23: Metabolic stability of CPD11 in human male hepatocytes [μM]

Human Male Hepatocytes CPD11					
time [min]	Concentration [μM]				
	5 μM	10 μM	25 μM	50 μM	100 μM
1	3.85	8.52	13.23	23.65	49.63
	na	na	13.87	23.39	52.85
mean	na	na	13.55	23.52	51.24
15	3.23	8.04	9.89	21.14	48.97
	na	na	10.69	22.08	45.68
mean	na	na	10.29	21.61	47.33
30	3.18	7.38	10.10	22.52	48.14
	na	na	12.01	20.73	56.61
mean	na	na	11.06	21.63	52.38
60	2.04	6.34	8.81	18.01	42.18
	na	na	8.85	18.60	44.96
mean	na	na	8.83	18.30	43.57
120	1.08	3.81	6.30	20.75	41.51
	na	na	5.67	16.00	38.70
mean	na	na	5.98	18.38	40.10
180	0.79	2.50	4.08	13.17	35.16
	na	na	5.34	15.63	35.53
mean	na	na	4.71	14.40	35.35
240	0.25	1.55	4.71	12.22	34.18
	na	na	3.78	9.83	33.44
mean	na	na	4.24	11.03	33.81
300	0.17	1.19	3.87	11.21	32.36
	na	na	3.15	8.80	34.52
mean	na	na	3.51	10.01	33.44
1440	0.06	0.14	0.27	1.18	31.06
	na	na	na	na	na
mean	na	na	na	na	na

Table 24: Metabolic stability of CPD11 in human male hepatocytes [%]

Human Male Hepatocytes CPD11					
time [min]	Percent [%]				
	5 μ M	10 μ M	25 μ M	50 μ M	100 μ M
1	77	85	53	47	50
	na	na	55	47	53
mean	na	na	54	47	51
15	65	80	40	42	49
	na	na	43	44	46
mean	na	na	41	43	47
30	64	74	40	45	48
	na	na	48	41	57
mean			44	43	52
60	41	63	35	36	42
	na	na	35	37	45
mean	na	na	35	37	44
120	22	38	25	42	42
	na	na	23	32	39
mean	na	na	24	37	40
180	16	25	16	26	35
	na	na	21	31	36
mean	na	na	19	29	35
240	5	16	19	24	34
	na	na	15	20	33
mean	na	na	17	22	34
300	3	12	15	22	32
	na	na	13	18	35
mean	na	na	14	20	33
1440	1	1	1	2	31
	na	na	na	na	na
mean	na	na	na	na	na

The time points between 1 min and maximum 300 min represent the most valuable information. After that time point viability of the hepatocytes may rapidly decrease, which could lead to false results. However, for informative purposes also sampling at time point 1140 min was performed.

As can be seen in Table 24, already 1 min after incubation approximately 15-50% of CPD11 was metabolized and after 300 min only 3-33% of CPD11 could still be quantitated in the samples. With a concentration of 31.06 μM after 1440 min CPD11 seemed to be stable at the incubation concentration of 100 μM .

- Cryopreserved Human Female Hepatocytes

CPD11 was incubated in cryopreserved human female hepatocytes in incubation medium at a concentration of 10 μM and 20 μM . Sampling time points and results in μM and percent are depicted in Table 25.

Table 25: Metabolic stability of CPD11 in human female hepatocytes [μM and %]

Human Female Hepatocytes CPD11			Human Female Hepatocytes CPD11		
time [min]	Concentration [μM]		time [min]	Percent [%]	
	10 μM	20 μM		10 μM	20 μM
1	9.47	19.09	1	97	95
15	8.27	17.26	15	83	86
30	7.47	14.41	30	75	72
60	5.71	11.78	60	57	59
120	3.00	6.99	120	30	35
180	1.89	4.67	180	19	23
240	1.26	3.16	240	13	16
300	0.49	2.68	300	5	13
1440	0.06	0.15	1440	1	1

Table 25 shows that degradation of CPD11 amounts approximately 5%, 1 min after incubation. Sixty min after incubation 50% of CPD11 was already metabolized and 300 min later 11.5% of the compound was still quantifiable.

CPD11 was stable in human female hepatocytes for 30 min after incubation. After 60 min a decrease of approximately 50% was observed. When comparing 10 μ M data of human male hepatocytes with human female hepatocytes no significant differences at time points between 1 min and 300 min were detectable.

- Comparison: Cryopreserved Human Male and Female Hepatocytes

Figure 19 presents the concentration versus time curves of CPD11 in human male and female hepatocytes (metabolic stability).

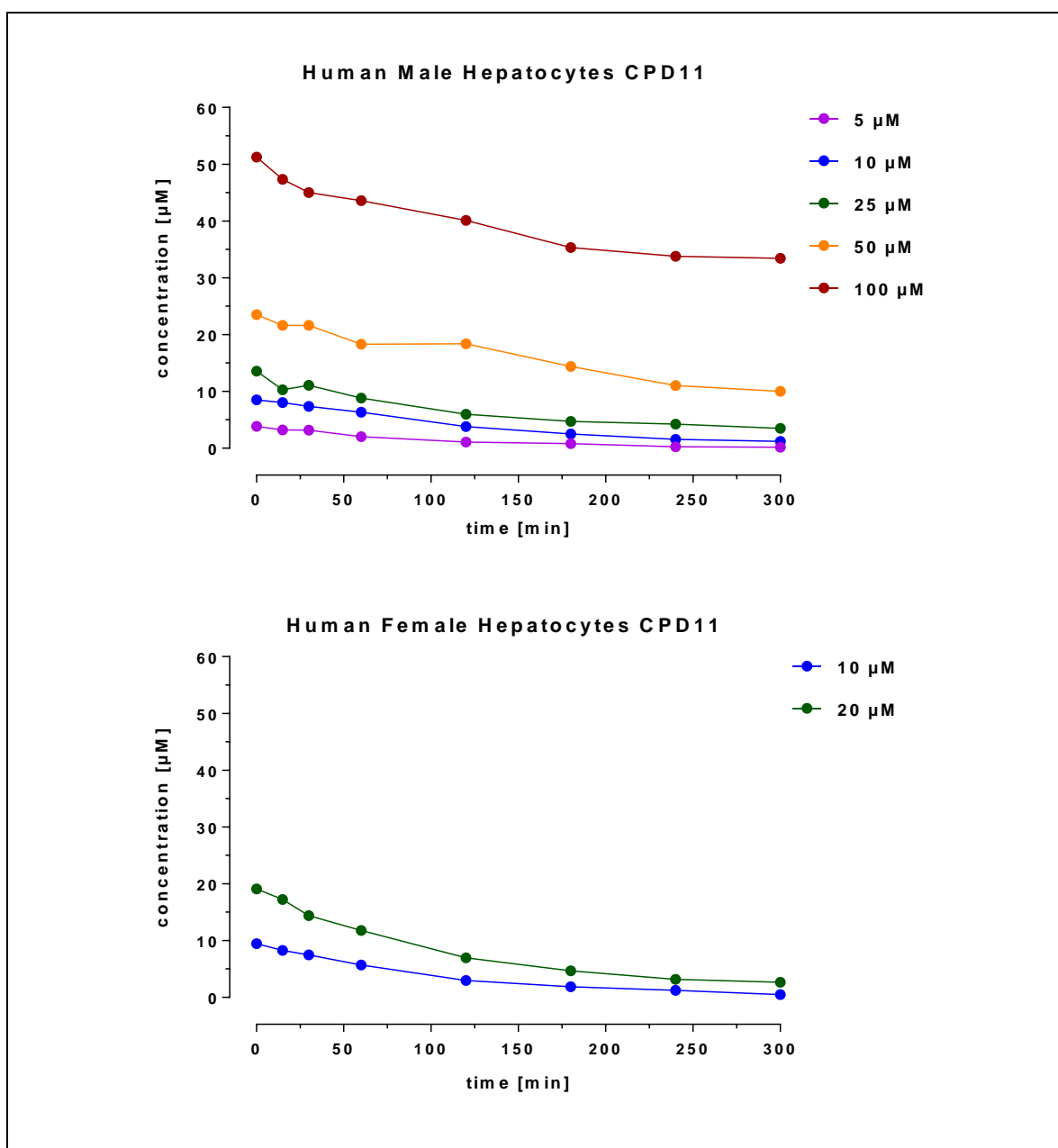


Figure 19: Hepatocytes metabolic stability of CPD11 in human hepatocytes

- **Cryopreserved Rat Hepatocytes**

CPD11 was incubated in cryopreserved rat hepatocytes in incubation medium at concentrations of 5 µM, 10 µM, 25 µM, 50 µM and 100 µM. Duplicate incubations were conducted with all concentrations. Sampling time points and results are depicted in Table 26 and Table 27.

Table 26: Metabolic stability of CPD11 in rat hepatocytes [μM]

Rat Hepatocytes CPD11					
time [min]	Concentration [μM]				
	5 μM	10 μM	25 μM	50 μM	100 μM
1	3.48	7.04	12.99	26.37	53.52
	3.35	7.67	11.74	25.71	52.76
mean	3.42	7.35	12.36	26.04	53.14
15	2.87	6.52	12.95	24.20	50.61
	2.85	6.41	12.08	23.84	53.00
mean	2.86	6.46	12.51	24.02	51.81
30	2.58	5.52	10.65	25.76	59.16
	2.55	5.83	10.70	23.20	47.88
mean	2.57	5.68	10.67	24.48	47.88
60	2.18	4.95	8.11	18.34	44.10
	2.17	5.12	7.80	18.77	42.94
mean	2.18	5.03	7.95	18.56	43.52
120	1.93	3.95	5.94	14.48	37.78
	1.71	3.75	6.96	14.78	35.69
mean	1.82	3.85	6.45	14.63	36.74
180	1.42	3.63	3.81	10.77	34.61
	1.38	3.77	3.76	12.86	32.93
mean	1.40	3.70	3.79	11.81	33.77
240	1.30	3.11	3.38	10.40	32.29
	1.23	3.12	3.28	10.37	36.87
mean	1.27	3.11	3.33	10.39	34.58
300	1.21	3.04	na	na	na
	1.05	2.98	na	na	na
mean	1.13	3.01	na	na	na
1440	0.12	1.11	0.23	0.72	25.65
	na	na	0.25	0.83	25.53
mean	na	na	0.24	0.78	25.59

Table 27: Metabolic stability of CPD11 in rat hepatocytes [%]

Rat Hepatocytes CPD11					
time [min]	Percent [%]				
	5 μ M	10 μ M	25 μ M	50 μ M	100 μ M
1	70	70	52	53	54
	67	77	47	51	53
mean	68	74	49	52	53
15	57	65	52	48	51
	57	64	48	48	53
mean	57	65	50	48	52
30	52	55	43	52	59
	51	58	43	46	48
mean	51	57	43	49	48
60	44	50	32	37	44
	43	51	31	38	43
mean	44	50	32	37	44
120	39	40	24	29	38
	34	38	28	30	36
mean	36	39	26	29	37
180	28	36	15	22	35
	28	38	15	26	33
mean	28	37	15	24	34
240	26	31	14	21	32
	25	31	13	21	37
mean	25	31	13	21	35
300	24	30	na	na	na
	21	30	na	na	na
mean	23	30	na	na	na
1440	2	11	1	1	26
	na	na	1	1	26
mean	na	na	1	1	26

The percentage results in Table 27 ranged from 49 to 74%, 1 min after incubation. At time point 15 min after incubation, already ~50% of CPD11 was metabolized and after 180 min only ~30% of the compound was still quantifiable.

- Cryopreserved Monkey Hepatocytes

CPD11 was incubated in cryopreserved monkey hepatocytes in incubation medium at concentrations of 10 μ M and 20 μ M. Sampling time points and results are listed in Table 28.

Table 28: Metabolic stability of CPD11 in monkey hepatocytes [μ M and %]

Monkey Hepatocytes CPD11			Monkey Hepatocytes CPD11		
time [min]	Concentration [μ M]		time [min]	Percent [%]	
	10 μ M	20 μ M		10 μ M	20 μ M
1	9.62	19.40	1	96	97
15	8.40	17.54	15	84	88
30	7.59	14.65	30	76	73
60	5.80	11.97	60	58	59
120	3.05	7.11	120	31	36
180	1.92	4.74	180	19	22
240	1.28	3.21	240	13	16
300	0.50	2.73	300	5	14
1140	0.06	0.16	1140	1	1

As depicted in Table 28, ~5% of CPD11 was metabolized after 1 min incubation and nearly 30% after 30 min incubation period. 180 min later ~30% of CPD11 could still be quantitated in the samples. Metabolic stability assay in monkey hepatocytes predict similar results in both investigated concentrations. CPD11 is metabolically stable at concentrations of 10 μ M and 20 μ M until time point 30 min. At time point 60 min ~50% of the compound was already metabolized.

- Comparison: Cryopreserved Rat and Monkey Hepatocytes

Figure 20 illustrates concentration versus time curves of the rat and monkey hepatocytes metabolic stability results.

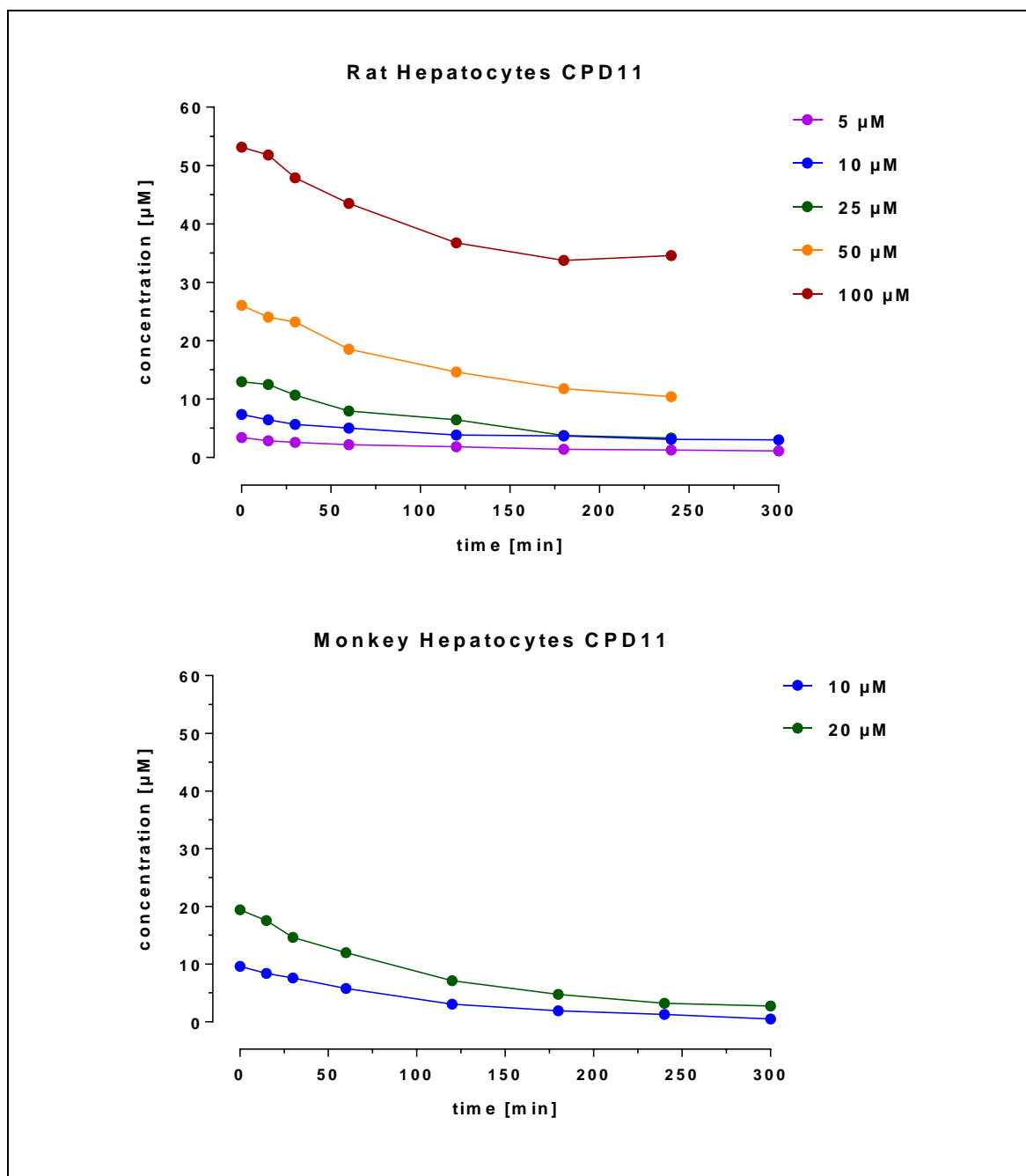


Figure 20: Hepatocyte metabolic stability of CPD11 in rat and monkey hepatocytes

Pharmacokinetic Calculations

Table 29 lists the results of the key PK parameters of CPD11 in human male, human female, rat and monkey hepatocytes. 24 hour values were excluded for the PK calculations.

These parameters, along with the metabolic stability results, increase our understanding of the metabolism of new chemical entities. The hepatic CL_{int} was between 0.4 and 20.2 $\mu\text{L}/\text{min}/10^6$ cells. The scaled CL_{int} was between 1.0 and 72.2 $\text{mL}/\text{min}/\text{kg}$, and the $t_{1/2}$ ranged from 1.1 to 5.8 h. The projected in vivo CL_{met} was between 0.4 and 28.1 $\text{mL}/\text{min}/\text{kg}$.

Table 29: PK calculations of CPD11 in hepatocytes experiments

Species	Conc.	k_{el}	$t_{1/2}$	Hepatic CL_{int}	Scaled CL_{int}	Scaled CL_{met}	Area
	μM		h	$\mu\text{L}/\text{min}/10^6 \text{ cells}$	$\text{mL}/\text{min}/\text{kg}$		
Rat	5	0.0040	2.9	8.0	38.4	22.6	145
Rat	10	0.0034	3.4	6.8	32.6	20.5	348
Rat	25	0.0060	1.9	12.0	57.6	28.1	432
Rat	50	0.0040	2.9	8.0	38.4	22.6	654
Rat	100	0.0020	5.8	4.0	19.2	3.7	880
Monkey	10	0.0094	1.2	18.8	72.2	27.3	289
Monkey	20	0.0069	1.7	13.8	53.0	24.0	549
Human Female	10	0.0094	1.2	18.8	47.4	14.6	249
Human Female	20	0.0069	1.7	13.8	37.8	13.1	544
Human Male	5	0.0106	1.1	21.2	53.4	15.1	237
Human Male	10	0.0069	1.7	13.8	34.8	13.1	342
Human Male	25	0.0044	2.6	8.8	22.2	10.8	531
Human Male	50	0.0028	4.1	5.6	14.1	8.4	818
Human Male	100	0.0002	57.8	0.4	1.0	0.4	1098

Metabolites and Rearrangement Products

Metabolites and rearrangement products (M) of CPD11 in cryopreserved human female, human male, rat and monkey hepatocytes are shown in Figure 21 to Figure 25.

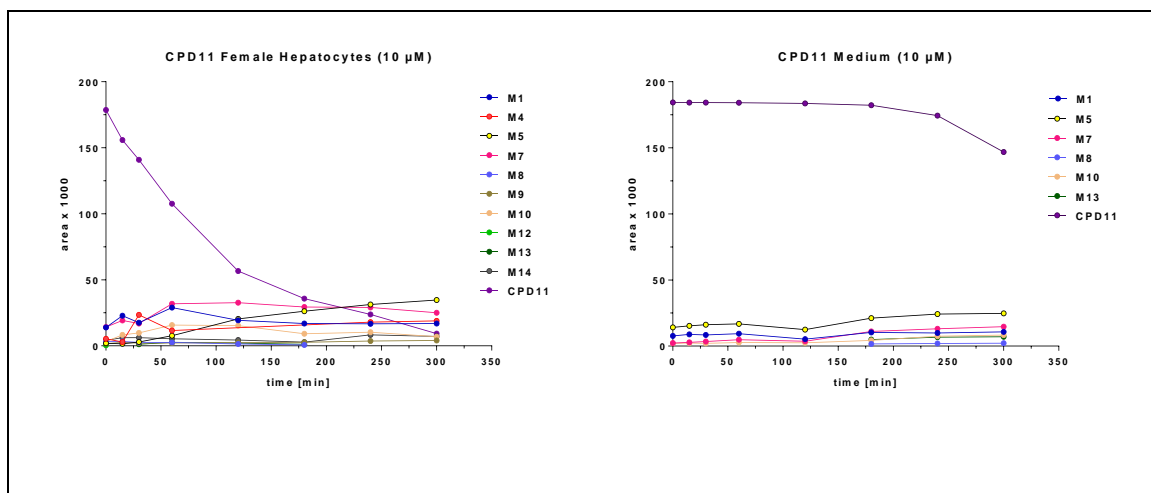


Figure 21: Metabolites and rearrangement products of CPD11 in human female hepatocytes at 10 μ M

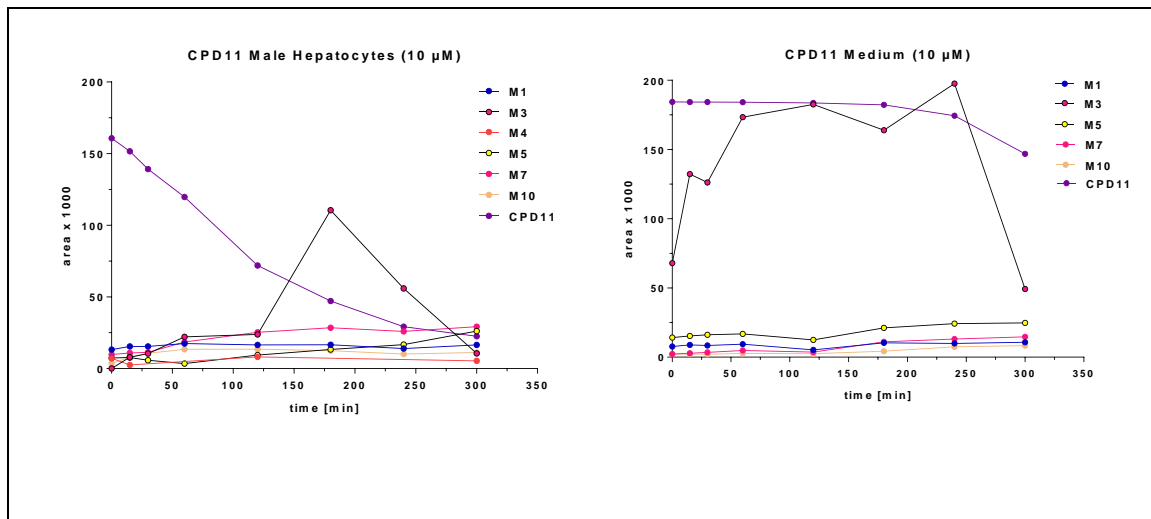


Figure 22: Metabolites and rearrangement products of CPD11 in human male hepatocytes at 10 μ M

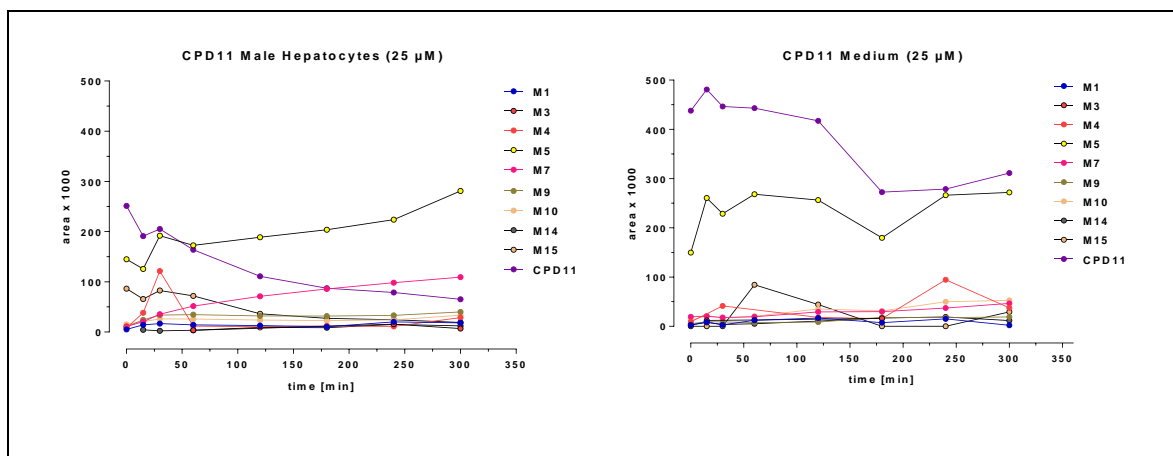


Figure 23: Metabolites and rearrangement products of CPD11 in human male hepatocytes at 25 µM

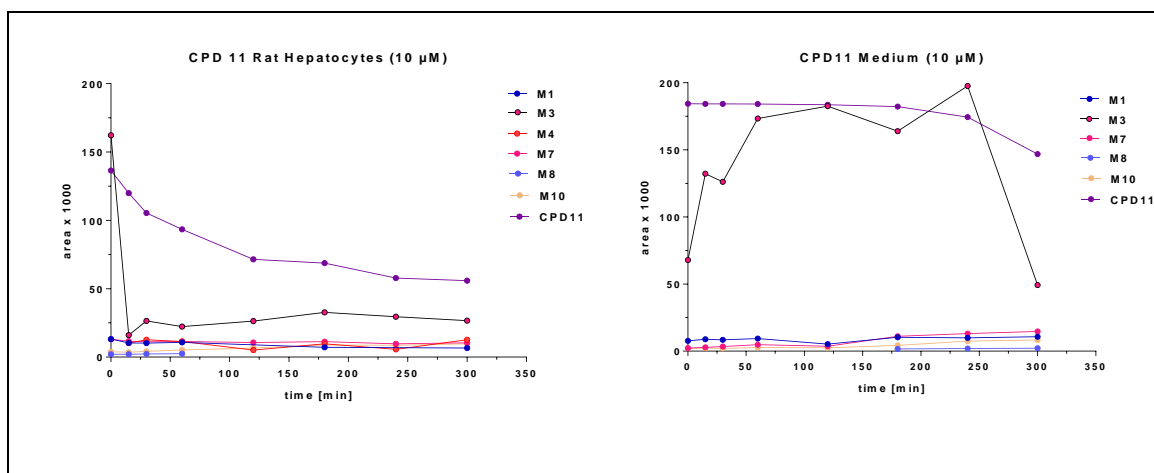


Figure 24: Metabolites and rearrangement products of CPD11 in rat hepatocytes at 10 µM

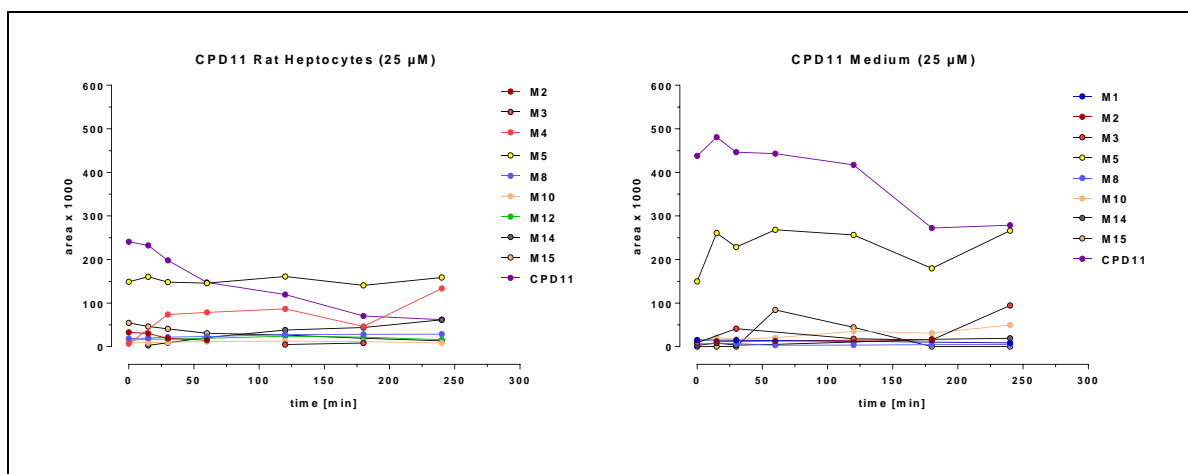


Figure 25: Metabolites and rearrangement products of CPD11 in rat hepatocytes at 25 µM

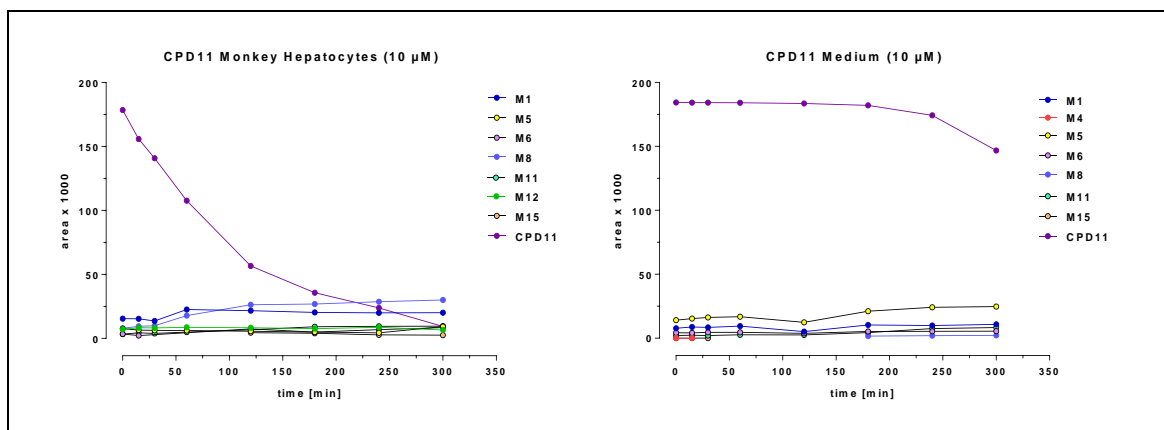


Figure 26: Metabolites and rearrangement products of CPD11 in monkey hepatocytes at 10 µM

In all hepatocyte species, 0 to 4 metabolites or rearrangement products (when comparing with medium samples) were detected, whereby a distinct peak was not recognizable. The metabolites or rearrangement products that were repeatedly perceived were M4 and M12.

Chromatograms in Figure 27 compare 10 µM CPD11 spiked in rat hepatocytes and 10 µM CPD11 spiked in incubation medium. Solely between 12 and 14 min traces of possible metabolites or rearrangement products can be seen, but not definitely assigned.

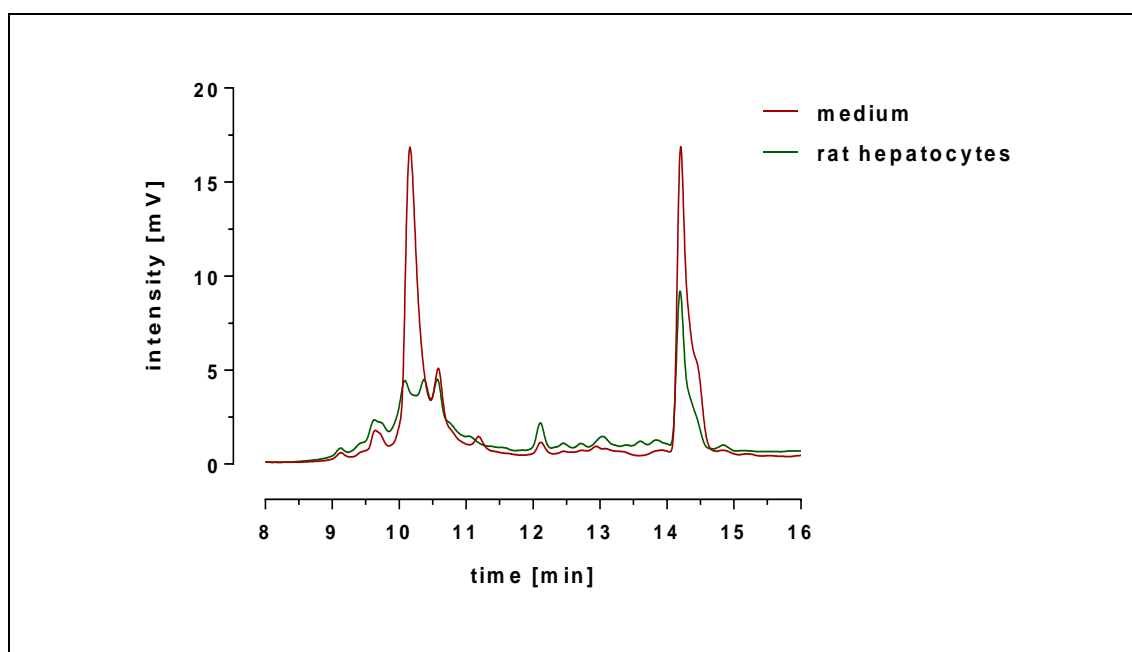


Figure 27: 10 µM CPD 11 spiked in rat hepatocytes and incubation medium

Figure 28 shows chromatograms of CPD11 spiked in incubation medium at a concentration of 10 μ M. As illustrated, CPD11 degrades in incubation medium as well as in the absence of hepatocytes. At retention times between 12 and 14 min also in incubation medium rearrangement products were generated.

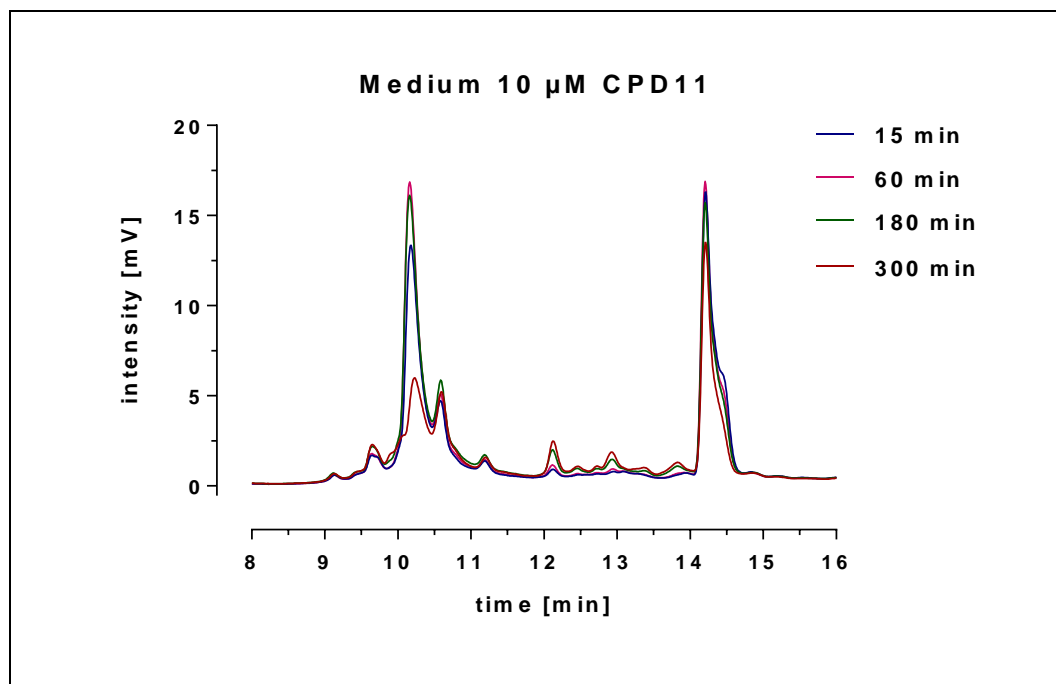


Figure 28: 10 μ M CPD11 spiked in incubation medium

Figure 29 compares chromatograms of 10 μ M CPD11 spiked in human male, human female, rat and monkey hepatocytes. The chromatograms are similar to each other and also nearly the same possible metabolites or rearrangement products were formed.

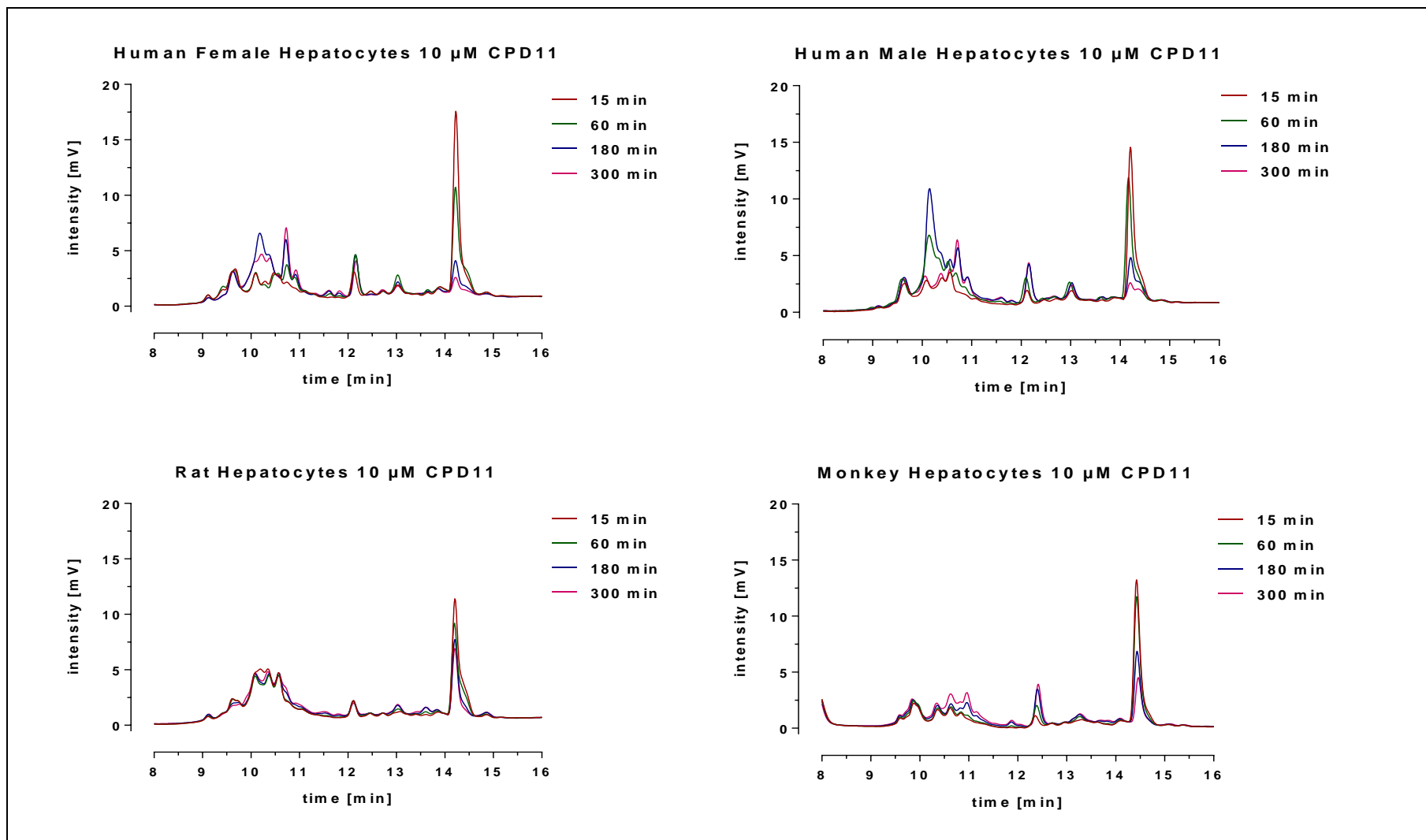


Figure 29: Comparison of chromatograms of CPD11 in different hepatocytes models at a concentration of 10 μ M

4.3.2 CPD22

Calibration Curve

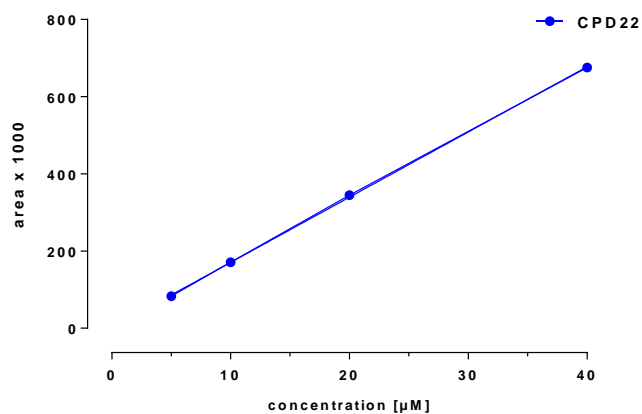


Figure 30: Calibration curve of CPD22 in incubation medium

The calibration curve of CPD22 in incubation medium was linear over the range from 5 to 40 μM, prepared by plotting peak area against sample concentration (Figure 30). Detailed information about the regression parameters are presented in Table 30. For calculation of CPD22 concentrations in incubation medium the transformed formula $x = y/16.89$ was used.

Table 30: Regression parameters of the calibration curve of CPD22 in incubation medium

CPD22	
Best-fit values	
Slope	16.89 ± 0.1641
Y-intercept when X=0.0	1.670 ± 3.781
X-intercept when Y=0.0	-0.09882
1/slope	0.05919
95% Confidence Intervals	
Slope	16.19 to 17.60
Y-intercept when X=0.0	-14.60 to 17.94
X-intercept when Y=0.0	-1.100 to 0.8360
Goodness of Fit	
R square	0.9998
Sy.x	4.398
Is slope significantly non-zero?	
F	10605
DFn, DFd	1.000, 2.000
P value	< 0.0001
Deviation from zero?	Significant
Data	
Number of X values	4
Maximum number of Y replicates	1
Total number of values	4
Number of missing values	0
Equation	
$Y = 16.89 * X + 1.670$	

Metabolic Stability

CPD22 is a prodrug of CPD11 which results through esterases and oxidation as demonstrated in Figure 31. Metabolic stability assay of CPD22 was implemented to obtain metabolic information of CPD22 and its metabolite CPD11.

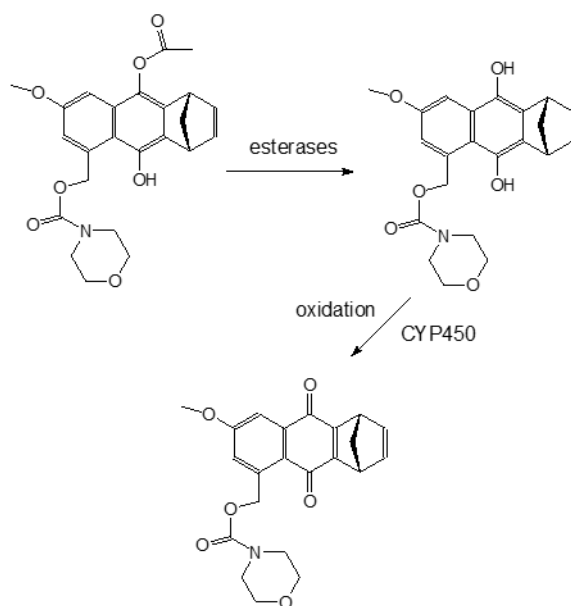


Figure 31: Esterases and oxidation from CPD22 to CPD11

- Cryopreserved Human Female Hepatocytes

CPD22 was incubated in cryopreserved human female hepatocytes at concentrations of 12.5 μM and 25 μM . Sampling time points and results in μM are depicted in Table 31.

Table 31: Metabolic stability of CPD22 in human female hepatocytes [μM]

Human Female Hepatocytes CPD22				
Concentration [μM]				
time [min]	CPD22 12.5 μM	CPD11	CPD22 25 μM	CPD11
0	12.50	0.00	25.00	0.00
1	1.93	9.74	4.45	20.90
15	0.14	11.66	3.00	24.85
30	LOQ	9.82	0.57	23.50
60	LOQ	4.95	LOQ	17.79
120	LOQ	2.26	LOQ	9.67
180	LOQ	1.14	LOQ	5.10
240	LOQ	0.78	LOQ	3.37
300	LOQ	0.61	LOQ	1.09
1440	LOQ	0.13	LOQ	0.58

As presented in Table 31 CPD22 is unstable in human female hepatocytes and was completely metabolized to CPD11 after almost 15 min (12.5 μM) and 30 min (25 μM). The highest concentration of CPD11 in the hepatocytes was reached after 15 min.

Figure 32 shows the concentration versus time curves of the human female metabolic stability data. These results verify that CPD22 was nearly immediately metabolized to CPD11.

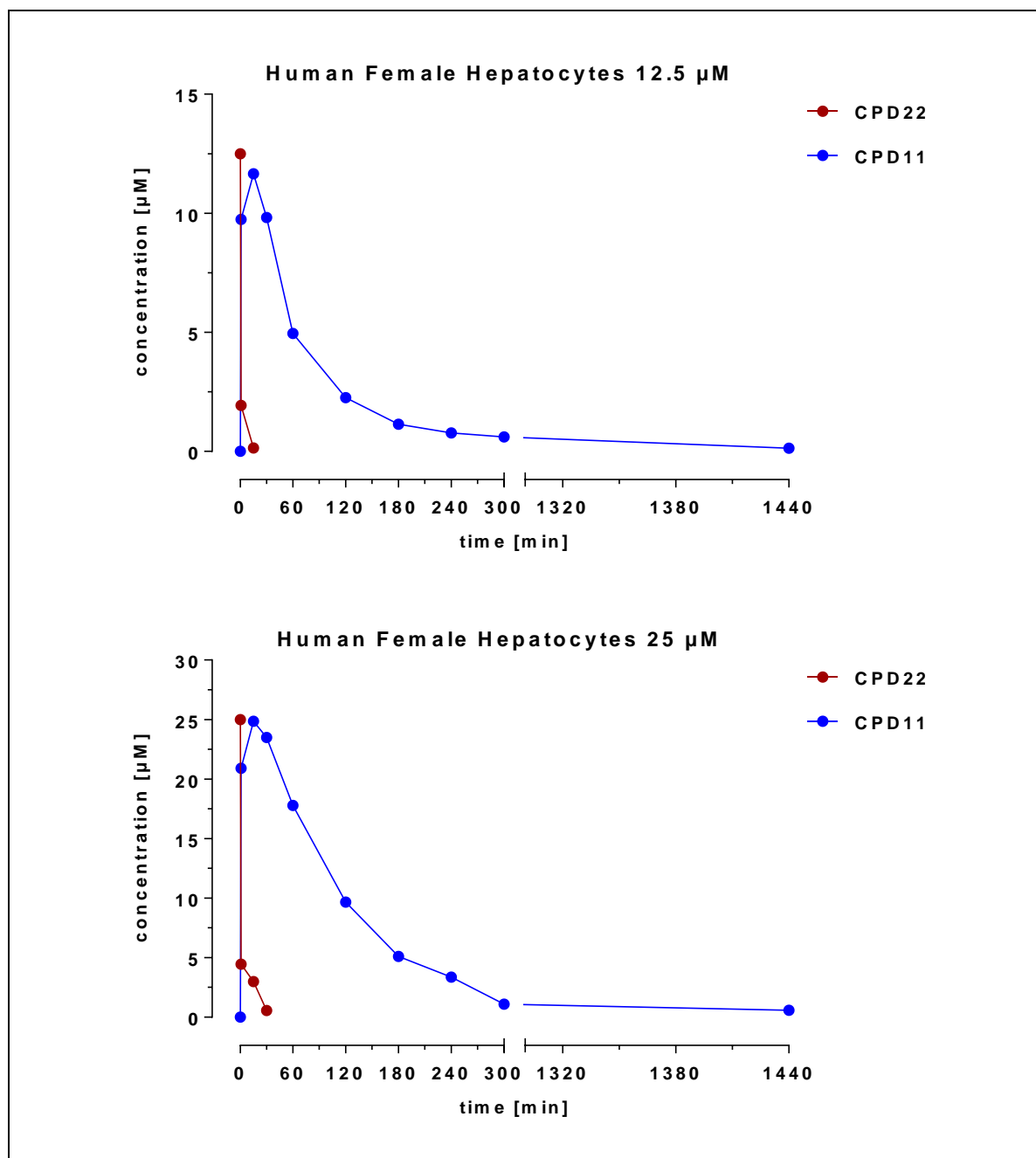


Figure 32 Hepatocyte metabolic stability of CPD22 in human female hepatocytes

- Cryopreserved Monkey Hepatocytes

CPD22 was incubated in cryopreserved monkey hepatocytes at concentrations of 12.5 μM and 25 μM . Sampling time points and results in μM are listed in Table 32.

Table 32: Metabolic stability of CPD22 in monkey hepatocytes [μM]

Monkey Hepatocytes CPD22				
time [min]	Concentration [μM]			
	CPD22	CPD11	CPD22	CPD11
	12.5 μM		25 μM	
0	12.50	0.00	25.00	0.00
1	4.80	6.95	9.16	12.83
15	1.53	11.06	3.78	21.54
30	0.49	11.49	1.37	25.06
60	LOQ	10.63	LOQ	24.66
120	LOQ	8.62	LOQ	20.93
180	LOQ	7.07	LOQ	17.12
240	LOQ	5.74	LOQ	13.54
300	LOQ	4.60	LOQ	10.98
1440	LOQ	0.73	LOQ	5.83

Table 32 shows a decrease of approximately 95% of CPD22, 30 min after incubation. The highest concentration of CPD11 was reached 30 min after incubation for both concentrations. 1440 min after incubation CPD11 was still quantifiable in the samples.

Figure 33 shows the concentration versus time curves of monkey metabolic stability data. These results verify that CPD22 was immediately metabolized to CPD11.

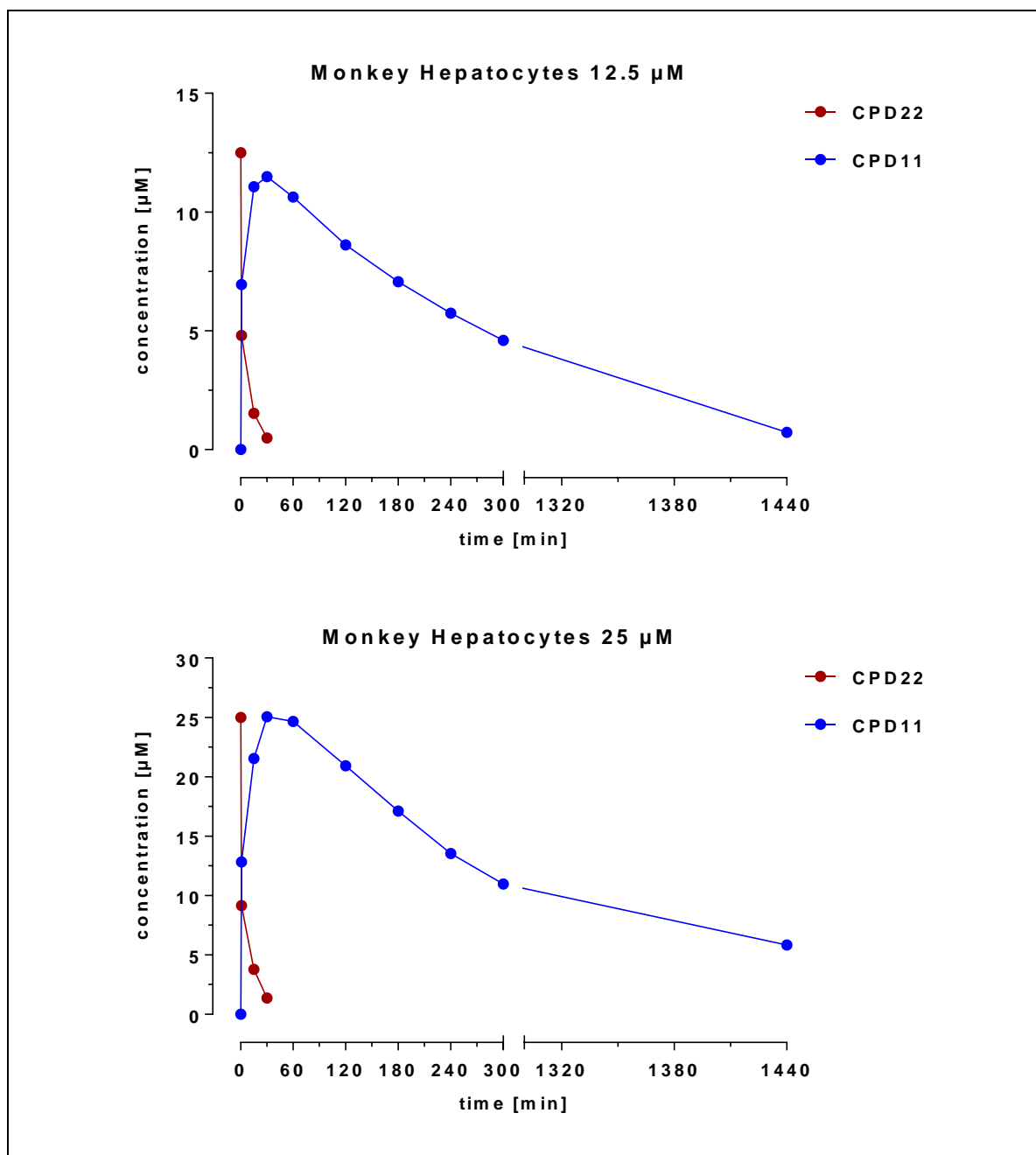


Figure 33: Hepatocytes metabolic stability of CPD22 in monkey hepatocytes

- Cryopreserved Rat Hepatocytes

CPD22 was incubated in cryopreserved rat hepatocytes at concentrations of 12.5 μM and 25 μM . Sampling time points and results in μM are listed in Table 33.

Table 33: Metabolic stability of CPD22 in rat hepatocytes [μM]

Rat Hepatocytes CPD22				
time [min]	Concentration [μM]			
	CPD22	CPD11	CPD22	CPD11
	12.5 μM		25 μM	
0	12.50	0.00	25.00	0.00
1	0.10	8.48	0.37	20.81
15	0.04	7.38	0.05	18.85
30	LOQ	6.07	LOQ	15.36
60	LOQ	4.51	LOQ	12.70
120	LOQ	3.82	LOQ	9.36
180	LOQ	3.15	LOQ	9.13
240	LOQ	2.87	LOQ	8.73
300	LOQ	2.64	LOQ	8.76
1440	LOQ	1.61	LOQ	5.43

The metabolic stability assay in rat hepatocytes show similar results as in human female and monkey hepatocytes, verifying that CPD22 was completely metabolized to CPD11 after maximum 30 min.

Figure 34 shows the concentration versus time curves of rat hepatocytes metabolic stability results, which also depicts the rapid metabolism of CPD22 prodrug to its CPD11 metabolite.

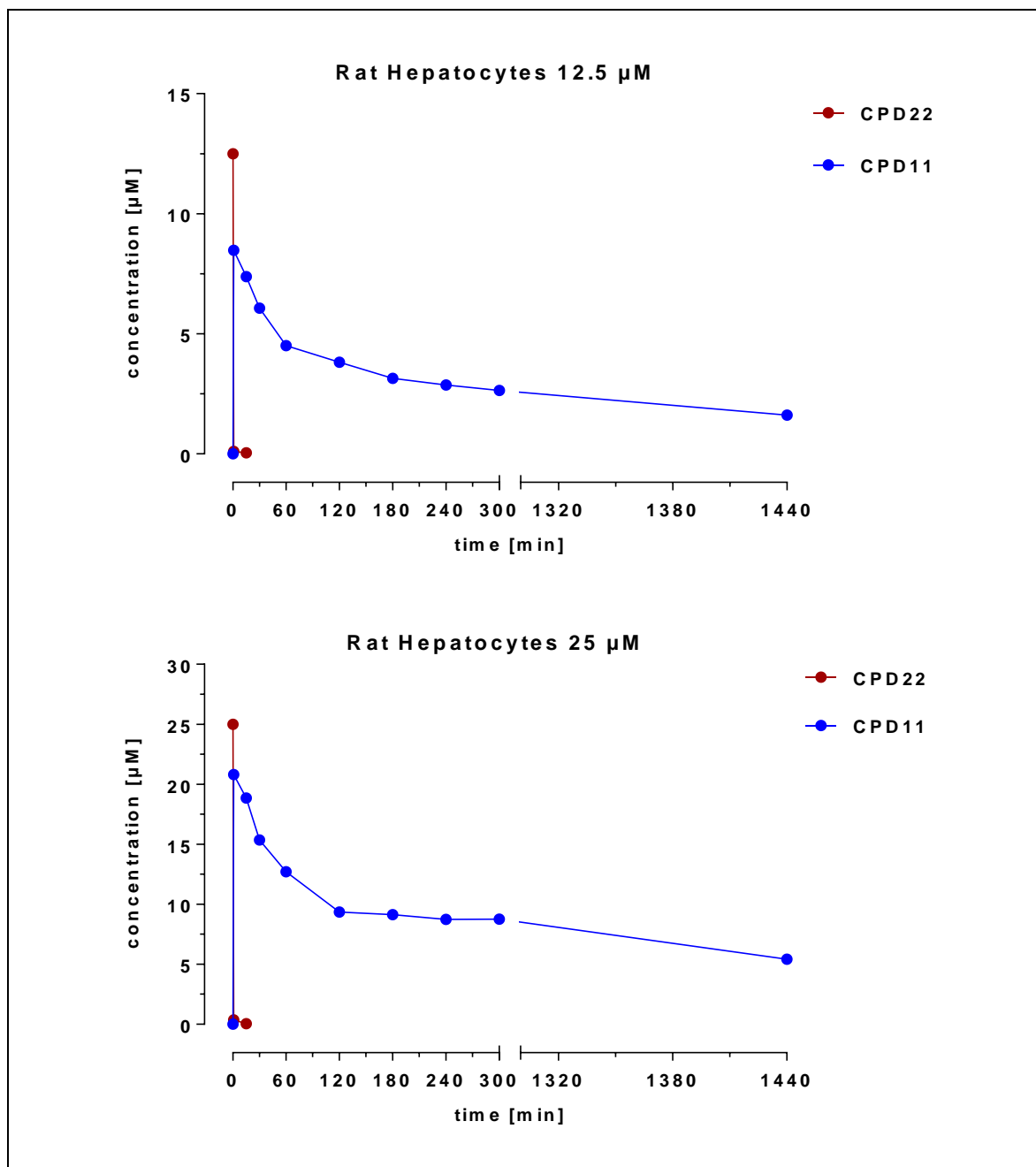


Figure 34: Concentration versus time curve of metabolic stability of CPD22 in rat hepatocytes

- Comparison: Cryopreserved Human Female, Rat and Monkey Hepatocytes

Figure 35 compares chromatograms of metabolic stability assays of CPD22 in human female, monkey and rat hepatocytes, 60 min after incubation with chromatograms of blank incubation samples, not containing hepatocytes. Incubation volume was 10 μM for both samples. The green line depicts the chromatograms of the blank samples and the red line of the hepatocyte samples.

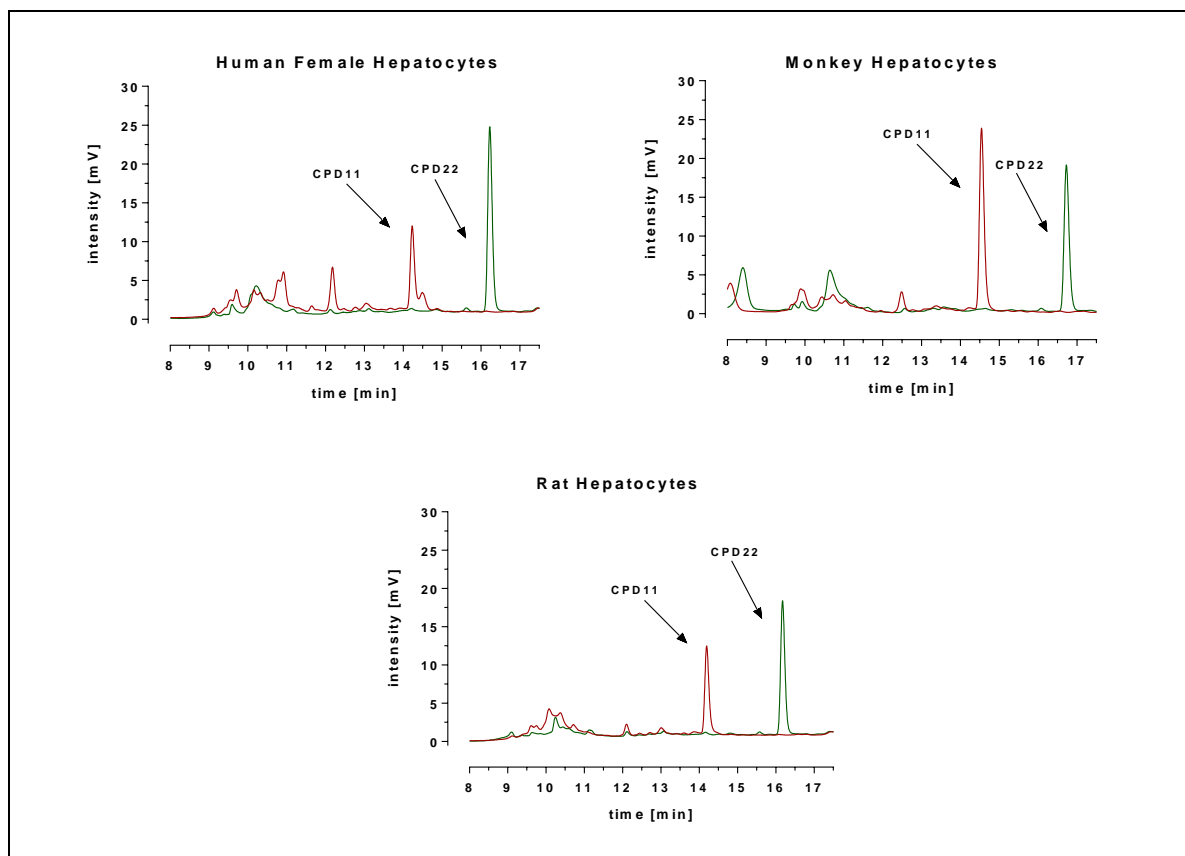


Figure 35: Chromatograms of metabolic stability of CPD22 in different hepatocytes 60 min after incubation. Incubation volume: 10 μ M

As can be seen in Figure 35 CPD22 cannot be quantified in the hepatocyte samples 60 min after compound incubation, while the blank samples show a clear CPD22 peak.

Pharmacokinetic Calculations

Table 34 lists the results of the PK calculations of the transformation product, CPD11, in human female, rat and monkey hepatocytes. Time point values corresponding to 1140 min were excluded for PK calculations. Some data points were not calculated, as only three data points were available. In CPD22, the $t_{1/2\alpha}$ (half-life of distribution) was below 1 min, and $t_{1/2\beta}$ (half-life of elimination) ranged from 2.3 to 10.6 min. For rat and female human hepatocytes, $t_{1/2\alpha}$ was not calculable because the concentration decline was too rapid.

The $t_{1/2\text{form}}$ (half-life of formation) ranged from 9.5 to 0.9 min, and $t_{1/2\beta}$ was between approximately 1 to 4 h in all species.

RESULTS

Table 34: PK calculations of transformation product; *na: only three data points available.*

CPD22								
Species	Conc.	alpha	r ²	t _{1/2} α	beta	r ²	t _{1/2} β	Area
	μM	min ⁻¹		min	min ⁻¹		min	
Rat	12.5	na	na	na	0.0654	1.000	10.6	7
	25.0	na	na	na	0.2971	0.936	2.3	16
Monkey	12.5	3.3762	1.000	0.2	0.0759	1.000	9.1	68
	25.0	3.5743	1.000	0.2	0.0677	1.000	10.2	146
Human Female	12.5	na	na	na	0.2516	0.924	2.8	22
	25.0	na	na	na	0.1107	1.000	6.3	97
Metabolite CPD11								
Species	Conc.	formation rate	r ²	t _{1/2} form	beta	r ²	t _{1/2} β	Area
	μM	min ⁻¹		min	min ⁻¹		min	
Rat	12.5	0.7304	1.000	1.0	0.0029	0.912	242.6	1180
	25.0	0.7392	1.000	0.9	0.0020	0.895	353.4	3243
Monkey	12.5	0.1138	0.968	6.1	0.0035	0.999	199.7	2373
	25.0	0.0603	0.941	11.5	0.0034	0.997	203.1	5507
Human Female	12.5	0.1727	1.000	4.0	0.0101	0.943	68.3	955
	25.0	0.0734	0.912	9.5	0.0111	0.975	62.6	2967

Metabolites and Rearrangement Products

Metabolites and rearrangement products of CPD22 in cryopreserved human female, rat and monkey hepatocytes are shown in Figure 36, Figure 37 and Figure 38. Incubation volume was 25 μ M.

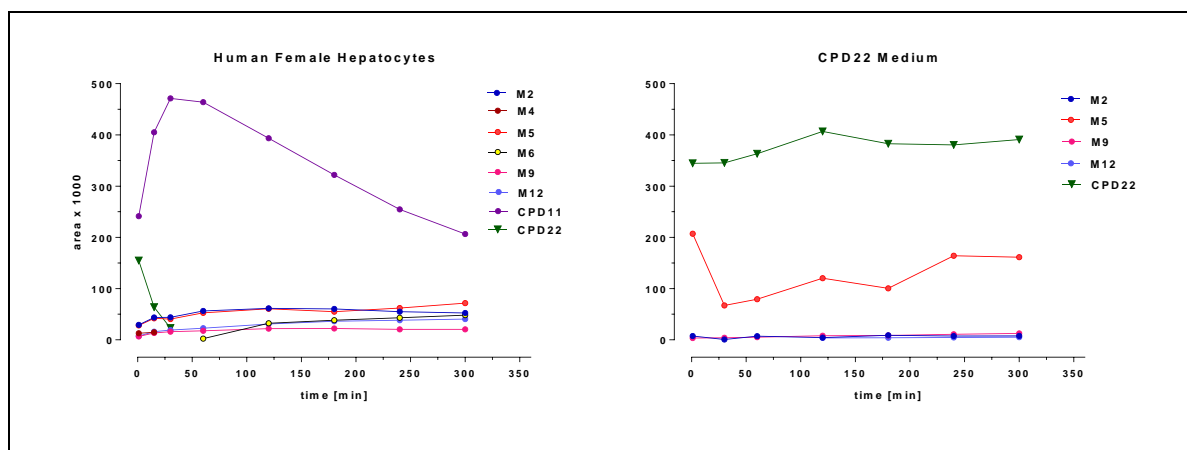


Figure 36: Human female hepatocytes spiked with 25 μ M CPD22

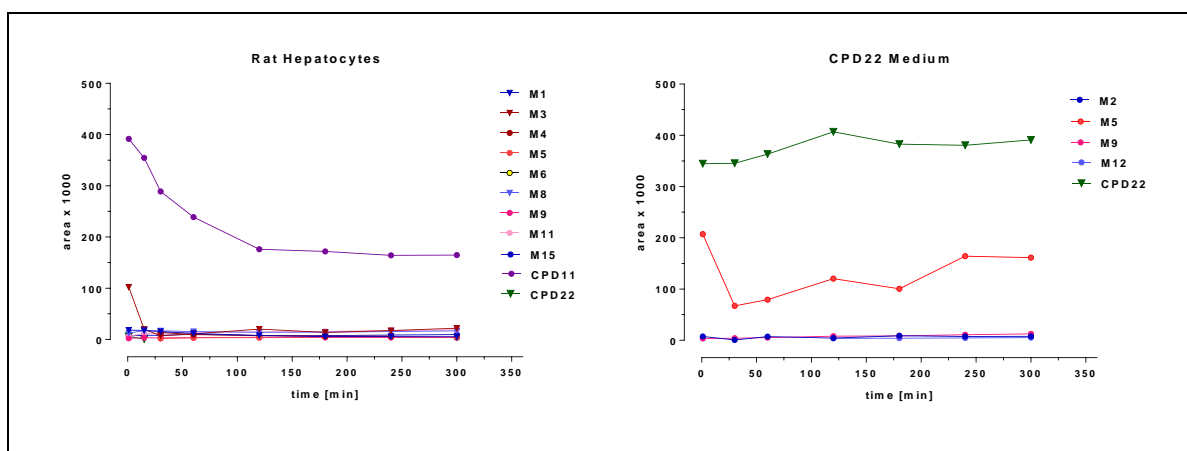


Figure 37: Rat hepatocytes spiked with 25 μ M CPD22

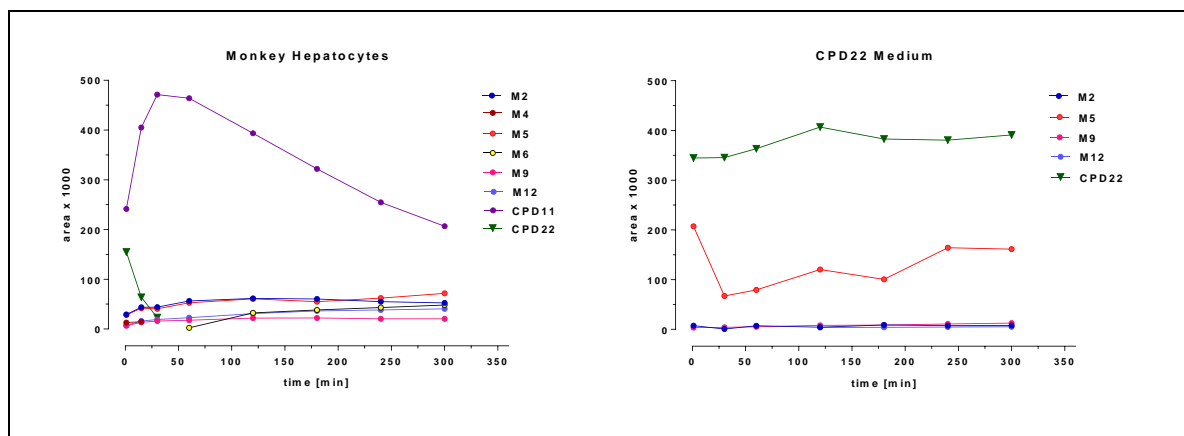


Figure 38: Monkey hepatocytes spiked with 25 μ M CPD22

As can be seen in Figure 36, Figure 37 and Figure 38, the main metabolite of CPD22 (CPD11 - purple line) reached its maximum peak concentration approximately 30 min after incubation in human female and monkey hepatocytes. Whereas in rat hepatocytes the maximum peak concentration occurred within 5 min. Metabolic profiling in rat hepatocytes showed six products, while in female and monkey hepatocytes two unknown products were detectable (when not including the products also formed in medium samples). Metabolites or rearrangement products M4 and M6 could be quantitated in all species.

4.3.3 Testosterone

Calibration Curve

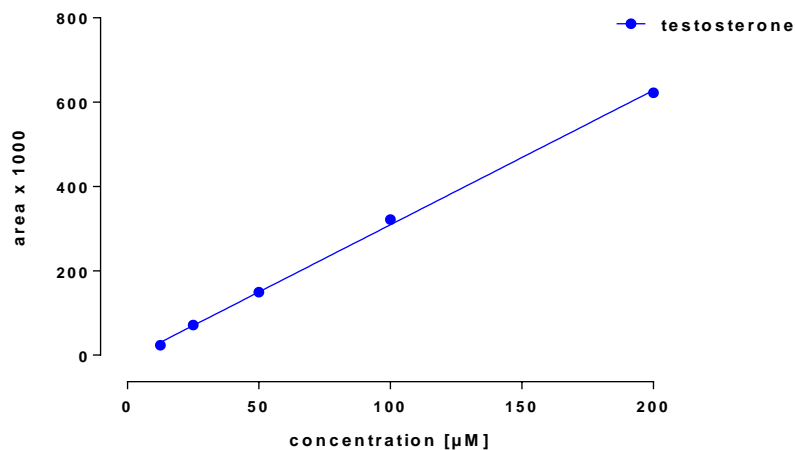


Figure 39: Calibration curve of testosterone in incubation medium

The calibration curve of testosterone in incubation medium was linear over the range from 12.5 to 200 μM, prepared by plotting peak area against sample concentration. Figure 39 shows correlation between peak area versus concentration. Detailed information about the regression parameters are depicted in Table 35. For calculation of testosterone concentrations in incubation medium, the transformed equation $x = y/3.19$, was used.

Table 35: Regression parameters of the calibration curve of testosterone in incubation medium

Testosterone	
Best-fit values	
Slope	$3,189 \pm 0,05718$
Y-intercept when X=0.0	$-9,671 \pm 5,903$
X-intercept when Y=0.0	3.033
1/slope	0.3136
95% Confidence Intervals	
Slope	3,007 to 3,371
Y-intercept when X=0.0	-28,45 to 9,111
X-intercept when Y=0.0	-2,986 to 8,565
Goodness of Fit	
R square	0.999
Sy.x	8.719
Is slope significantly non-zero?	
F	3110
DFn, DFd	1,000, 3,000
P value	< 0,0001
Deviation from zero?	Significant
Data	
Number of X values	5
Maximum number of Y replicates	1
Total number of values	5
Number of missing values	0
Equation	
$Y = 3,189 * X - 9,671$	

Metabolic Stability

For validation reasons testosterone was used as a reference compound. Testosterone was incubated in cryopreserved human female, human male, rat and monkey hepatocytes in incubation medium at a substrate concentration of 50 μ M. Sampling time points and results in μ M and percent are depicted in Table 36 Table 39.

Table 36: Metabolic stability of testosterone in human male hepatocytes [μM and %]

Human Male Hepatocytes Testosterone		Human Male Hepatocytes Testosterone	
	Concentration [μM]		Percent [%]
time [min]	50 μM	time [min]	50 μM
0	45.11	0	90
15	32.66	15	65
30	27.02	30	54
60	15.86	60	32
120	9.34	120	19
180	LOQ	180	LOQ

Table 37: Metabolic stability of testosterone in human female hepatocytes [μM and %]

Human Female Hepatocytes Testosterone		Human Female Hepatocytes Testosterone	
	Concentration [μM]		Percent [%]
time [min]	50 μM	time [min]	50 μM
0	40.12	0	80
15	31.22	15	62
30	20.47	30	41
60	16.80	60	34
120	10.13	120	20
180	1.88	180	4

Table 38: Metabolic stability of testosterone in rat hepatocytes [μM and %]

Rat Hepatocytes Testosterone		Rat Hepatocytes Testosterone	
	Concentration [μM]		Percent [%]
time [min]	50 μM	time [min]	50 μM
0	38.97	0	78
15	26.58	15	53
30	20.47	30	41
60	4.14	60	8
120	1.72	120	3
180	LOQ	180	LOQ

Table 39: Metabolic stability of testosterone in monkey hepatocytes [μM and %]

Monkey Hepatocytes Testosterone		Monkey Hepatocytes Testosterone	
	Concentration [μM]		Percent [%]
time [min]	50 μM	time [min]	50 μM
0	34.55	0	69
15	28.31	15	57
30	22.07	30	44
60	17.96	60	36
120	11.16	120	22
180	1.19	180	2

Figure 40 and Figure 41 illustrate concentration versus time curves of human male, human female, rat and monkey hepatocytes testosterone metabolic stability experiments.

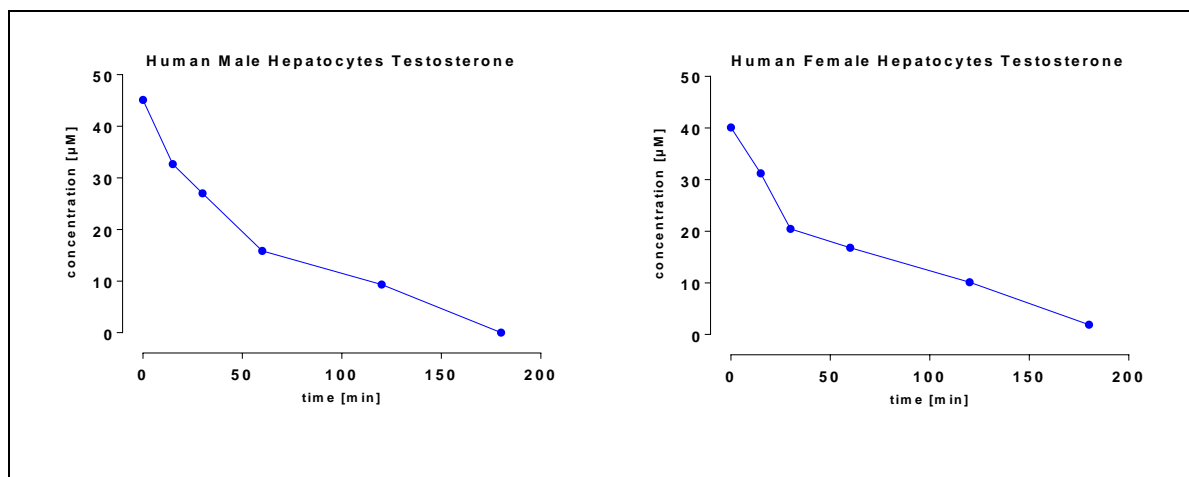


Figure 40: Concentration versus time curves of metabolic stability of testosterone in human male and female hepatocytes

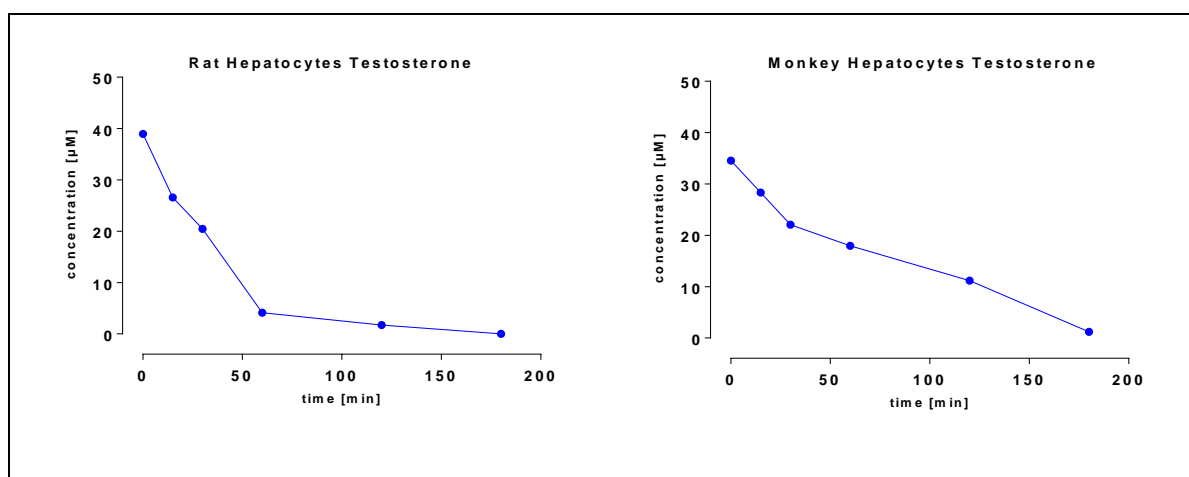


Figure 41: Concentration versus time curves of metabolic stability of testosterone in rat and monkey hepatocytes

As described in the below Tables and Figures testosterone is metabolically unstable. After 180 min nearly no traces of the compound was quantifiable in the assay. These results are in accordance with the literature and therefore give evidence for the significance and exactness of the results obtained from CPD11 and CPD22 metabolic stability studies. [68]

Pharmacokinetic Calculations

Table 40 shows the results of the PK calculations of testosterone in human male, human female, rat and monkey hepatocytes.

Based on these results $t_{1/2}$ values were predicted to be between 0.4 and 0.9 h. The hepatic CL_{int} were found to be 54.8, 33.6, 30.7 and 25.9 $\mu\text{L}/\text{min}/10^6$ cells, in rat, monkey, human female and human male, respectively. The scaled CL_{int} was between 65.2 and 263.0 $\text{mL}/\text{min}/\text{kg}$, showing high discrepancies within the species. Scaled CL_{met} was determined to be between 15.9 and 45.5 $\text{mL}/\text{min}/\text{kg}$.

Table 40: PK calculations of testosterone in hepatocytes experiments

Species	Conc.	k_{el}	$t_{1/2}$	Hepatic CL_{int}	Scaled CL_{int}	Scaled CL_{met}	Area
	μM		h	$\mu L/min/10^6$ cells	mL/min/kg		
Rat	50	0.0274	0.4	54.8	263.0	45.5	225
Monkey	50	0.0168	0.7	33.6	129.0	32.8	426
Human Female	50	0.0154	0.8	30.7	77.5	16.5	432
Human Male	50	0.0129	0.9	25.9	65.2	15.9	346

4.4 Preliminary Pharmacokinetics of CPD3 and CPD11

4.4.1 Calibration curves

Calibration curve of CPD3

The calibration curve of CPD3 in plasma was linear over the range from 1.56 to 100.0 $\mu\text{g/mL}$, prepared by plotting peak area against sample concentration. The graph below (Figure 42) shows an excellent correlation between peak area versus concentration. Detailed information about the regression parameters are listed in Table 41. For calculation of CPD3 concentrations in plasma the transformed formula $x = y/4.978$ was used, whereby 4.978 represents the slope regression line.

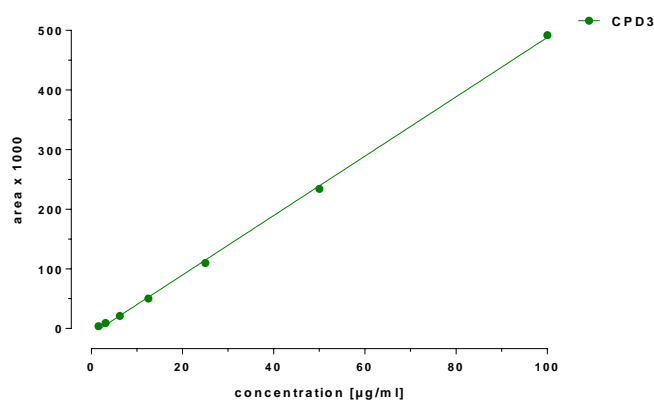


Figure 42: Calibration curve of CPD3 in plasma

Table 41: Regression parameters of the calibration curve of CPD3 in plasma

CPD3	
Best-fit values	
Slope	4.978 ± 0.05428
Y-intercept when X=0.0	-9.700 ± 2.369
X-intercept when Y=0.0	1.948
1/slope	0.2009
95% Confidence Intervals	
Slope	4.839 to 5.118
Y-intercept when X=0.0	-15.79 to -3.610
X-intercept when Y=0.0	0.7384 to 3.117
Goodness of Fit	
R square	0.9994
Sy.x	4.765
Is slope significantly non-zero?	
F	8413
DFn, DFd	1.000, 5.000
P value	< 0.0001
Deviation from zero?	Significant
Data	
Number of X values	7
Maximum number of Y replicates	1
Total number of values	7
Number of missing values	0
Equation	
	$Y = 4.978 * X - 9.700$

Calibration Curve CPD11

The slope was 7.417 ± 0.1096 . Please refer to section 4.1.2 for detailed results.

4.4.2 CPD3 in vivo Data

Plasma Concentration Raw Data

Table 42 shows plasma concentrations of CPD3 after a single iv dose of 12.5 mg or 20 mg CPD3. For rat 1 iv 6 blood samples at different time points were taken and for rat 2 and rat 3 iv, blood samples at 5 different time points were drawn.

Table 42: Plasma concentrations [$\mu\text{g/mL}$] of CPD3 after iv administration

Rat intravenous CPD3			
Rat ID	time [min]	Dose [mg]	CPD3 [$\mu\text{g/mL}$]
1 iv	3	12.5	22.40
1 iv	7	12.5	17.60
1 iv	42	12.5	1.90
1 iv	43	12.5	1.00
1 iv	156	12.5	0.60
1 iv	171	12.5	0.00
2 iv	2	20.0	29.53
2 iv	30	20.0	25.33
2 iv	40	20.0	22.21
2 iv	60	20.0	15.07
2 iv	159	20.0	1.08
3 iv	2	20.0	25.87
3 iv	30	20.0	23.67
3 iv	39	20.0	20.45
3 iv	60	20.0	15.44
3 iv	157	20.0	0.71

Plasma concentrations of CPD3 were in a very similar order of magnitude at sampling time points of 3-7 min. Immediately after iv bolus injection, concentrations varied approximately from 22 to 29 $\mu\text{g/mL}$. When the dose of 12.5 mg is taken into account then this concentration lies between approximately 25 and 35 $\mu\text{g/mL}$ ($20/12.5 = 1.6$). In rat 1 iv only traces of CPD3

were detectable after 42 min, whereas in rat 2 and 3 iv, even after one hour, CPD3 was quantifiable in the samples. Quantification of CPD3 was possible in 15 out of 16 samples.

Table 43 shows plasma concentrations of CPD3 after a single ip administration of 20 mg CPD3. For rat 1, rat 2 and rat 3 ip blood samples at 5 different time points were taken.

Table 43: Plasma concentrations [$\mu\text{g/mL}$] of CPD3 after ip administration

Rat intraperitoneal CPD3			
Rat ID	time [min]	Dose [mg]	CPD3 [$\mu\text{g/mL}$]
1 ip	0	20.0	0.00
1 ip	18	20.0	6.00
1 ip	37	20.0	6.40
1 ip	55	20.0	5.90
1 ip	160	20.0	3.20
2 ip	0	20.0	0.00
2 ip	17	20.0	3.40
2 ip	37	20.0	3.90
2 ip	54	20.0	3.20
2 ip	160	20.0	1.50
3 ip	0	20.0	0.00
3 ip	20	20.0	3.40
3 ip	39	20.0	3.20
3 ip	55	20.0	2.10
3 ip	161	20.0	2.90

Contrary to iv bolus injections, plasma concentrations increased after ip administration, reaching the c_{max} within 20 to 40 min with a peak concentration of 3.4-6.4 $\mu\text{g/mL}$ (mean 5.6 $\mu\text{g/mL}$). After 160 min plasma concentrations dropped to ~ 2.5 $\mu\text{g/mL}$.

Plasma Concentration versus Time Curves

The resulting plasma concentration [$\mu\text{g/ml}$] versus time [min] data obtained from rats after iv and ip administration of CPD3 are illustrated in Figure 43. As can be seen in the upper insert, rat 1 iv only received 12.5 mg CPD3, hence the plasma concentrations of rat 1 iv was lower comparing to rat 2 and rat 3 iv.

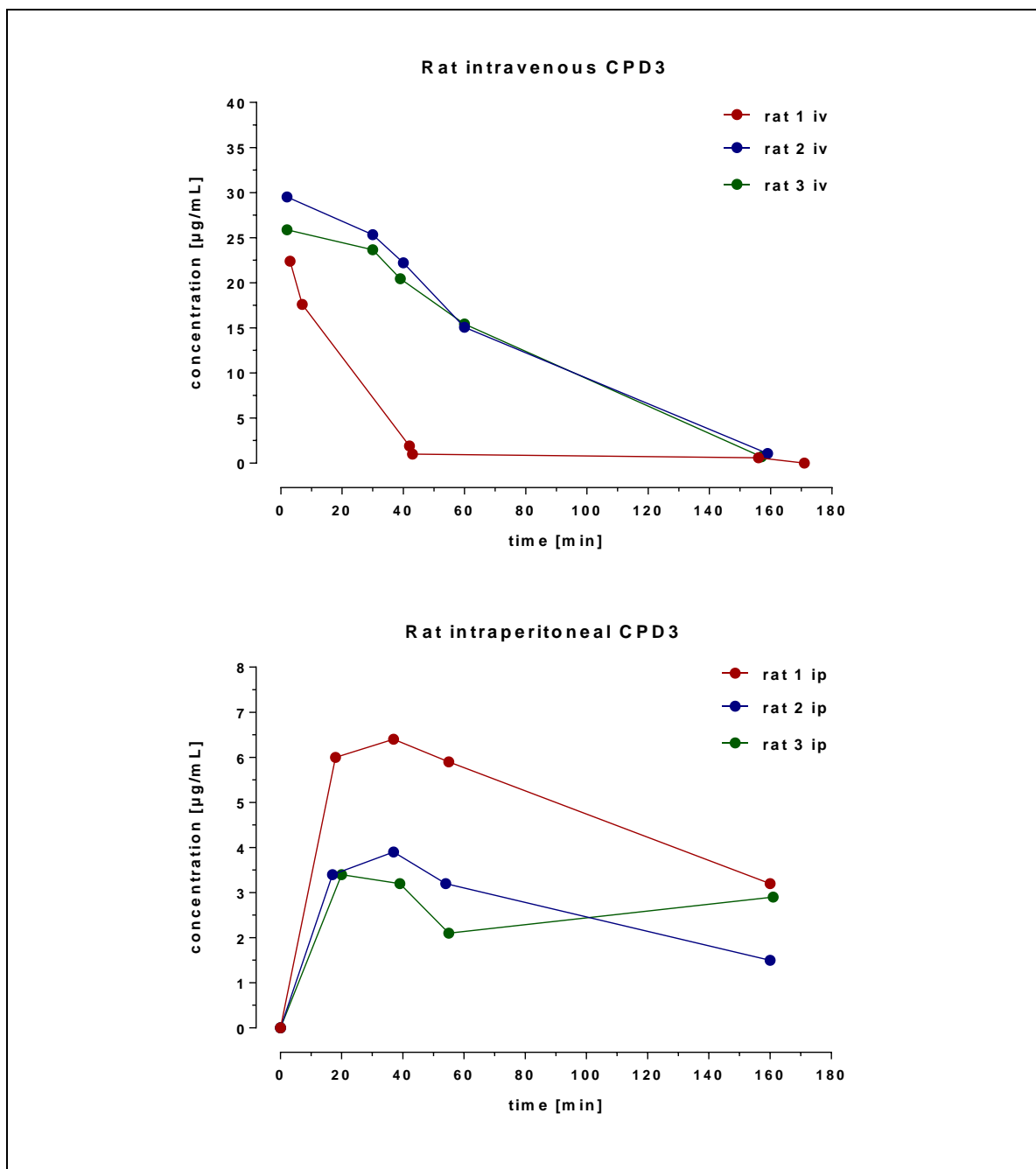


Figure 43: Plasma concentration [$\mu\text{g/mL}$] versus time [min] curves of CPD3

4.4.3 CPD11 in vivo Data

Figure 44 shows chromatograms of CPD11 in mouse plasma 5, 10, 30, 60, 180 and 360 min after iv drug administration. For better resolution, the chromatograms were truncated from 0 to 8 min and from 20 to 42 min, therefore the gradient profile is not visible.

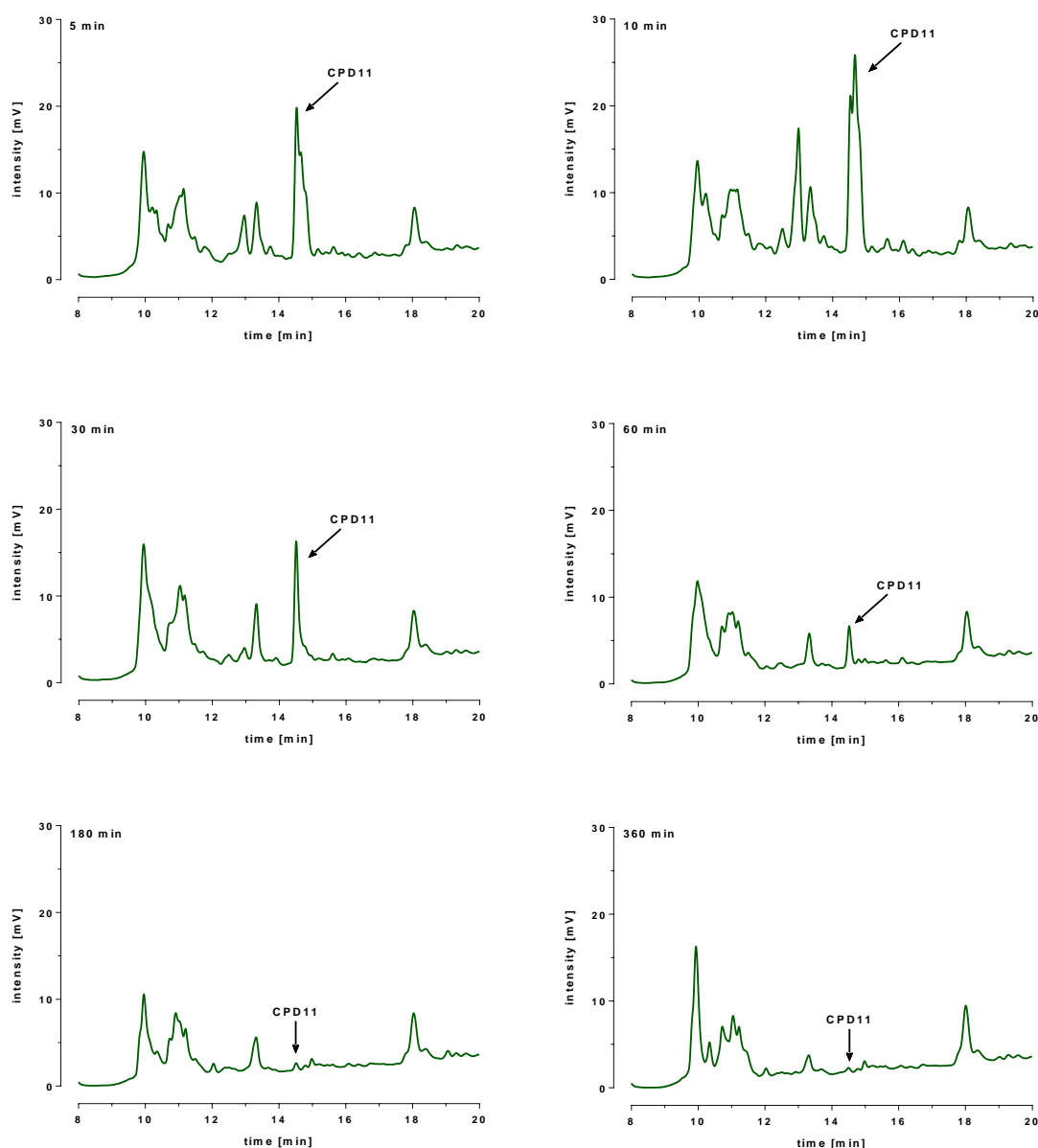


Figure 44: Temporal concentration gradients of CPD11 in plasma of mouse 2 iv

The CPD11 peak of interest is marked by an arrow in Figure 44, showing a double peak in chromatograms obtained after 5 and 10 min. 360 min after CPD11 administration only a small amount of the compound was detectable in the plasma samples.

Figure 45 compares chromatograms of blank mouse plasma with plasma of mouse 2 iv, 30 min after CPD11 administration.

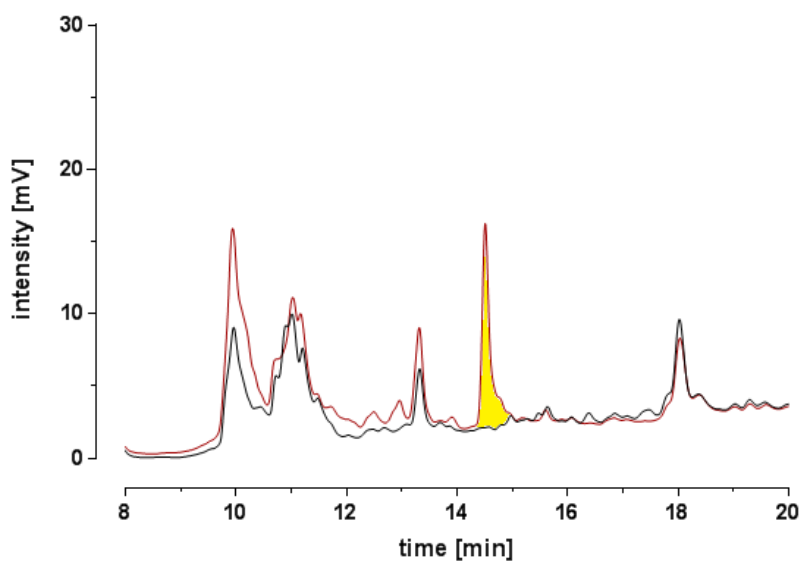


Figure 45: Comparison between chromatograms of blank mouse plasma (black line) and plasma of mouse 2 iv (red line)

In Figure 45 the CPD11 peak is highlighted in yellow. Within the first 15 min after the start of HPLC-analysis, a number of unknown peaks were detectable.

Figure 46 shows chromatograms of CPD11 in rat plasma 3, 8, 18, 42, 81 and 184 min after iv drug administration. For better resolution the chromatograms were also truncated.

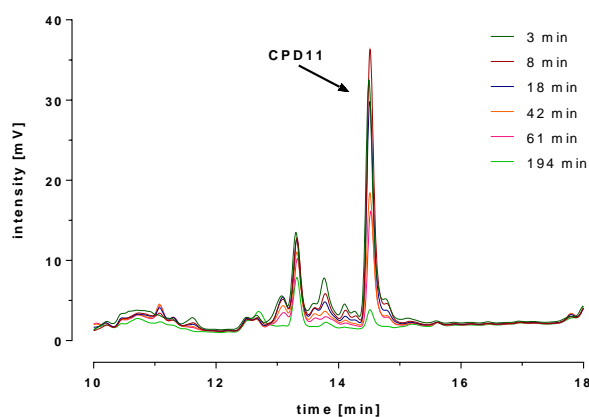


Figure 46: Temporal concentration gradients of CPD11 in plasma of rat 3 iv

The CPD11 peak of interest is marked by an arrow in Figure 46. The CPD11 peaks eluted in rat chromatograms as a sharp single peak at a retention time of 14.5 min. Three metabolites or rearrangement products were detected between 13.5 and 14.1.

Plasma Concentration Raw Data

Table 44 shows plasma concentrations [$\mu\text{g/mL}$] of CPD11 in 3 rats after a single iv dose of 20 mg of CPD11. Six blood samples at different time points were drawn. In Table 44 time point 0 min is from the PK-perspective the intersection point of the concentration versus time curve with the y-axis. For rat 2 iv and rat 3 iv, plasma concentrations of CPD11 were in a similar order of magnitude at sampling time points 0-8 min. The plasma concentrations of CPD11 in rats iv at time point 0-3 min ranged from 66.0-94.0 $\mu\text{g/mL}$. At time point 11-18 min all three animals showed similar plasma concentrations of CPD11 (mean = 52 $\mu\text{g/mL}$). Traces of CPD11 were quantifiable in all three rats, even after 145-194 min (mean = 39 $\mu\text{g/mL}$). Quantification of CPD11 was feasible in all 18 samples.

Table 44: Plasma concentrations [$\mu\text{g/mL}$] of CPD11 after iv administration in rats

Rat intravenous CPD11			
Rat ID	time [min]	Dose [mg]	CPD11 [$\mu\text{g/mL}$]
1 iv	0	20.0	94.00
1 iv	2	20.0	78.10
1 iv	13	20.0	58.30
1 iv	28	20.0	32.20
1 iv	46	20.0	21.90
1 iv	145	20.0	4.98
2 iv	0	20.0	66.00
2 iv	2	20.0	56.00
2 iv	11	20.0	45.60
2 iv	25	20.0	31.00
2 iv	45	20.0	19.83
2 iv	143	20.0	3.55
3 iv	3	20.0	66.80
3 iv	8	20.0	67.60
3 iv	18	20.0	52.10
3 iv	42	20.0	34.30
3 iv	61	20.0	25.00
3 iv	194	20.0	4.30

Table 45 shows plasma concentrations [$\mu\text{g/mL}$] of CPD11 in 3 rats after ip administration of 20 mg CPD11. Four blood samples at different time points were drawn. The earliest blood sampling time points were between 16 and 17 min, which also reflected the highest plasma concentration in all animals. Whereby rat 1 ip depicted at all time points the significantly highest plasma concentrations, when compared to rat 2 ip and rat 3 ip.

Table 45: Plasma concentration [$\mu\text{g/mL}$] of CPD11 after ip administration in rats

Rat intraperitoneal CPD11			
Rat ID	time [min]	Dose [mg]	CPD11 [$\mu\text{g/mL}$]
1 ip	16	20.0	43.20
1 ip	33	20.0	21.50
1 ip	52	20.0	28.20
1 ip	159	20.0	16.10
2 ip	17	20.0	15.40
2 ip	34	20.0	7.47
2 ip	53	20.0	6.31
2 ip	159	20.0	3.40
3 ip	17	20.0	25.00
3 ip	34	20.0	18.23
3 ip	53	20.0	13.69
3 ip	159	20.0	8.60

Table 46 shows plasma concentrations [$\mu\text{g/mL}$] of CPD11 in 3 mice-groups ($n = 24$) after a single iv administration of 0.58 mg CPD11. Blood samples at 7 different time points were taken. The dosage was lower than in rat studies, which was clearly recognizable in the plasma concentrations. After 360 min only minor traces of CPD11 were detectable (mean = 0.08 $\mu\text{g/mL}$). Quantification of CPD11 was possible in all 21 samples.

Table 46: Plasma concentrations [$\mu\text{g/mL}$] of CPD11 after iv administration in mice

Mouse intravenous CPD11			
Mouse ID	time [min]	Dose [mg]	CPD11 [$\mu\text{g/mL}$]
1 iv	5	0.58	5.13
1 iv	10	0.58	3.31
1 iv	15	0.58	4.26
1 iv	30	0.58	2.21
1 iv	60	0.58	0.53
1 iv	180	0.58	0.14
1 iv	360	0.58	0.05
2 iv	5	0.58	4.71
2 iv	10	0.58	7.01
2 iv	15	0.58	5.58
2 iv	30	0.58	2.51
2 iv	60	0.58	0.59
2 iv	180	0.58	0.10
2 iv	360	0.58	0.10
3 iv	5	0.58	4.21
3 iv	10	0.58	4.70
3 iv	15	0.58	5.58
3 iv	30	0.58	1.73
3 iv	60	0.58	0.63
3 iv	180	0.58	0.10
3 iv	360	0.58	0.10

Table 47 and Table 48 show plasma concentrations [$\mu\text{g/mL}$] of CPD11 in 2 mice after ip and 2 mice after sc administration of 0.75 mg CPD11. Blood samples at 4 (ip) or 3 (sc) different time points were drawn. At this point it should be noted, once again, that mice within the ip group and mice within the sc group were treated with CPD11, dissolved in different solvents. The mice in the ip group reached their highest plasma concentrations at time points 6 and 34 min and mice in the sc group at time points 17 and 26 min, respectively. After 90 to 120 min $\sim 0.55 \mu\text{g/mL}$ of CPD11 were quantifiable in the mouse ip group. Whereas, in the sc group,

~60 min after study drug administration, ~0.15 µg/mL of CPD11 were detectable in the plasma samples.

Table 47: Plasma concentrations [µg/mL] of CPD11 after ip administration in mice

Mouse intraperitoneal CPD11			
Mouse ID	time [min]	Dose [mg]	CPD11 [µg/mL]
0 ip	6	0.75	0.48
0 ip	34	0.75	0.93
0 ip	61	0.75	0.78
0 ip	120	0.75	0.50
2 ip	6	0.75	2.55
2 ip	26	0.75	1.60
2 ip	59	0.75	1.06
2 ip	90	0.75	0.61

Table 48: Plasma concentrations [µg/mL] of CPD11 after ip administration in mice

Mouse subcutaneous CPD11			
Mouse ID	time [min]	Dose [mg]	CPD11 [µg/mL]
1 sc	26	0.75	0.79
1 sc	46	0.75	0.43
1 sc	59	0.75	0.11
3 sc	17	0.75	0.37
3 sc	25	0.75	0.81
3 sc	60	0.75	0.21

Plasma Concentration versus Time Curves

Figure 47 shows plasma concentration [$\mu\text{g}/\text{mL}$] versus time [min] profiles obtained from rats after iv and ip administration of 20 mg CPD11.

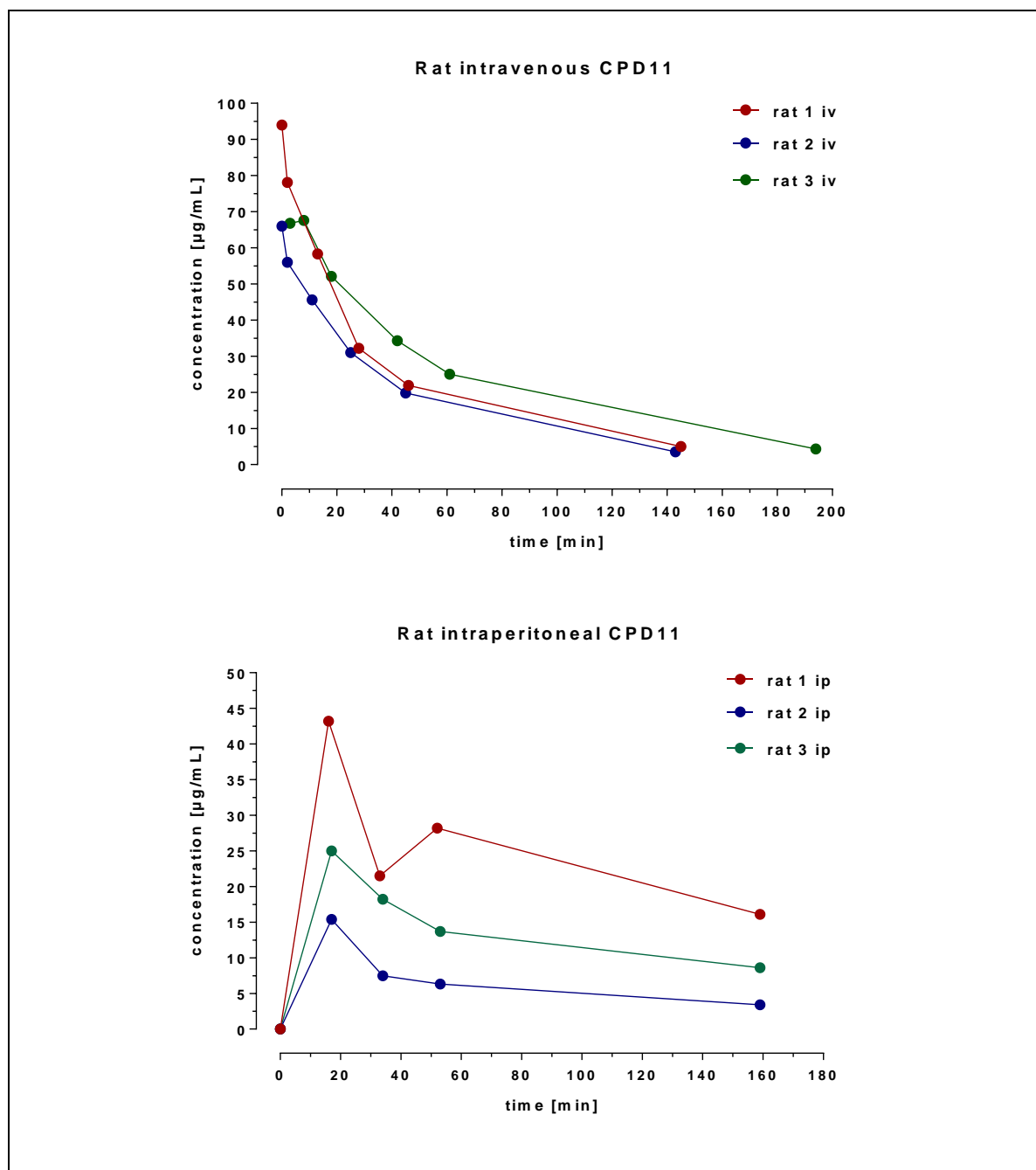


Figure 47: Plasma concentration [$\mu\text{g}/\text{mL}$] versus time [min] curves of CPD11 in rats

As illustrated in Figure 47, the concentration versus time curves of rat 1-3 iv show minimal variability, homogenous curves and represents a one-compartment model. Due to the small amount of blood samples, PK calculations were performed for a non-compartment model.

Figure 48 shows plasma concentration [$\mu\text{g/ml}$] versus time [min] profiles obtained from 3 mice-groups ($n = 24$) after iv administration of 0.58 mg CPD11. The concentration versus time curves were observed to be akin in rat and mice samples.

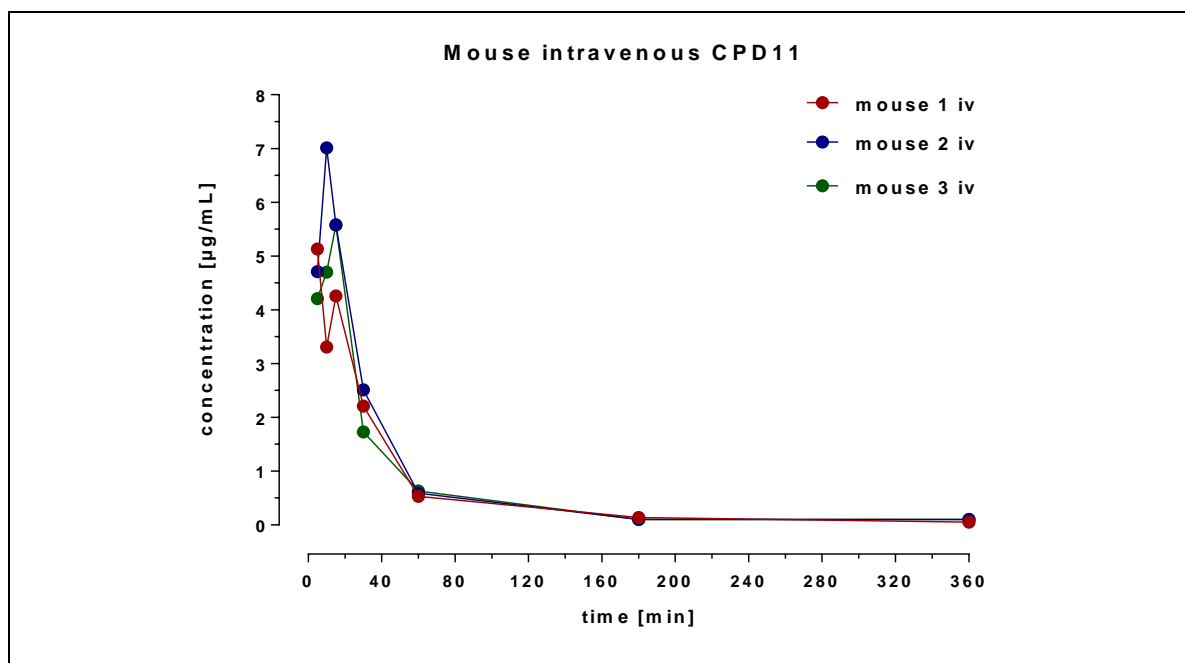


Figure 48: Plasma concentration [$\mu\text{g/mL}$] versus time [min] curves of CPD11 in mice

Figure 49 shows plasma concentration [$\mu\text{g/ml}$] versus time [min] profiles obtained from mice after ip and sc administration of 0.75 mg CPD11.

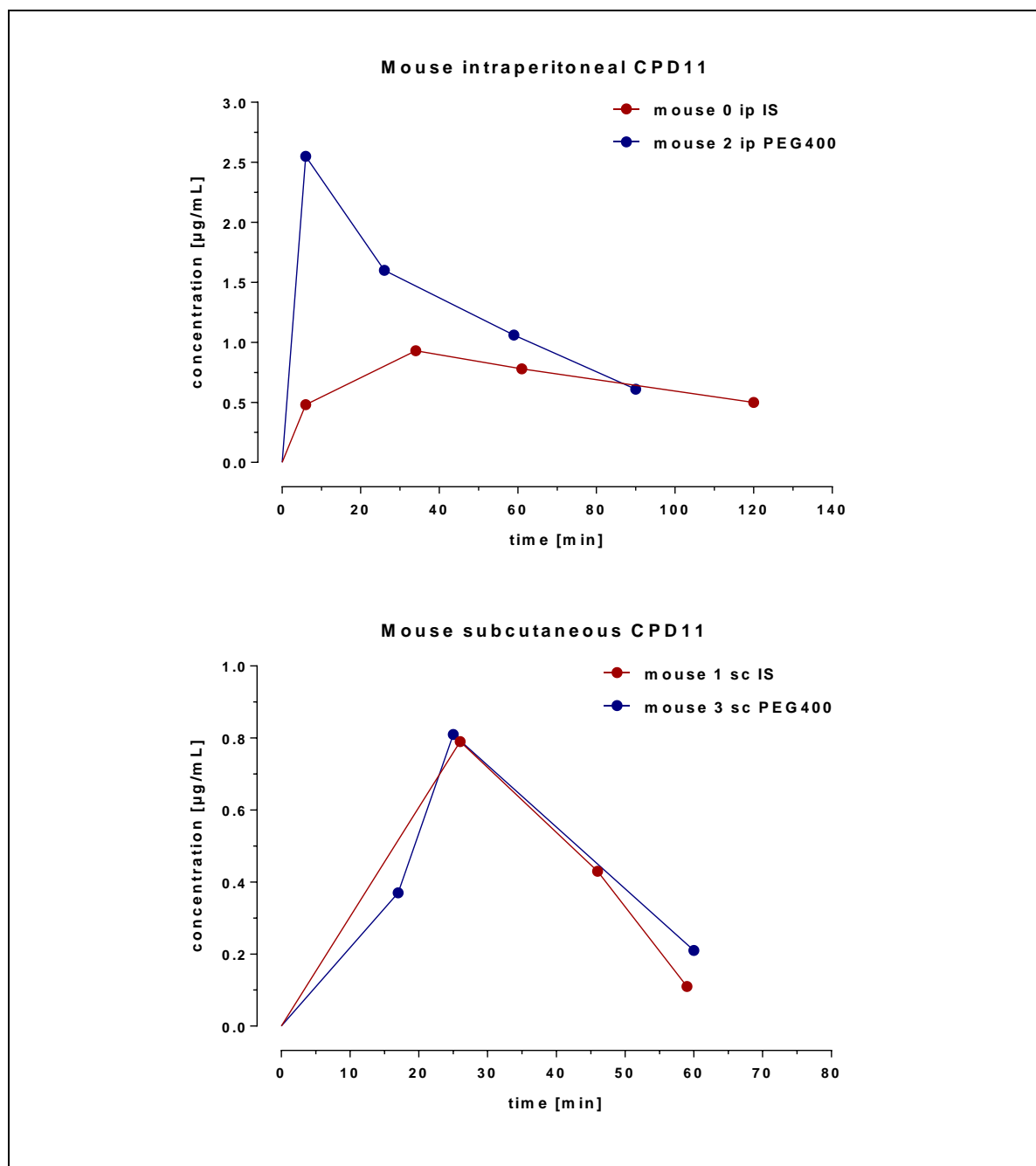


Figure 49: Plasma concentration [$\mu\text{g/mL}$] versus time [min] curves of CPD11 in mice

As can be seen in Figure 49 plasma concentration versus time curves of mice sc hardly differ from each other, whereas mice ip plasma concentration versus time curves show significant differences.

4.4.4 Pharmacokinetic Parameters

The following tables contain the PK data of CPD3 and CPD11. Plasma concentration versus time data were fitted with the software Phoenix WinNonlin Version 6.1 or Kinetica Software Version 5.1 using a NCA PK model. For WinNonlin, “model 200” was used for extravascular calculations and “model 201” for intravasal calculations. For Kinetica, the “NCA iv bolus” and “NCA extravascular” models were utilized.

The PK parameters of CPD3 and CPD11 are depicted in Table 49 and Table 50. For a better overview PK parameters were reduced to ten parameters.

As shown in Table 49 for CPD3, C_{\max} was reached within 2 and 3 min in the rat iv group, whereas in the rat ip group, the mean C_{\max} was attained after 31 min. The average C_{\max} in rats iv was 25.9 $\mu\text{g/mL}$, while this value was 4.6 $\mu\text{g/mL}$ in rats ip. The MRT in rats iv was 38 min, as compared with 753 min in rats ip. The CL in rats iv ranged from 11.1 to 21.1 mL/min, and it ranged from 3.6 to 33.5 mL/min rats ip. The mean $t_{1/2\text{el}}$ was calculated to be 55 min in rats iv and 106 min in rats ip (mean values).

Table 50 indicates clear differences in the PK parameters of rats iv and ip after CPD11 administration. C_{\max} was reached within ~3 min in the rat iv group and after 17 min in the rat ip group. The average C_{\max} in iv rats was 75.90 $\mu\text{g/mL}$, while this value in ip rats was 27.87 $\mu\text{g/mL}$. The MRT in iv rats ranged from 52 to 68 mL/min, while it ranged from 160 to 261 mL/min in ip rats and from 60 to 71 mL/min in iv mice. The mean $t_{1/2\text{el}}$ was 44 min in the rat iv group, 135 min in the rat ip group and 71 min in the mouse iv group. The C_{\max} was reached within approximately 10 min in the mouse iv group.

As already mentioned, the mouse 0 ip and mouse 1 sc received CPD11 dissolved in IS and PBS, whereas the mouse 2 ip and mouse 3 sc received the same dose of CPD11 dissolved in PEG400 and PBS. The C_{\max} values ranged from 0.78 to 2.55 $\mu\text{g/mL}$, and the T_{\max} values ranged from 6 to 34 min. The average $t_{1/2\text{el}}$ was calculated to be 71 min in the mouse ip group compared with 14.5 min in the mouse sc group.

RESULTS

CPD3

Table 49: NCA PK parameters of CPD3 in rats

Species & ID	Administration	Dose	C _{max}	T _{max}	AUC _{last}	AUC _{tot}	t _{1/2el}	MRT	CL	Vd	C _{last}	T _{last}
		mg	µg/mL	min	µg/mL*min	µg/mL*min	min	min	mL/min	mL	µg/mL	min
Rat 1 iv	intravenous	12.5	22.40	3	490	592	116	28	21.1	1665.4	0.60	156
Rat 2 iv	intravenous	20	29.53	2	1956	1998	27	44	10.0	470.3	1.08	159
Rat 3 iv	intravenous	20	25.87	2	1782	1806	23	43	11.1	497.3	0.71	157
Mean	intravenous	17.5	25.93	2	1409	1465	55	38	14.1	877.7	0.80	157
SD	intravenous	4.3	3.6	0.6	801.0	762.5	52.6	9.1	6.1	682.4	0.3	1.5
CV [%]	intravenous	24.7	13.7	24.7	56.8	52.0	95.0	24.0	43.6	77.8	31.4	1.0
Rat 1 ip	intraperitoneal	20	6.40	37	741	1269	116	181	15.8	2854.8	3.20	160
Rat 2 ip	intraperitoneal	20	3.90	37	400	598	87	146	33.5	4868.3	1.50	160
Rat 3 ip	intraperitoneal	20	3.40	20	404	5611	116	1933	3.6	6891.1	2.90	161
Mean	intraperitoneal	20	4.60	31	515	2492	106	753	17.6	4871.4	2.53	160
SD	intraperitoneal	0	1.6	9.8	195.7	2721.5	16.7	1022.1	15.0	2018.2	1.0	1.0
CV [%]	intraperitoneal	0	35.2	31.3	38.0	109.2	15.7	135.7	85.5	41.4	35.818	0

RESULTS

CPD11

Table 50: NCA PK parameters of CPD11 in rats and mice

Species & ID	Administration	Dose	C _{max}	T _{max}	AUC _{last}	AUC _{tot}	t _{1/2el}	MRT	CL	Vd	C _{last}	T _{last}
		mg	µg/mL	min	µg/mL*min	µg/mL*min	min	min	mL/min	mL	µg/mL	min
Rat 1 iv	intravenous	20	94.00	0	3188	3504	43	56	5.7	320.3	4.98	145
Rat 2 iv	intravenous	20	66.00	0	2534	2729	39	52	7.3	404.8	3.55	143
Rat 3 iv	intravenous	20	67.60	8	4242	4527	50	68	4.4	302.2	4.30	194
Mean	intravenous	20	75.90	3	3321	3587	44	59	5.8	342.4	4.28	161
SD	intravenous	0	15.7	4.6	861.4	901.7	5.6	8.5	1.5	54.7	0.7	28.9
CV [%]	intravenous	0	20.7	173.2	25.9	25.1	12.7	14.4	25.0	16.0	16.7	18.0
Rat 1 ip	intraperitoneal	20	43.02	16	3845	8523	173	261	2.3	613.3	16.10	159
Rat 2 ip	intraperitoneal	20	15.40	17	947	1498	116	160	13.4	2139.5	3.40	159
Rat 3 ip	intraperitoneal	20	25.00	17	2039	3590	116	188	5.6	1047.1	8.60	159
Mean	intraperitoneal	20	27.87	17	2277	4537	135	203	7.1	1266.6	9.37	159
SD	intraperitoneal	0	14.1	0.6	1464.0	3607.0	33.0	52.3	5.7	786.4	6.4	0.0
CV [%]	intraperitoneal	0	50.7	3.5	64.3	80.0	24.4	25.7	79.8	62.1	68.2	0.0
Mouse 1 iv	intravenous	0.58	5.13	5	186	191	87	71	3.0	215.1	0.05	360
Mouse 2 iv	intravenous	0.58	7.01	10	221	225	58	60	2.6	155.3	0.10	360
Mouse 3 iv	intravenous	0.58	5.58	15	193	198	69	69	2.9	202.0	0.10	360
Mean	intravenous	0.58	5.91	10	200	205	71	67	2.8	190.8	0.08	360
SD	intravenous	0	1.0	5.0	19.0	17.6	14.6	5.8	0.2	31.4	0.0	0.0
CV [%]	intravenous	0	16.6	50.0	9.3	8.6	20.5	8.6	8.3	16.5	34.6	0.0
Mouse 0 ip	intraperitoneal	0.75	0.93	34	88	155	99	143	4.8	689.7	0.50	120
Mouse 2 ip	intraperitoneal	0.75	2.55	6	117	154	43	64	4.9	313.3	0.61	90
Mouse 1 sc	subcutaneous	0.75	0.78	26	25	27	12	36	28.0	1011.3	0.11	59
Mouse 3 sc	subcutaneous	0.75	0.81	25	26	30	17	41	24.7	1020.3	0.21	60

4.5 In vitro and in vivo Topic Studies of CPD11

4.5.1 Calibration curves

Calibration Curve of Caffeine in PBS

The calibration curve of caffeine in PBS was linear over the range of 1.25-20.0 $\mu\text{g/mL}$, prepared by plotting peak area against sample concentration (Figure 50), with a correlation coefficient >0.9989 . The slope was 125.7 ± 2.365 , as shown in Table 51.

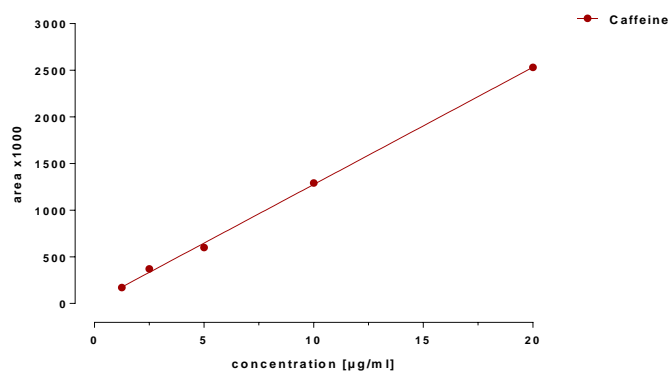


Figure 50: Calibration curve of caffeine in PBS

Table 51: Regression parameters of the calibration curve of caffeine in PBS

Caffeine	
Best-fit values	
Slope	125.7 ± 2.365
Y-intercept when X=0.0	18.79 ± 24.42
X-intercept when Y=0.0	-0.1496
1/slope	0.007958
95% Confidence Intervals	
Slope	118.1 to 133.2
Y-intercept when X=0.0	-58.90 to 96.48
X-intercept when Y=0.0	-0.8048 to 0.4488
Goodness of Fit	
R square	0.9989
Sy.x	36.07
Is slope significantly non-zero?	
F	2822
DFn, DFd	1.000, 3.000
P value	< 0.0001
Deviation from zero?	Significant
Data	
Number of X values	5
Maximum number of Y replicates	1
Total number of values	5
Number of missing values	0
Equation	
	$Y = 125.7 * X + 18.79$

Calibration Curve of CPD11 in PBS

The calibration curve of CPD11 in PBS was linear over the range of 1.25-20.0 $\mu\text{g/mL}$ (Figure 51). The slope was 31.72 ± 1.532 . The regression parameters are listed in Table 52.

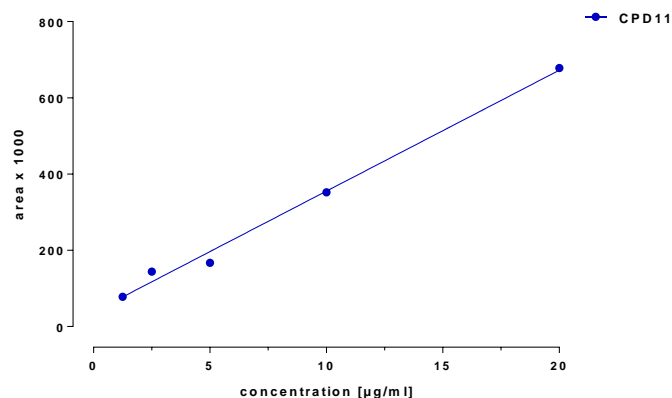


Figure 51: Calibration curve of CPD11 in PBS

Table 52: Regression parameters of the calibration curve of CPD11 in PBS

CPD11	
Best-fit values	
Slope	31.72 ± 1.532
Y-intercept when X=0.0	38.00 ± 15.82
X-intercept when Y=0.0	-1.198
1/slope	0.03153
95% Confidence Intervals	
Slope	26.84 to 36.59
Y-intercept when X=0.0	-12.33 to 88.32
X-intercept when Y=0.0	-3.178 to 0.3488
Goodness of Fit	
R square	0.993
Sy.x	23.36
Is slope significantly non-zero?	
F	428.6
DFn, DFd	1.000, 3.000
P value	0.0002
Deviation from zero?	Significant
Data	
Number of X values	5
Maximum number of Y replicates	1
Total number of values	5
Number of missing values	0
Equation	
	$Y = 31.72 * X + 38.00$

4.5.2 LOQ & LOD

LOQ of CPD11 in PBS was 0.06 $\mu\text{g/mL}$ and LOD was 0.03 $\mu\text{g/mL}$ and in plasma LOQ was 0.07 $\mu\text{g/mL}$ and LOD was 0.035 $\mu\text{g/mL}$. For detailed results please refer to section 4.1.2.

4.5.3 In vitro EpiDerm™ Model

Permeation of Caffeine

Caffeine was used in this in vitro model for validation purposes. The results are shown in Figure 52. For better resolution, the chromatograms were truncated; therefore the isocratic profile is not visible.

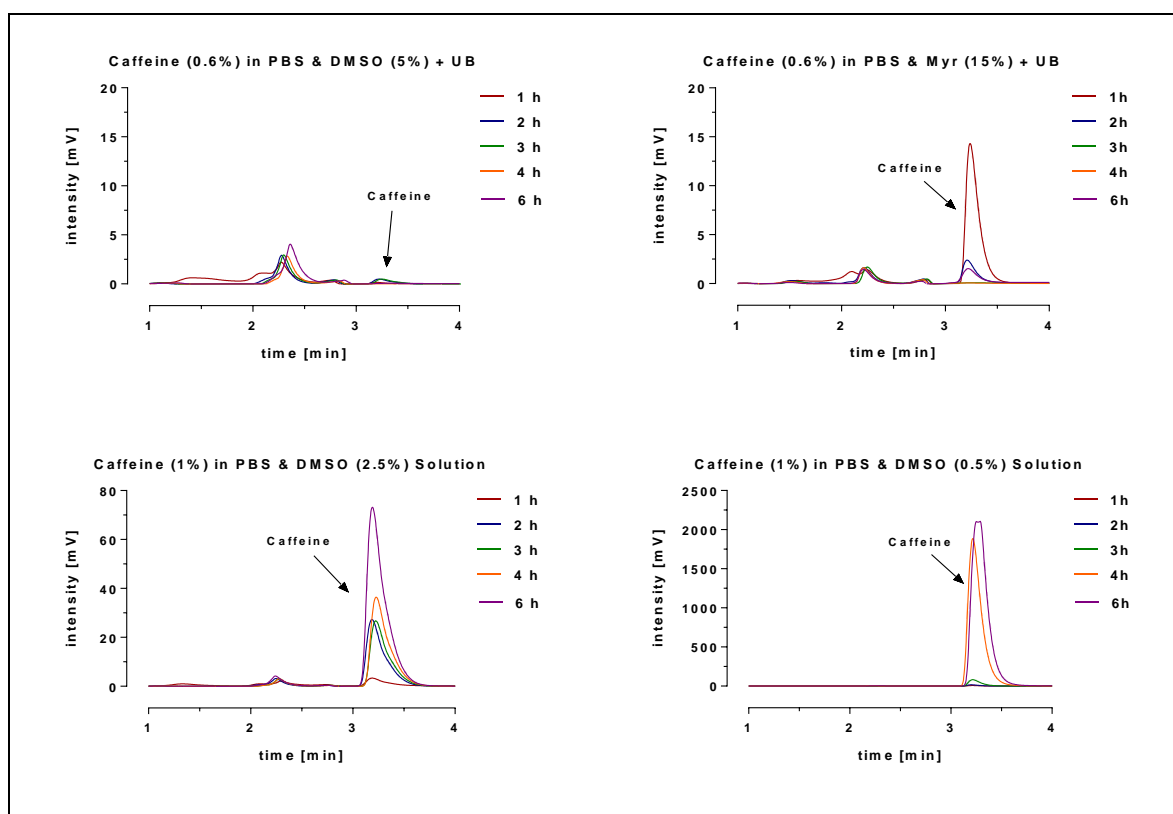


Figure 52: Chromatograms of caffeine in the EpiDerm™ skin model.

Figure 52 depicts the permeation of caffeine and shows, as anticipated, that caffeine permeates through the EpiDerm™ skin model regardless of the formulation used.

Furthermore, these results showed that the EpiDerm™ model could be used with different formulations and solvents, as drugs are able to permeate in solutions and as ointment bases, e.g., ultrabase through the skin.

Table 53 provides an overview of the peak areas of caffeine in different formulations, which were later used to calculate the permeated active substance proportion. For the purpose of better presentation, the peak areas were cumulated, and the data are also shown in Table 53.

Table 53: Peak areas x 1000 and peak areas x 1000 accumulation of the different caffeine formulations

	Solution		Ultrabase	
	Caffeine (1%) in PBS & DMSO (2.5%)	Caffeine (1%) in PBS & DMSO (0.5%)	Caffeine (0.6%) in PBS & DMSO (5%) + UB	Caffeine (0.6%) in PBS & Myr (15%) + UB
time [h]	area x 1000			
1	38	60	12	127
2	339	145	9	20
3	333	724	10	6
4	451	17195	13	5
6	906	24064	7	12
time [h]	Cumulation: area x 1000			
1	38	60	12	127
2	377	205	21	147
3	710	929	31	153
4	1161	18124	44	158
6	2067	42188	51	170

Figure 53 shows the logarithmic presentation of the accumulation results. These results clarify that caffeine in the form of a solution can permeate the skin better than caffeine incorporated in an ointment base. Furthermore, the formulations with a lower DMSO content showed greater permeation. This relationship initially appeared incomprehensible because DMSO is usually a penetration catalyst. However, it should be noted that a high concentration of DMSO may destroy the cells of the EpiDerm™ skin model and could result in an alteration of the permeation behaviour.

RESULTS

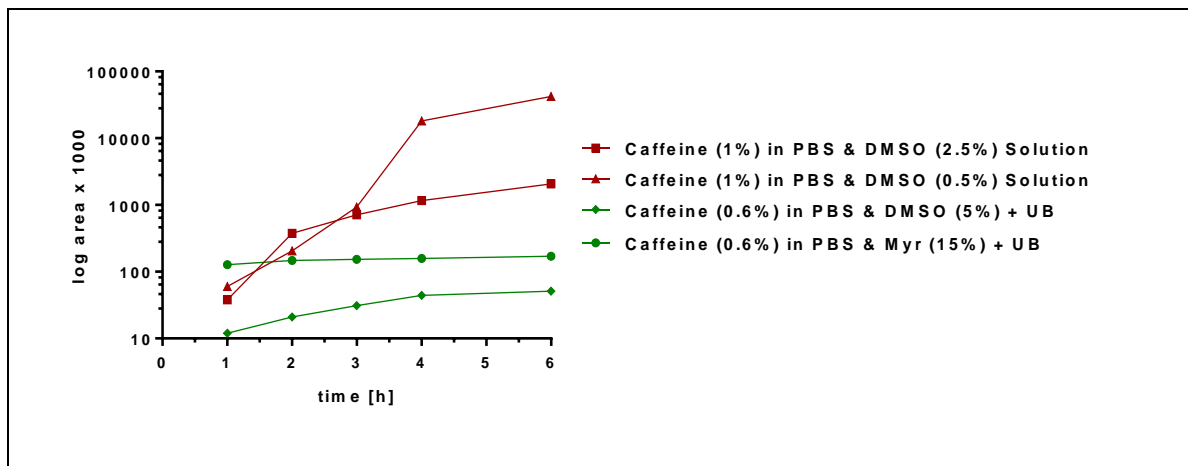


Figure 53: Logarithmic presentation of caffeine accumulation results

Table 54 depicts the proportion of caffeine in $\mu\text{g/mL}$, which permeates through the skin membrane.

Table 54: Permeated proportions of caffeine in different formulations in $\mu\text{g/mL}$

	Solution		Ultrabase	
	Caffeine (1%) in PBS & DMSO (2.5%)	Caffeine (1%) in PBS & DMSO (0.5%)	Caffeine (0.6%) in PBS & DMSO (5%) + UB	Caffeine (0.6%) in PBS & Myr (15%) + UB
time [h]	$\mu\text{g/mL}$			
1	0.302	0.477	0.095	1.010
2	2.697	1.154	0.072	0.160
3	2.649	5.760	0.080	0.048
4	3.588	136.794	0.103	0.040
6	7.208	191.44	0.056	0.095

Figure 54 shows the concentration versus time curves of different caffeine concentrations in $\mu\text{g/mL}$ in different formulations.

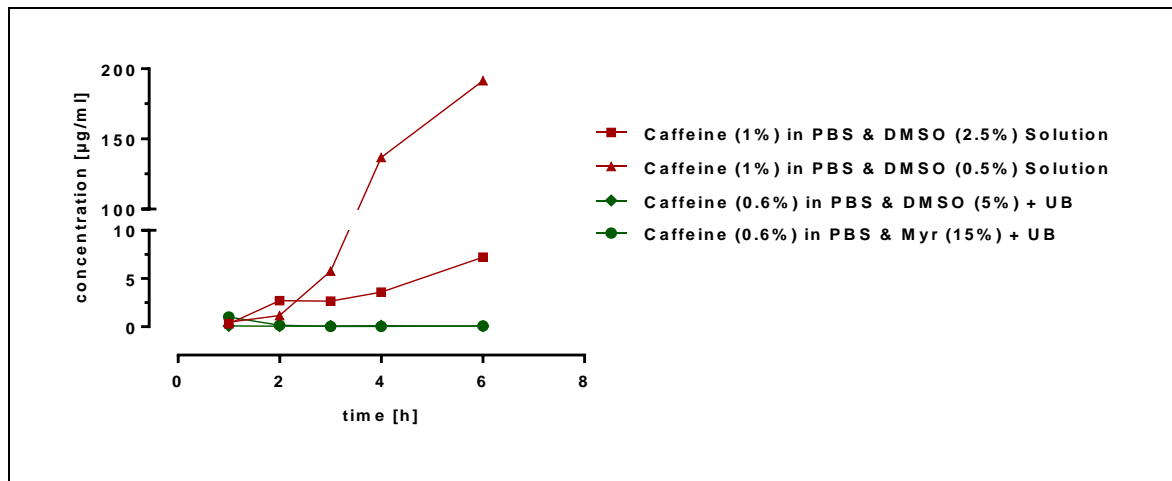


Figure 54: Concentration versus time curves of caffeine in various formulations [$\mu\text{g/mL}$]

Blank Samples

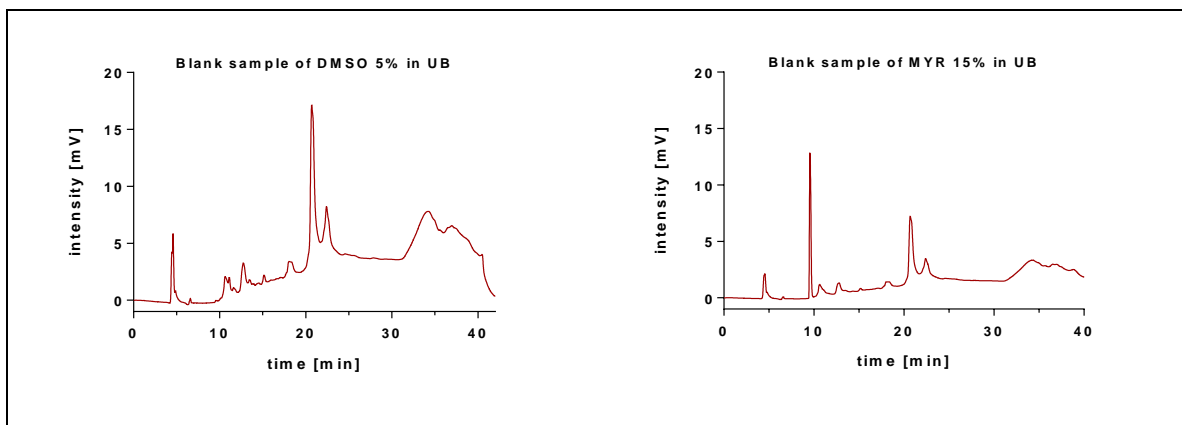


Figure 55: Chromatograms of blank samples

As the formulations of both blank samples did not contain any compounds, the peaks that appeared were the results of the solvents and bases and/or of the PBS (acceptor solution). To accurately assign CPD11 peaks in the chromatograms, an analysis of these two blank samples was performed with different solvent/base concentrations (Figure 55).

Permeation of CPD11

Figure 56 shows the chromatograms of 1% CPD11 diluted in 15% myristyl alcohol in 5% DMSO incorporated in ultrabase. Additionally, the figure shows the chromatogram of 0.01% CPD11 dissolved in 0.5% DMSO and further diluted in PBS.

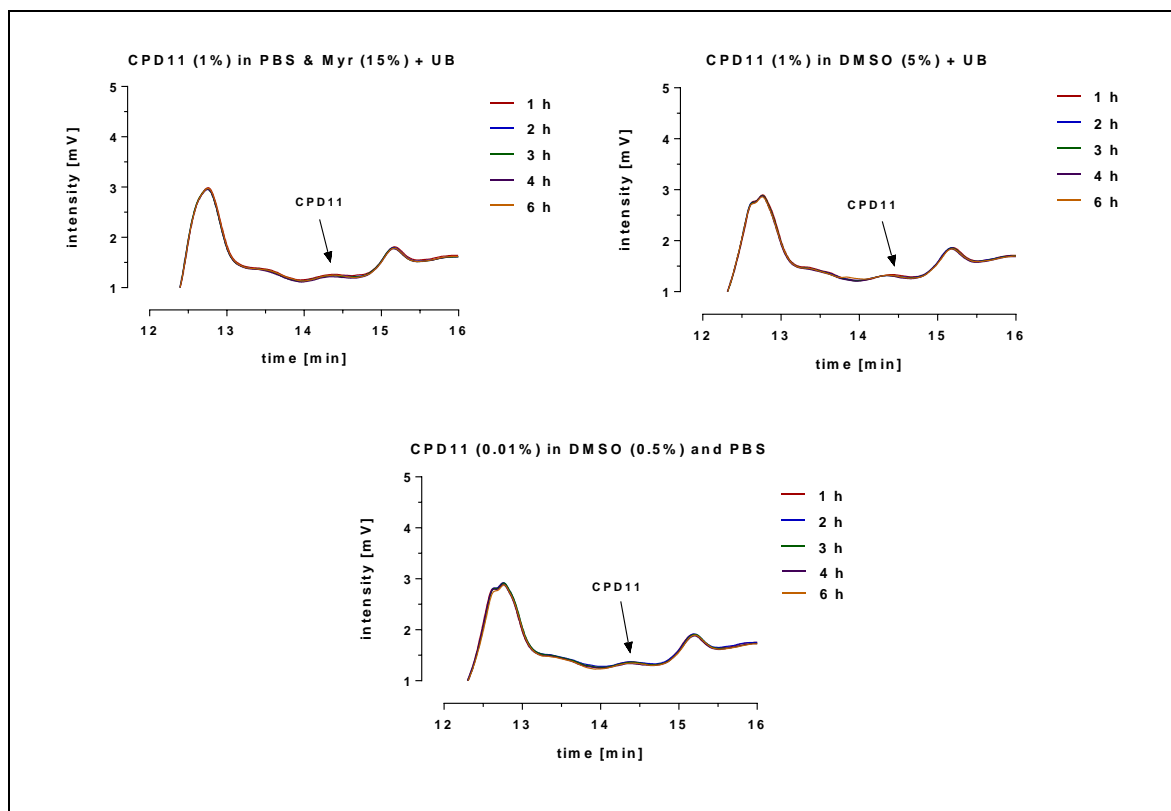


Figure 56: Chromatograms of CPD11 in EpiDerm™ model with different formulations

Figure 57 shows two different chromatograms from the test experiment. Chromatogram A illustrates perforated skin (skin number 7), where after the first test run, CPD11 (1%) diluted in 5% DMSO and ultrabase was reapplied onto the skin. Chromatogram B shows skin perforated from the beginning and the subsequent application of CPD11 (1%) diluted in 0.5% DMSO and PBS. For better resolution, the chromatograms were truncated; the gradient profile is not shown.

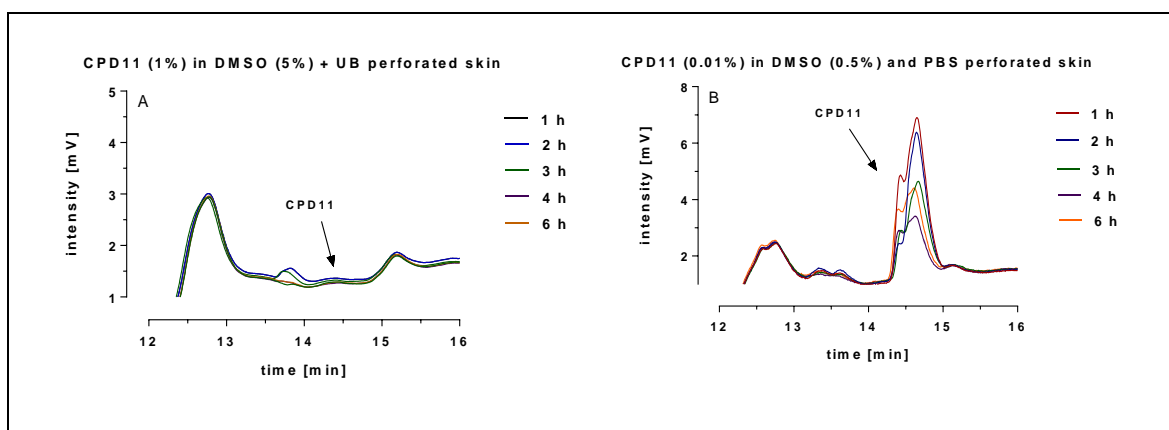


Figure 57: Chromatograms of CPD11 on perforated skin in the EpiDerm™ model

Table 55 gives an overview of the performed EpiDerm™ model results. As shown in this table, CPD11 concentrations throughout the intact skin model were above the LOQ. For the perforated skin experiments, traces of CPD11 were only quantifiable in skin numbers 24-26. For the test experiments, in which one sample was taken after 6 h, CPD11 was also not detectable (skin numbers 6, 10 and 14).

Table 55: Overview of the CPD11 concentration [$\mu\text{g/mL}$] results in the in vitro EpiDerm™ model

Skin No.	Conc. [%]	Solvent	Base	Skin	1 h [$\mu\text{g/mL}$]	2 h [$\mu\text{g/mL}$]	3 h [$\mu\text{g/mL}$]	4 h [$\mu\text{g/mL}$]	6 h [$\mu\text{g/mL}$]	1 x 6 h [$\mu\text{g/mL}$]
3	1	DMSO (2.5 %)	Ultrabase	intact	LOQ	LOQ	LOQ	LOQ	LOQ	nd
4	1	DMSO (2.5 %)	Ultrabase	intact	LOQ	LOQ	LOQ	LOQ	LOQ	nd
5	1	DMSO (2.5 %)	Ultrabase	intact	LOQ	LOQ	LOQ	LOQ	LOQ	nd
6	1	DMSO (2.5 %)	Ultrabase	intact	nd	nd	nd	nd	nd	LOQ
7	1	DMSO (5 %)	Ultrabase	intact	LOQ	LOQ	LOQ	LOQ	LOQ	nd
8	1	DMSO (5 %)	Ultrabase	intact	LOQ	LOQ	LOQ	LOQ	LOQ	nd
9	1	DMSO (5 %)	Ultrabase	intact	LOQ	LOQ	LOQ	LOQ	LOQ	nd
10	1	DMSO (5 %)	Ultrabase	intact	nd	nd	nd	nd	nd	LOQ
11	1	Myristyl alcohol (15 %)	Ultrabase	intact	LOQ	LOQ	LOQ	LOQ	LOQ	nd
12	1	Myristyl alcohol (15 %)	Ultrabase	intact	LOQ	LOQ	LOQ	LOQ	LOQ	nd
13	1	Myristyl alcohol (15 %)	Ultrabase	intact	LOQ	LOQ	LOQ	LOQ	LOQ	nd
14	1	Myristyl alcohol (15 %)	Ultrabase	intact	nd	nd	nd	nd	nd	LOQ
15	0.01	PBS & DMSO (0.5 %)	Solution	intact	LOQ	LOQ	LOQ	LOQ	LOQ	nd
16	0.01	PBS & DMSO (0.5 %)	Solution	intact	LOQ	LOQ	LOQ	LOQ	LOQ	nd
17	0.01	PBS & DMSO (0.5 %)	Solution	intact	LOQ	LOQ	LOQ	LOQ	LOQ	nd
18	0.01	PBS & DMSO (0.5 %)	Solution	intact	LOQ	LOQ	LOQ	LOQ	LOQ	nd
19	0.01	PBS & DMSO (0.5 %)	Solution	intact	LOQ	LOQ	LOQ	LOQ	LOQ	nd
3	1	DMSO (2.5 %)	Ultrabase	perforated	nd	LOQ	LOQ	LOQ	LOQ	nd
7	1	DMSO (5 %)	Ultrabase	perforated	nd	LOQ	LOQ	LOQ	LOQ	nd
24	0.01	PBS & DMSO (0.5 %)	Solution	perforated	2.90	0.50	0.66	LOQ	20.21	nd
25	0.01	PBS & DMSO (0.5 %)	Solution	perforated	2.43	LOQ	LOQ	LOQ	LOQ	nd
26	0.01	PBS & DMSO (0.5 %)	Solution	perforated	2.33	2.21	1.04	0.32	0.79	nd

(nd = note done)

4.5.4 In vivo Model

Figure 58 shows the chromatograms of guinea pigs 4 and 6. These represented negative control samples that served to identify whether CPD11 penetrated through the skin and would therefore be detected in the plasma. The peaks in these chromatograms could be due to the anaesthetics, as the animals were narcotized, as previously described in section 3.6.4.

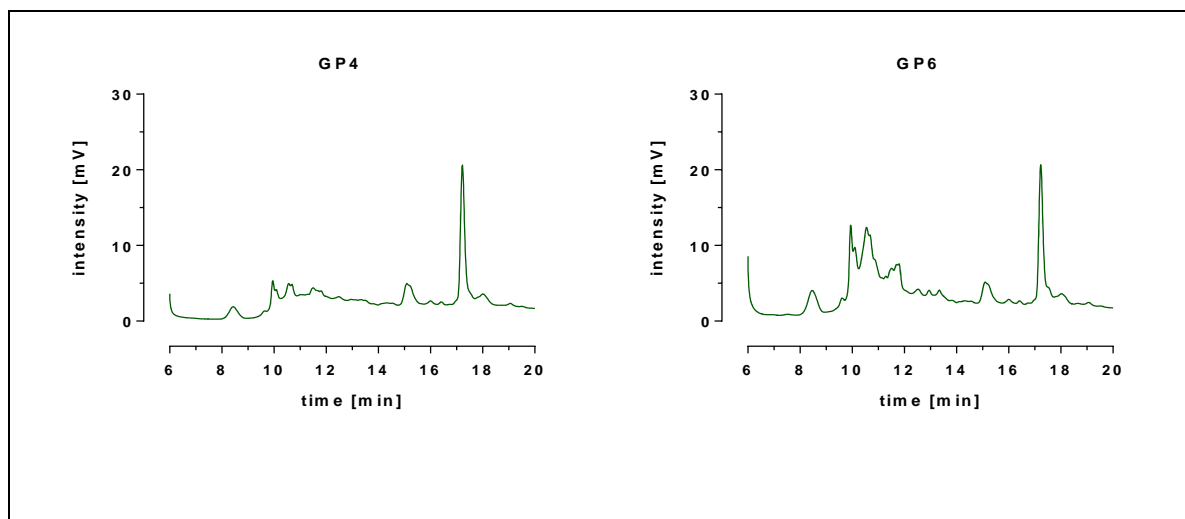


Figure 58: Chromatograms of negative control guinea pigs number 4 and 6 samples

The chromatograms of GP1, GP2 and GP3 are depicted in Figure 59. The guinea pigs were treated with different formulations, which contained 1% CPD11.

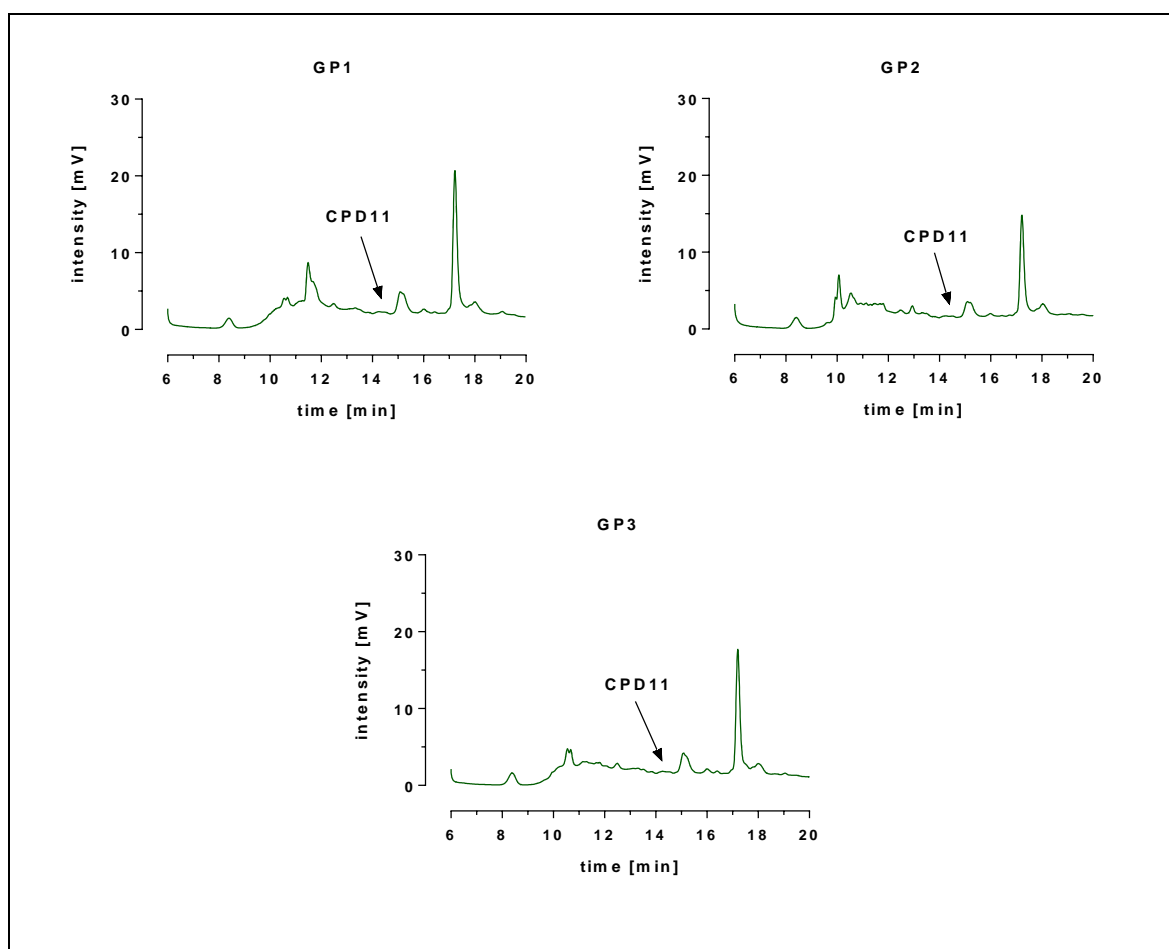


Figure 59: Chromatograms of guinea pigs number 1-3 plasma samples

Furthermore, it was very important for these investigations that the peak of CPD11 did not overlap with the peaks of the anaesthetics. As seen in Figure 58 and Figure 59, no peak overlapping occurred.

5 Discussion

5.1 Validation

The first RP-HPLC method, validated for GLP-ICH, confirmed the analysis of the given group of new antibacterial naphthoquinones Figure 1 a-h). While the complete validation of the method was implemented with only the most active and non-toxic lead compound CPD11, only a partial validation was performed for an extended set of seven test compounds (CPD3, CPD5, CPD6, CPD7, CPD10, CPD13, CPD17).

This low-cost analytical method is simple and robust, assuring quantification in various biological matrices, such as plasma, hepatocyte cell cultures and liver tissue. Showing a relatively low LOQ, the method was deemed appropriate for the determination of the analyte, even at low plasma concentrations, which is especially important when predicting the compound PK. The analytical results showed repeatable recoveries within a specific biological matrix, but a substantial difference appeared when comparing recoveries in different matrices. The two-thirds decrease of CPD11 in crude liver extracts might occur due to the intense and irreversible binding of the compound to liver tissue proteins or other biopolymers.

Furthermore, the aim was to keep the sample preparation as rapid and as simple as possible by using protein precipitation, considering that RP-HPLC methods usually require more time and/or expensive procedures, such as liquid-liquid or solid-phase extraction, prior to analysis. To our knowledge, this is the first report presenting a fully validated analytical assay for the quantification of this class of compounds. In the pharmaceutical industry in particular, where investigations of several compounds are required, it would be of great benefit, saving both time and costs, to use the same validated method for all compounds instead of developing new procedures for each compound. Hence, the presented method could be of great advantage for scientific institutions or the pharmaceutical industry when working with similar or related derivatives.

5.2 Binding and Distribution Experiments

In this study, a matrix-free method was applied for the prediction of various relevant PK values, explicit PPB, AGP, HSA, intestinal absorption and microsomal binding. This method, also referred to as the TRANSIL^{XL} kit, determines the binding of compounds by estimating their affinity to different immobilized biological matrices. Thirty-one new chemical entities from SeaLife were investigated using this method. Moreover, for validation purposes, already established drugs with diverse pharmacological and physicochemical properties were analysed using the same test system under identical conditions. For additional information on drug properties, PK calculations were performed for 26 SeaLife compounds by utilizing the ADMET Predictor software.

Some available methods already enable the measurement of PPB. Among these, the most common approaches are equilibrium dialysis, column equilibrium gel filtration and ultrafiltration using tubes equipped with special membranes. According to previous publications and studies, equilibrium dialysis seems to be the gold standard because the method is easy and inexpensive. These methods have a disadvantage because they require saturation of the membrane with the tested drug to avoid false results resulting from binding of the compound to the membrane or vial instead of the protein and they are also time-consuming. Considering the chemical properties of the investigated compounds, we found the TRANSIL^{XL} system to be the most convenient model due to the high insolubility of certain compounds in PBS. TRANSIL^{XL} offers the great advantage of dissolving the test compounds in diluted DMSO, which leads to adequate dissolved amounts of the drug for further binding experiments. Nonetheless, it is important not to exceed a certain amount of DMSO, which could lead to underestimation of the binding results and destruction of the membranes. [50, 58]

Therefore, the TRANSIL^{XL} system appears to have certain advantages compared to the other methods. Protein and/or tissue binding occurs within milliseconds, and an equilibrium is reached a few minutes after starting the incubation. Separation of unbound from bound drug is achieved by centrifugation, which is followed by an accurate, selective and sensitive quantitation method (RP-HPLC). Incubating the same concentration of drug in 6 wells containing increasing amounts of immobilized biological phase enables a direct correlation of the binding between drug and binding molecule to be calculated.

Most of the 31 SeaLife compounds investigated show high PPB values ranging from 85 up to 99% (Table 18), possibly due the aqueous insolubility. Comparison with the data obtained from the ADMET Predictor software confirmed our in vitro results, with only the values obtained from CPD4, CPD16 and CPD25 showing higher discrepancies, which may be related to solubility problems of these compounds. Although some established drugs have similarly high PPB values (cardiac glycosides, thyroid preparations, irinotecan, docetaxel, erlotinib, psychotropic drugs), a high binding rate decreases the systemic bioavailability of the drug in the blood. This condition would lead to a high Vd, which would ultimately require the administration of high doses of the drug in order to obtain plasma concentrations above the threshold. High doses of a drug often are associated with undesired and toxic side effects. Thus, future strategies will focus on improving the water solubility of the most SeaLife compounds without losing their pharmacological activity, which might lead to lower PPB and Vd values. Furthermore, recent studies have demonstrated that newly developed antibiotics have distinctly lower PPB values (<90%), perhaps because drugs showing high PPB require a higher dose to achieve their minimal inhibitory concentration (MIC). The data obtained from the TRANSIL^{XL} method estimated a PPB of 93.9% for erlotinib, which is in accordance with the current literature. The PPB of linezolid was predicted to be 44.9%, which is approximately 15% higher than described in the literature. [87, 88, 89, 90]

fHSA [%] values ranged from 82.5 to 99.8% and were predicted to be rather high. Whereas fAGP [%] results were approximately between 1.5 and 96.5%, showing a high variety of the binding rates within the SeaLife compounds (Table 19). Additionally, the AGP and HSA f_u values of the test compounds were correlated with each other. Figure 60 illustrates a close correlation between the two protein fractions with most of the test compounds within the 95% confidence interval ($r = 0.78$). Only three compounds, CPD26, CPD29 and CPD30, were far from the regression line.

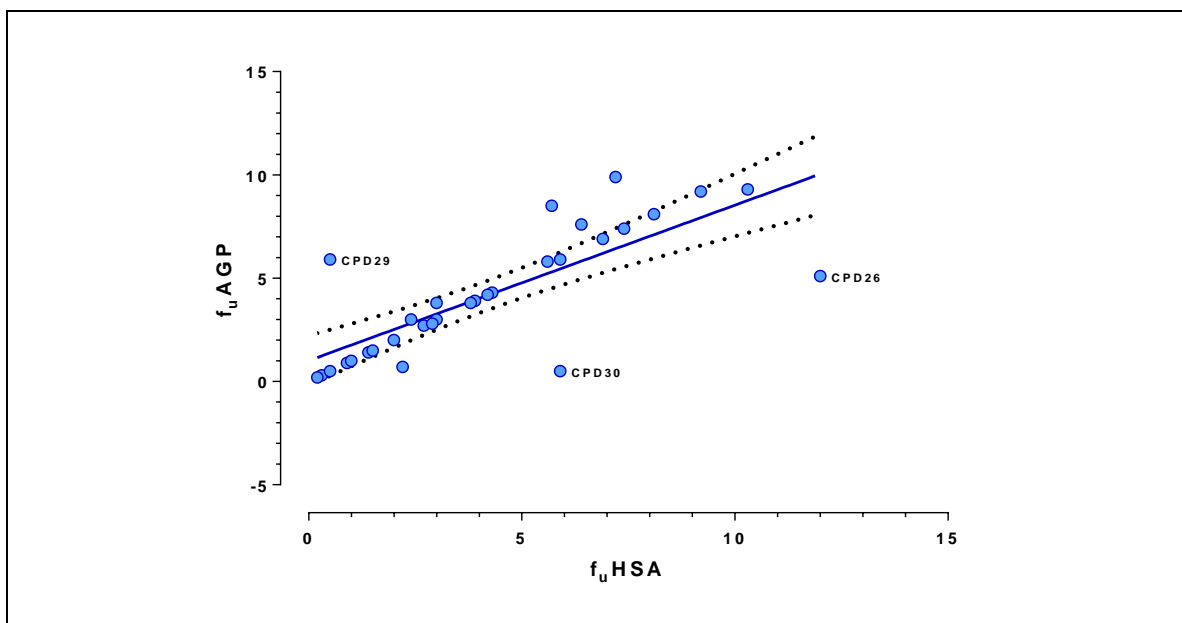


Figure 60: Correlation of f_u HSA and f_u AGP values

The f_u values of the test compounds were below 10% for AGP and below 13% for HSA, giving evidence of strong protein binding. The highest binding rate amounted to 99.8%, in which almost the entire amount of the drug is bound to proteins. The reference drugs showed a better correlation between the two proteins, with a wide range of binding rates from 5 to 85% and a correlation coefficient of $r = 0.99$ (data not shown).

Figure 61 compares the $\log MA_{int}$ data with the $\log MA_{micro}$ data; it can be seen that these data are independent from each other. This independence can be visualized by interlinking the values, and no trend is recognizable. Interestingly, the mean affinity of the test compounds for the different membranes was nearly identical, with the value of $\log MA_{int}$ being 2.85 and that of $\log MA_{micro}$ being 2.88. CPD7 with a $\log MA_{int}$ of 2.50 was distributed 316-fold stronger into the membrane than into the PBS, and CPD21 with a $\log MA_{int}$ of 3.50 was distributed 3162-fold stronger. Thus, 99.68% of CPD7 and 99.97% of CPD21 are bound to the membrane. This conversion to percentage values shows that the difference between these two compounds was minimal. A $\log MA$ below 1.50 would be more interesting, as this would imply that the compounds would have difficulty in passing through membranes. By contrast, compounds with a very high $\log MA$ affinity (> 5.00) would bind to the membrane without further diffusion.

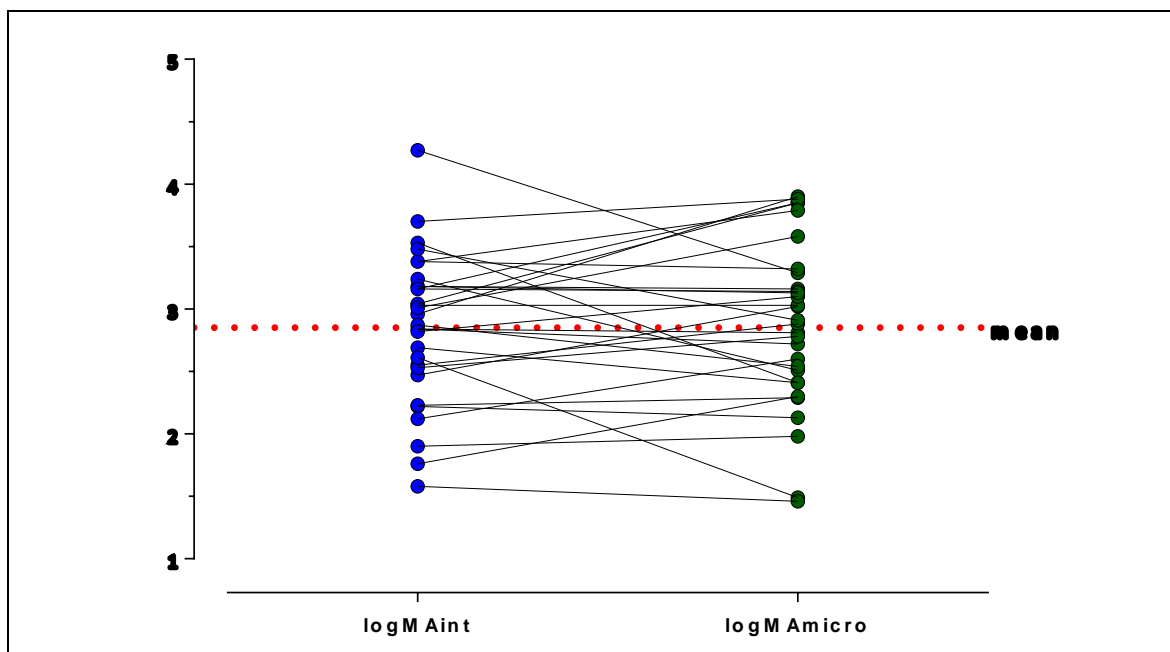


Figure 61: Comparison of the affinity of SeaLife compounds to intestinal and microsomal membranes, expressed as $\log MA_{\text{int}}$ (blue circles) and $\log MA_{\text{micro}}$ (green circles); red line: mean value.

The in vitro protein binding of the SeaLife compounds in TRANSIL^{XL} was compared with the PPB data of the same compounds obtained by the scientific ADMET Predictor software. As seen in Figure 62, most of the calculated binding rates of the test compounds show a good agreement and are within a similar order of magnitude. Generally, the binding rates determined by the TRANSIL^{XL} system were slightly higher than the values calculated by the ADMET Predictor, with the exception of compounds CPD5, CPD16 and CPD26, among which CPD5 and CPD26 showed approximately 5-10% and CPD16 approximately 25% lower binding. CPD4 and CPD25 appeared to have significantly lower PPB [%] in the ADMET Predictor. CPD11 and CPD15 showed lower PPB [%] in both systems. Nevertheless, these ADMET Predictor data are convincing and confirm the meaningfulness of in silico predictions of protein binding rates.

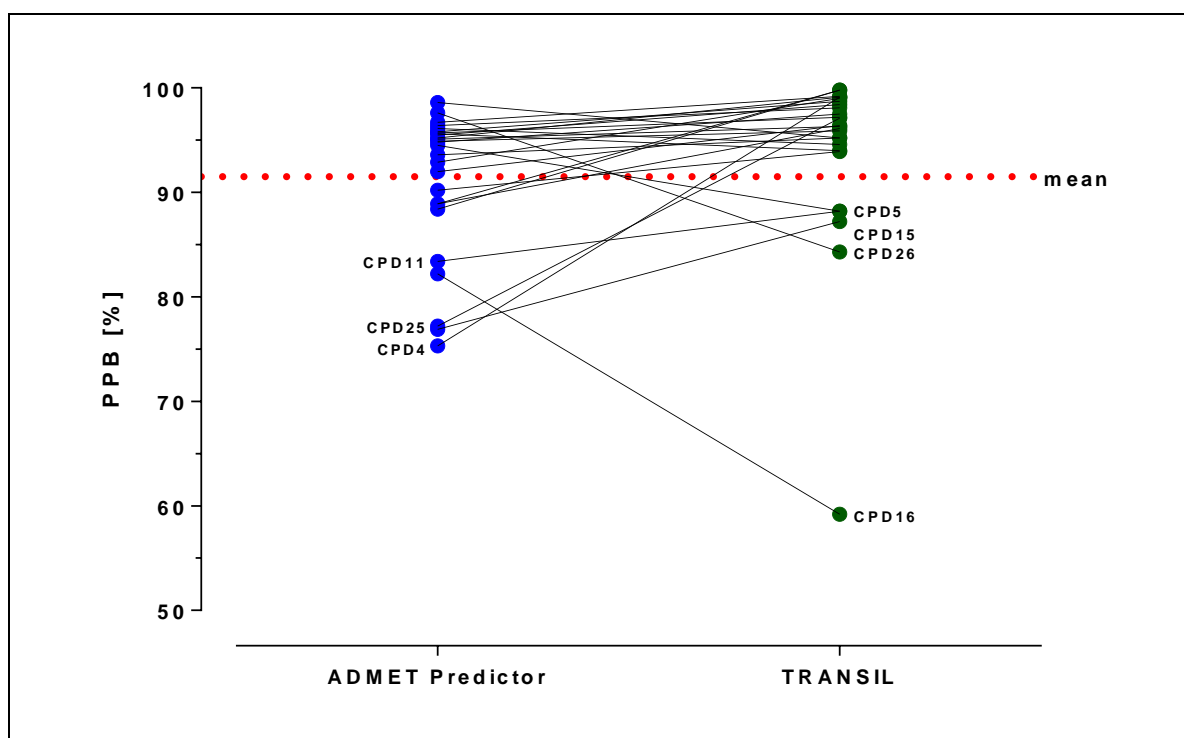


Figure 62: Comparison of PPB [%] values obtained from ADMET Predictor software (blue circles) and TRANSIL^{XL} (green circles); red line: mean value

5.3 Cryopreserved Hepatocytes

The importance of the usage of cryopreserved hepatocytes for metabolic stability studies is increasing. One major advantage of cryopreserved hepatocytes, in comparison to freshly prepared hepatocytes, is that they enable long-term storage. Furthermore, hepatocytes (fresh and cryopreserved) possess all metabolizing enzymes and transporters, in contrast to microsomes for example; therefore, hepatocytes represent the gold standard in hepatic metabolism studies. [91, 92, 93]

Metabolic stability assays in cryopreserved human male, human female, rat and monkey hepatocytes were performed. These experiments are very useful to differentiate metabolically stable compounds from less stable compounds. This information is of great value to select drug candidates for further development.

Metabolic stability studies of CPD11 in human male hepatocytes (Table 23) showed that the compound was more metabolically stable at concentrations of 5 μ M and 10 μ M until the 60 min time point. After that time, CPD11 seemed to be more stable in higher incubation concentrations (25, 50 and 100 μ M). With a concentration of 31.06 μ M after 1440 min, CPD11 appeared to be very stable at a concentration of 100 μ M. The stability in higher incubation concentrations may also be due to the fact that hepatocytes were saturated and therefore lost their full viability.

CPD11 was stable in human female hepatocytes for 30 min after incubation (Table 25). After 60 min, a decrease of approximately 50% was observed. When comparing the data from 10 μ M of human male hepatocytes with human female hepatocytes, no significant difference within 300 min was detectable. The results shown in Figure 19 verify that CPD11 is a metabolically unstable compound.

When comparing the percentage results listed in Table 27 in rat hepatocytes, hardly any differences were detected at concentrations of 5 μ M and 10 μ M. Experiments at 25, 50 and 100 μ M also demonstrated minor variations of the outcomes. Only at the time point of 1440 min and concentration of 100 μ M were differences observed, which could be more or less neglected, as mentioned earlier, when comparing with the other 100 μ M incubation data. The rat hepatocyte results were in accordance with the results obtained from the human hepatocyte investigations.

As shown in Table 28, the metabolic stability assay in monkey hepatocytes predicted similar results at both investigated concentrations. CPD11 was metabolically stable at concentrations of 10 μM and 20 μM until the 30 min time point. At the 60 min time point, approximately 50% of the compound was already metabolized. The concentration versus time curves illustrated in Figure 20 verified that the CPD11 in monkey and rats hepatocytes was metabolically unstable, particularly in lower incubation concentrations.

Experiments with CPD11 incubated in incubation medium, without including hepatocytes, were analysed under the same conditions as the CPD11 hepatocyte experiments. This study showed that CPD11 itself was unstable in medium, as illustrated in Figure 63. CPD11 at a concentration of 25 μM seemed to be more stable in medium under incubation conditions (Figure 64).

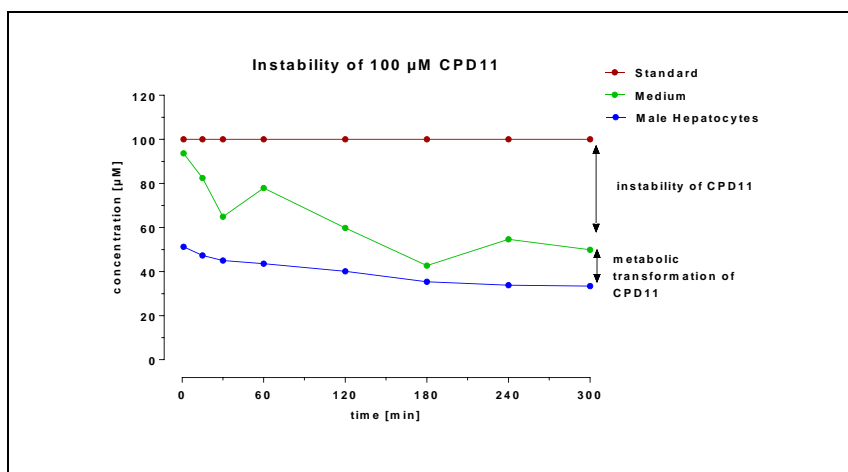


Figure 63: Instability of 100 μM CPD11 in incubation medium

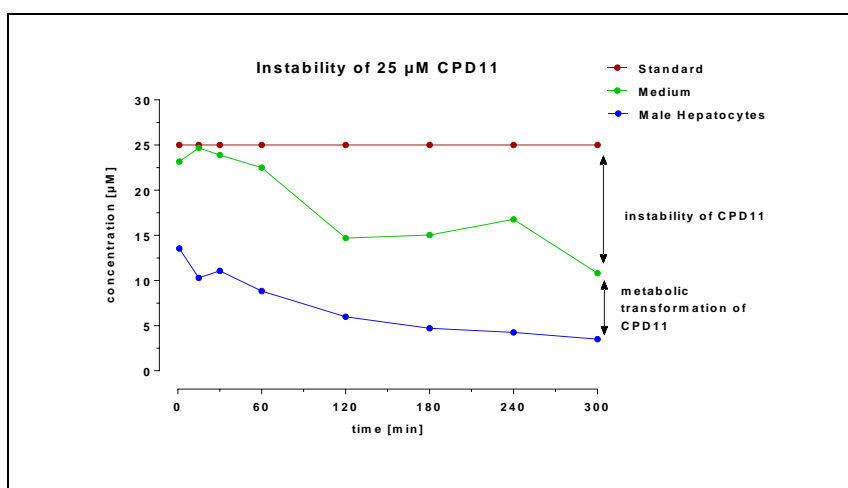


Figure 64: Instability of 25 μM CPD11 in incubation medium

Overall, it can be assumed that CPD11 is metabolically less stable. It should be noted that the compound itself also shows high instability in the absence of hepatocytes, especially at higher incubation concentrations. Therefore, it is recommended to perform metabolic studies with the investigated compounds at lower incubation concentrations. The CPD11 metabolic stability data of cryopreserved human male, human female, rat and monkey hepatocytes in general showed similar results. Consequently, in vivo studies in both rat and monkey could be conducted to evaluate in vivo human metabolic data.

The key PK parameters of CPD11 in human male, human female, rat and monkey hepatocytes listed in Table 29, along with the metabolic stability results, help to better understand the metabolism of new chemical entities. A high hepatic CL usually predicts a high metabolism. The calculated CL values show moderate results in comparison to the results of McGinnity et al. [65]. The scaled CL_{int} was between 1.0 and 72.2 mL/min/kg, showing high discrepancies within the species. The $t_{1/2}$ ranged from 1.1 to 5.8 h, which is predicted to be considerably short (when excluding the human male hepatocyte value at 100 μ M). Due to the saturation of hepatocytes, the clearances decreased with higher incubation concentrations within the system (Figure 65), whereas the $t_{1/2}$ increased with escalated drug concentrations. In the case of prodrugs, the hepatic CL_{int} can be predicted to be very high, e.g., due to the enzymatic hydrolysis of temocapril or candesartan cilexetil, whereas the CL_{int} values were calculated to be between 3000 and 7000 μ L/min/ 10^6 cells. [94]

In general, the PK results were comparable with each other, suggesting similar enzyme activity within the different hepatocyte species. Nonetheless, as depicted in Table 29, differences between rat hepatocytes and human male hepatocytes were detectable at a concentration of 5 μ M.

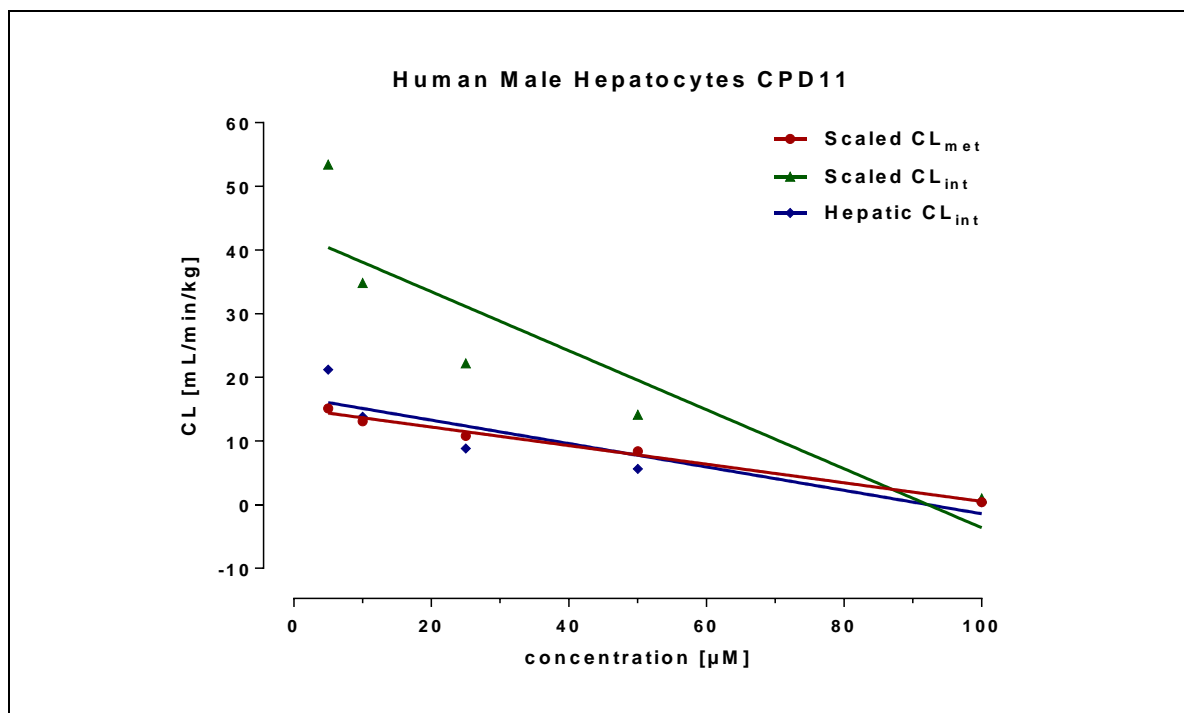


Figure 65: Correlation of PK results of spiked CPD11 concentration with scaled CL_{met} , scaled CL_{int} and hepatic CL_{int} in human male hepatocytes

With respect to the metabolites and rearrangement products of CPD11, Figure 21 to Figure 26 illustrate that in neither low nor high CPD11 concentrations was a distinct metabolite recognizable. The chromatograms in Figure 27 verify the above-mentioned assumption that there were no relevant metabolites of CPD11 formed in hepatocytes. Between 12 and 14 min, traces of possible metabolites or rearrangement products were quantifiable. However, to confirm this assumption, further investigations must be performed.

CPD22 is a prodrug of CPD11 resulting from esterases and oxidation (Figure 31). To obtain metabolic information about CPD22 and its metabolite CPD11, metabolic stability assays in different hepatocyte species were conducted. According to Table 31, Table 32 and Table 33, CPD22 was completely metabolized to CPD11 within 30 min after incubation in all species. The highest concentration of CPD11 occurred between 1 and 30 min. Figure 66 shows the chromatograms of the metabolic stability assays of CPD22 in human female, monkey and rat hepatocytes at the 1, 15, 120 and 300 min time points at an incubation concentration of 10 μ M. These chromatograms verify rapid turnover from CPD22 to CPD11 immediately after incubation.

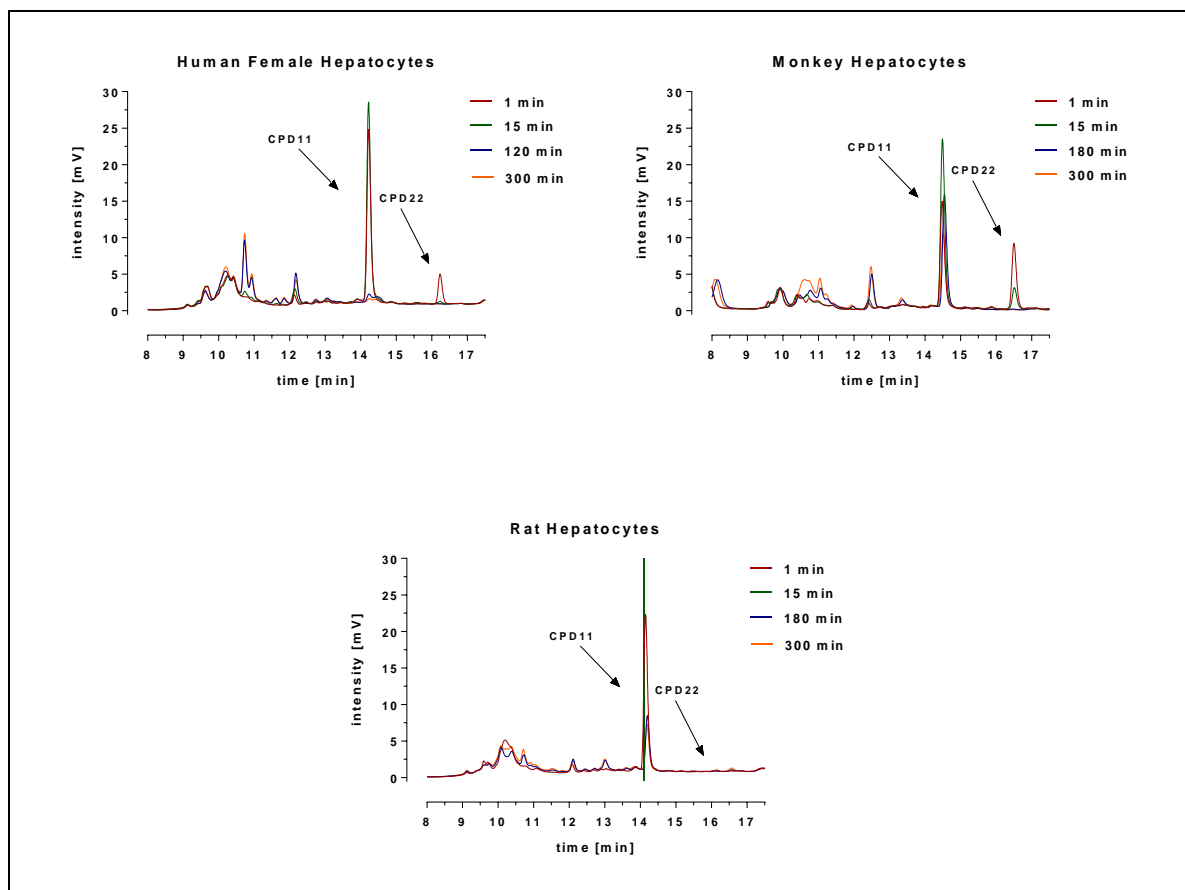


Figure 66: Chromatograms of metabolic stability of CPD22 in different hepatocytes species, incubation volume: 10 μ M

Ultimately, human female, rat and monkey hepatocyte metabolic stability assays of CPD22 showed that the compound is very unstable due to its rapid transformation to CPD11.

The calculated PK results of CPD22 and its metabolite CPD11 listed in Table 34 demonstrated that the $t_{1/2\beta}$ was below 10 min in all species. This evidence confirms the rapid conversion and degradation of CPD22 in hepatocytes. CPD22 was instantly biotransformed to the active compound CPD11 in rat hepatocytes ($t_{1/2\text{form}} = \sim 1$ min). In monkey and female hepatocytes, the $t_{1/2\text{form}}$ showed a similar order of magnitude (~ 4 -10 min). The metabolic conversion ($t_{1/2\beta}$) of CPD11 in the hepatocytes was rather slow: 1 h in human female, 3 h in monkey and 4 h in rat hepatocytes. The ratio of the area values ($F = 40$) were identical for monkey and human female hepatocytes. Furthermore, the metabolic profiling experiments of CPD22 revealed that the amount of metabolic conversion, other than the CPD11 conversion, was rather poor in all hepatocyte species.

5.4 Preliminary Pharmacokinetics of CPD3 and CPD11

Preliminary PK studies of CPD3 and CPD11 were conducted in rats and mice using different routes of administration.

Rats received CPD3 as an ip or iv bolus injection. As shown in Figure 43, the drug concentrations in plasma approximately 160 min after CPD3 administration were slightly higher in the ip group than in the iv group. This result is in accordance with the Dost'sche law. [95]

Rats and mice received CPD11 as an ip, sc or iv injection. Figure 44 shows a double peak in the chromatograms of mouse 2 iv samples, which may have been generated by a metabolite of the CPD11 compound but not from the matrix, as chromatograms after 30 min did not show any peak overlap at the CPD11 retention time. Figure 45 illustrates the peak distributions in the chromatograms in mouse 2 iv plasma samples. For this purpose, chromatograms of blank mouse plasma were compared with those of the mouse 2 iv plasma samples 30 min after CPD11 injection. It seems that the majority of these peaks were from the matrix or anaesthetics and not from CPD11, so the blank mouse and mouse 2 iv results show a more or less identical pattern of peaks. Between 12 and 13.5 min, some peaks could be detected that might represent metabolites or rearrangement products.

When comparing the chromatograms of iv mice and rats, considerable differences were seen. For instance, in rat chromatograms, virtually no matrix peaks within 8 to 12.5 min of HPLC-analysis were detected (Figure 67). The CPD11 peak eluted at the same retention time as in the mouse iv samples (tailed peak), whereas in rat chromatograms, this peak eluted as a sharper single peak. Figure 46 depicts the chromatograms superimposed on each other and shows that apart from the decrease of the CPD11 peak, new products (metabolites, rearrangement products) were formed with increasing time. Three main products were detected between 13.5 and 14.1. Due to the preliminary stage of the investigation, it was deliberately decided not to perform further analysis on these rearrangement products (HPLC MS/MS). In rat 1 iv and rat 2 iv, the same new rearrangement products were depicted.

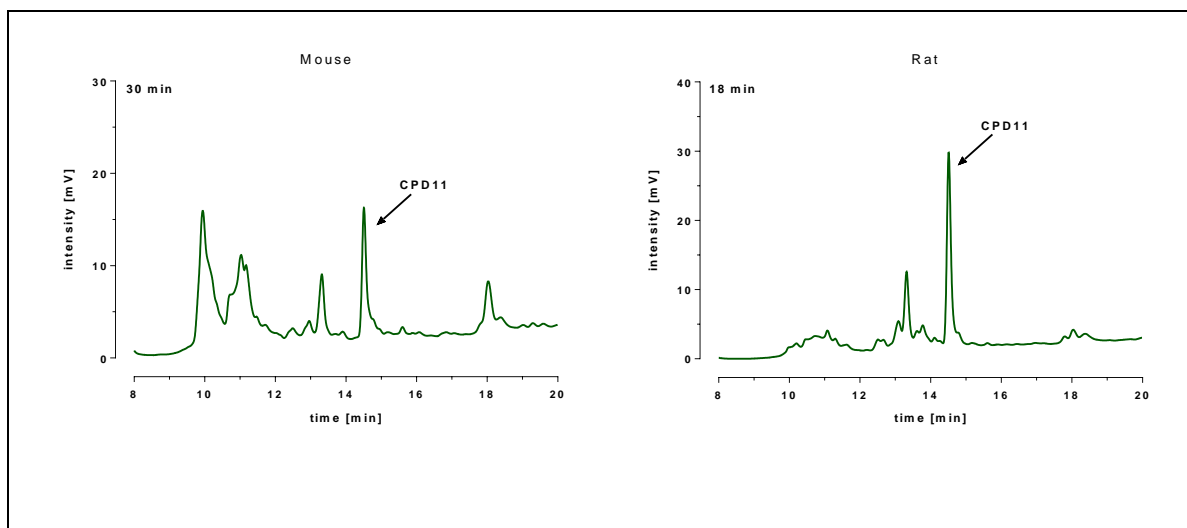


Figure 67: Comparison of CPD11 chromatograms in mouse (left) and rat (right)

Table 44 shows the plasma concentrations [$\mu\text{g/mL}$] of CPD11 in 3 rats after a single iv dose of 20 mg. For rat 2 and rat 3 iv, the plasma concentrations of CPD11 were of a similar order of magnitude at sampling time points from 0-8 min. The plasma concentrations of CPD11 in rat 1 iv at time point 0 min significantly differed ($94 \mu\text{g/mL}$) from those of rat 2 iv and rat 3 iv. As illustrated in Figure 47, the concentration versus time curves of iv rats 1-3 showed minimal variability with very homogenous curves, representing a one-compartment model. When comparing the time point 159 min in rats ip (Table 45) with the time points from 143-194 min in rats iv (Table 44) the mean values were higher in the ip administration group (mean = $9 \mu\text{g/mL}$) than in the iv group (mean = $4 \mu\text{g/mL}$). Table 46 shows the plasma concentrations [$\mu\text{g/mL}$] of CPD11 in mouse samples after a single iv bolus injection of 0.58 mg CPD11. For all mouse samples, the plasma concentrations of CPD11 were of a similar order of magnitude at the sampling time points from 5 to 360 min. Out of all the samples, mouse 2 iv showed the highest plasma concentration of CPD11 at 10 min ($7.01 \mu\text{g/mL}$). In contrast, mouse 1 iv and mouse 3 iv reached their highest peak concentrations after 15 min (mean = $5 \mu\text{g/mL}$). When comparing concentration versus time curves in the rat iv group with the mouse iv group, few differences in the curve progression were detectable, as illustrated in Figure 68 (attention: different scaling).

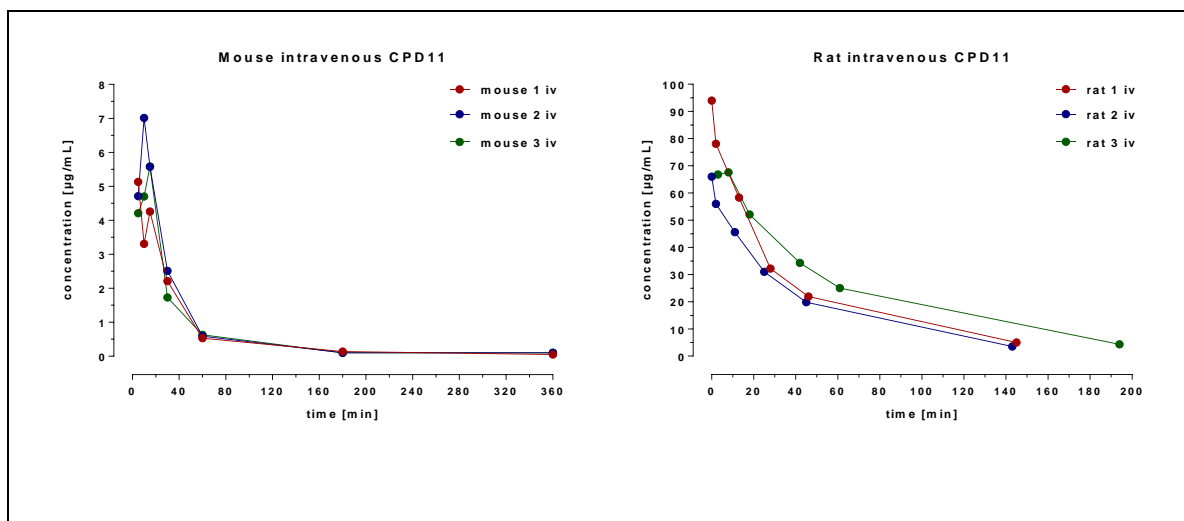


Figure 68: Comparison of concentration versus time curves [µg/mL] in mice (left) and rats (right) after an iv bolus injection of CPD11

Table 47 and Table 48 represent plasma concentrations [µg/mL] of CPD11 in 2 mice after ip and 2 mice after sc administration of 0.75 mg CPD11. It is important to note that the mice in the ip group and the mice in the sc group were treated with CPD11 dissolved in different solvents. This difference may explain the significant differences in the mouse 0 ip and mouse 2 ip plasma concentrations at the time point of 6 min. The mouse 2 ip showed a 5-fold higher plasma concentration than that in the mouse 0 ip. The concentration deviation decreased with increasing time. Discrepancies in the mouse 1 sc and mouse 3 sc were slightly lower than in the ip group. As shown in Figure 49, the plasma concentration time curves of the mouse sc group barely differed, whereas the mouse ip plasma concentration time curves showed significant differences. This relationship demonstrates that the ip administration of CPD11 in an IS formulation led to higher peak concentrations, which also decreased quickly. The mouse 2 ip showed more constant concentrations of CPD11 in plasma. Nevertheless, it must be noted that only two mice were included in each administration group, which provided limited informative value.

PK calculations (Table 49) in rats after CPD3 iv and ip administration showed that the CL values in rats iv (mean 14.1 mL/min) and rats ip (mean 17.6 mL/min) were similar. Vd was considerably higher in the ip rat group than in the rat iv group, at 878 mL versus 4871 mL. C_{last} was 3-fold higher in the ip rat group, while the AUC_{last} was 3-fold higher in the rat iv group than in the rat ip group (1409 µg/mL*min versus 515 µg/mL*min). While the AUC_{tot} in iv rats was nearly the same as the AUC_{last}, the AUC_{tot} in ip rats was five times higher than the AUC_{last}.

PK results after iv, ip and sc administration of CPD11 in rats and mice are shown in Table 50. The PK parameters in the rats iv and rats ip clearly differed from each other. The V_d was three times higher in the rat ip group (mean 1266.6 mL) than in the rat iv group (mean 342.4 mL). The mean residence time (MRT) values 203 min after ip administration in rats were nearly four times higher than those in the rat iv group (59 min). C_{max} was reached within approximately 3 min in the rat iv group but was obtained later in the rat ip group (at 17 min). The C_{max} after ip administration was comprehensible, as a compound after ip administration must first reach the systemic circulation, and only then can it be eliminated from the vascular system. As seen in Table 44, these data must be interpreted with caution, as the clinic incorrectly set 0 min as the first blood sampling time point in the rat 1 and 2 iv.

A comparison of the mouse iv and rat iv PK data in Table 50 shows some significant differences. It is difficult to directly compare C_{max} results because the CPD11 dose was much lower in mice than in rats. The CL of rats iv (mean 5.8 mL/min) was 2-fold higher than that of mice iv (2.8 mL/min). Additionally, the AUC values show major differences between the PK of mice and rats after CPD11 administration. The MRT was nearly identical in mice iv and rats iv (mean 62.81 min).

As the mouse 0 ip and mouse 1 sc received CPD11 dissolved in different formulations (IS and PBS) than for the mouse 2 ip and mouse 3 sc (PEG400 and PBS), it was not possible to compare these results. The MRT and V_d values showed distinctive differences within the mouse ip group. In contrast, the MRT and V_d in the mouse sc group seemed to be very similar. The calculated CL, AUC_{last} and AUC_{tot} results were more or less the same in the sc and ip groups and were furthermore independent from the utilized formulation. Nevertheless, it should be noted that the mouse ip and sc studies must be considered as preliminary investigations, as only one mouse with the same formulation was treated in each group.

In general, plasma concentrations after CPD11 administration were higher than after CPD3 administration. This observation is in accordance with the results obtained from the intestinal and microsomal in vitro binding tests, which predicted lower affinity of CPD11 towards membranes. As shown in Table 49 and Table 50, both drugs were eliminated rapidly from the blood, with an elimination $t_{1/2el}$ of approximately 45 min (CPD11) and 55 min (CPD3) in rat iv studies. CPD11 showed a distinct first-order kinetics according to a one-compartment model. Assuming a daily dose, the short $t_{1/2el}$ of CPD3 and CPD11 provided evidence for their rapid elimination without accumulation of the compounds in the body. After 5 times the $t_{1/2el}$ (= 225 min), only 3.2% of the C_{max} (~4 µg/mL) remained in the blood.

The MRT values in rats iv were very similar for both compounds. The peak concentrations amounted to approximately 3-fold higher in the CPD11 rat iv group than in the CPD3 rat iv group, resulting in 5-fold higher AUC_{last} values in CPD11 rats iv as well as in ip samples. The values for CL of CPD3 provided evidence that this compound was distributed and/or metabolized into the body at a distinctly higher level than CPD11 (compared to Vd).

The PK data derived from blood samples from the iv administration of CPD11 were in perfect correlation with the data found independently using the in vitro binding TRANSIL^{XL} assays, described in section 4.2. For instance, CPD11 showed a Vd of 0.98 L/kg in the vitro TRANSIL^{XL} experiments, which corresponds to a Vd of 67 litres (in consideration of an adult body weight of 70 kg). This value equates to approximately 10-fold of the total blood volume (5.5 litters for a healthy adult). PK calculations based on the in vivo data of CPD11 in rats iv revealed a Vd of approximately 340 mL. Dividing this amount by the blood volume of a 600 g rat (6 mL blood per 100 g body weight = 36 mL) gives a similar factor of 10. This consistency also implies that the Vd values found for CPD11 can be directly compared between rat and man.

5.5 In vitro and in vivo Topic Studies of CPD11

In vitro permeability experiments of CPD11 were performed using the EpiDerm™ system produced by MatTek. These investigations obtained information regarding the permeation ability of CPD11 through human skin prior to performing in vivo topical studies on guinea pigs. The sample chromatograms illustrated in Figure 56, verified that CPD11 did not permeate through the skin in concentrations higher than 0.06 µg/mL (= LOQ), and therefore this compound is assumed to only show an effect on the skin surface. Additionally, in the perforated skin model, as demonstrated by the chromatograms in Figure 57, no mentionable permeation of CPD11 in ointment formulations was observed. Solely in test experiments using CPD11 (0.01%) diluted in 0.5% DMSO and PBS was a permeation of the compound through the perforated skin detected. As shown in Table 55, CPD11 could not be quantified in the intact skin samples (= LOQ, 0.06 µg/mL). In comparison to the experiments conducted with the standard drug caffeine, a high permeation in solution as well as in ointment bases could be shown, which is in accordance with the current literature. [96]

After the in vitro investigations, in vivo topical studies on guinea pigs were performed using the same formulations as in the in vitro skin studies. When comparing the chromatograms (Figure 58) of negative control samples (GP4 and GP6) with the chromatograms of guinea pig (GP1 – GP3) samples (Figure 59) treated with CPD11, no major differences in the patterns of the chromatograms were visible; they were more or less identical.

The findings in the in vivo guinea pig model are in accordance with the in vitro results and verify that CPD11 most likely does not permeate through the intact skin in a plasma concentration higher than the LOQ (0.07 µg/mL).

6 Conclusion

ADMET parameters obtained from *in vitro*, *in vivo* and *in silico* studies provide important information about drug properties and are therefore very useful for the selection of potential drug candidates. Nevertheless, for the selection of a drug candidate, both the pharmacological and PK properties of the drug ought to be involved in the decision regarding whether a compound should be further clinically investigated.

To conduct all experiments described in this thesis, a simple, robust and low-cost RP-HPLC method was first developed and validated for the quantification of this new group of compounds, complying with the requirements of preclinical research. This analytical method provided the basis for all *in vitro* and *in vivo* analyses of the above-mentioned antibacterial candidates. The target was to develop a single RP-HPLC method that can be used for the quantification of one compound class, which also shows chemical inhomogeneity. To date, 31 new synthetic test compounds have been successfully analysed with this method, whereas special attention was given to the lead compound CPD11. Due to pending patent matters, only 8 out of 31 chemical structures could be published. CPD11 showed an LOQ of 0.07 µg/mL and excellent recoveries in plasma, ranging from 93.5 to 104%. Sample preparation using a one-step protein precipitation yielded an excellent recovery *in vivo* and *in vitro*.

SeaLife compounds show good pharmacological activity against a wide range of gram-positive bacteria, as investigated initially by SeaLife Pharma itself. Despite this advantageous pharmacological activity, the aqueous solubility of the compounds must be improved to reduce their high PPB rates (up to 99%). Using this strategy, lower doses could be administered to prevent toxic side effects. The TRANSIL^{XL} system has proven to be a very reliable and time-saving method for predicting the SeaLife compounds' PK properties. Comparison with results calculated using the *in silico* ADMET Predictor software verified the TRANSIL^{XL} system's outcome. Additionally, a comparison of the binding study results with the data obtained from the *in vivo* rat studies revealed a similar outcome. Thus, we recommend the validated TRANSIL^{XL} system when working on drug development to predict valuable information regarding the PK properties of a new compound as early, efficiently and rapidly as possible to save time and money on future drug investigations with compounds showing insufficient results.

For the evaluation of the metabolism of CPD11 and its prodrug CPD22, different cryopreserved hepatocyte species were utilized. Overall, it could be concluded that the lead

compound was metabolically less stable, especially at high incubation concentrations in all species. However, the compound itself also showed a high instability solely in incubation medium without the addition of hepatocytes. Consequently, it can be recommended to perform metabolic stability experiments of this class of compounds at lower incubation concentrations, which also prevents hepatocyte overload that could lead to incorrect results. The evaluation of possible metabolites or rearrangement products showed no distinctive metabolite of CPD11 in all hepatocyte species. Metabolic studies of CPD22 in hepatocytes showed that CPD22 was biotransformed to CPD11 immediately after incubation.

The PK results of CPD11 and CPD3 represented in this thesis showed a high variability between the two test compounds. The first dose in rats and mice revealed a rather short MRT after iv administration. These short $t_{1/2el}$ values together with the V_d , which was higher than the body weight, would make it necessary to administer a higher dose of the compound to exceed the minimal inhibitory concentrations in the blood. Therefore, the PK properties must be improved, as already mentioned above.

Additionally, topical studies with CPD11 were conducted in vitro (EpiDerm™ model) and in vivo (guinea pigs) to evaluate whether CPD11 could be a potential candidate for cutaneous applications. The represented results were coherent with each other, as desired, showing no systemic resorption of CPD11 through the skin above a plasma concentration of 0.07 µg/mL.

In conclusion, it can be stated that with regard to solubility, stability in biological matrices and PK properties, hydrophilic, stable compounds with favourable PK properties (e.g., prodrugs) would be more preferable. Prodrug CPD22 was already investigated in this study, yet from a pharmacological point of view, it appeared not to be the accurate drug candidate for further investigations.

7 Abstract

The emergence of antibiotic resistance has increased the need to develop new anti-infective compounds. Targeted research activities in the field of antibacterial compounds are therefore of growing relevance. The pharmacological properties of a drug candidate, along with its pharmacokinetic parameters, play an important role in determining the proper dose to avoid toxicity. Therefore, determinations of ADMET parameters along with preliminary pharmacokinetic studies are an essential part of preclinical drug development.

In this investigation, the protein, intestinal and microsomal binding of 31 new bicycloheptyl anellated naphthoquinones showing antibacterial activity was reported. The *in vitro* TRANSIL^{XL} system was used for this research, which allows the binding characteristics of compounds to be accurately described. In general, the plasma protein binding was 85-99%, mainly bound to human serum albumin, and the volume of distribution was predicted to be approximately 1.9 L/kg. Furthermore, metabolic stability studies were performed with the lead compound CPD11 and with CPD22, which is a prodrug of CPD11. In hepatocytes, this class of compounds appeared to be metabolically unstable. Finally, preliminary pharmacokinetic studies were conducted in rats and mice. The results showed that the drugs were eliminated rapidly from the blood with an elimination half-life of approximately 45 to 55 min. Another set of experiments was performed to determine the *in vitro* and *in vivo* permeability of CPD11 through the skin in case the drug is considered for topical applications. The results were coherent with each other, showing no systemic resorption of CPD11 through the skin with a plasma concentration higher than 0.07 µg/mL (= LOQ).

Eventually, to decrease the high protein binding rates and distribution volumes as well as to improve the metabolic stability, it is strongly recommended to chemically modify the compounds to improve their aqueous solubility and stability.

8 Zusammenfassung

Die steigende Progression der Antibiotikaresistenzen erhöht den Bedarf zur Entwicklung neuer anti-infektiöser Verbindungen. Eine gezielte Forschung im Bereich antibakterieller Arzneistoffe ist deshalb von steigender Relevanz. Sowohl pharmakologische als auch pharmakokinetische Eigenschaften eines Arzneistoffkandidaten spielen eine tragende Rolle bei der Evaluierung der geeigneten Dosis und damit der Vermeidung von Toxizitäten.

In Rahmen dieser Arbeit wurden unter anderem die Protein-, intestinale- und mikrosomale Bindung von 31 neuen bicycloheptyl anellierten Naphthoquinonen, welche antibakterielle Eigenschaften zeigen, untersucht. Für diese Untersuchungen wurde das in-vitro TRANSIL^{XL} System verwendet. Im Allgemeinen betrug die Plasma-Protein-Bindung 85–99%, hauptsächlich gebunden an humanem Serum Albumin mit einem Verteilungsvolumen von etwa 1.9 L/kg. Zusätzlich wurden auch Zellkulturstudien zur Ermittlung der metabolischen Stabilität mit dem Lead Compound CPD11 und CPD22, einem Prodrug von CPD11, durchgeführt. Die erfassten Hepatozyten-Daten zeigten, dass diese Wirkstoffklasse womöglich metabolisch instabil ist. Schließlich wurden pharmakokinetische Voruntersuchungen an Ratten und Mäusen durchgeführt. Die Ergebnisse zeigten, dass die untersuchten Arzneistoffe mit einer Eliminationshalbwertszeit von etwa 45 bis 55 min rasch aus dem Blut eliminiert wurden. Eine weitere Versuchsreihe zur Untersuchung der in-vitro und in-vivo Permeabilität von CPD11 durch die Haut wurde ebenfalls durchgeführt. Die Ergebnisse der beiden Untersuchungsreihen stimmten miteinander überein und zeigten, dass CPD11 nicht systemisch durch die Haut über eine Plasmakonzentration höher als 0.07 µg/mL resorbiert wurde.

Zusammenfassend wird dringend empfohlen die Verbindungen chemisch zu modifizieren um die Wasserlöslichkeit und Stabilität zu steigern und damit die hohe Plasma-Protein-Bindungsrate und das Verteilungsvolumen sowie auch die metabolischen Stabilität zu verbessern.

9 List of Abbreviations

ACN	acetonitrile
ADMET	absorption, distribution, metabolism, excretion and toxicology
AGP	alpha-1-acid glycoprotein
Aqua bidest.	Aqua bidestillata
AUC	area under the curve
AUC _{last}	area under the curve up to the last measurable concentration
AUC _{tot}	total area under the curve
CL	clearance
CL _{int}	intrinsic clearance
C _{max}	maximum plasma concentration
C _{last}	last measurable concentration
Conc.	concentration
CYP450	cytochrome P450
CV	coefficients of variation
DMSO	dimethylsulfoxid
f	fraction bound
fAGP	fraction alpha-1-acid glycoprotein
fHSA	fraction bound human serum albumin
fPPB	fraction bound plasma protein
f _u	fraction unbound
f _u AGP	fraction unbound alpha-1-acid glycoprotein
f _u HSA	fraction unbound human serum albumin
f _u PPB	fraction unbound plasma protein
HSA	human serum albumin
ip	intraperitoneal
iv	intravenous

LIST OF ABBREVIATIONS

IS	dimethylisosorbid
k	elimination constant
k'	capacity factor
K _D	dissociation constant
k _{el}	elimination constant
LOD	limit of detection
logMA	tissue binding
logMA _{micro}	microsomal binding
logMA _{int}	intestinal binding
logP	partition coefficient
LOQ	limit of quantification
LT	long tem
M	metabolites and rearrangement products
MA	membrane affinity
MAE	mean absolute error
MRT	mean residence time
N	number of theoretical plates
na	not applicable (not done)
nc	not calculated
nd	not done
NCA	non-compartmental pharmacokinetic data analysis
PBS	phosphate-buffered saline
PEG400	polyethylenglycol
P _{int}	predicted intestinal permeability coefficient
PK	pharmacokinetic
pK _a /pK _b	dissociation constant, acidic and basic
PPB	plasma protein binding
Q	quality samples

LIST OF ABBREVIATIONS

QI	quality index
r^2	correlation quality
RMSE	root mean squared error
RP-HPLC	reverse phase-high performance liquid chromatography
sc	subcutaneous
scaled CL_{int}	scaled intestinal clearance
scaled CL_{met}	scaled metabolic clearance
SD	standard deviation
SST	system suitability testing
$t_{1/2}$	half-life
$t_{12\alpha}$	half-life of distribution
$t_{12\beta}$	half-life of elimination
$t_{1/2el}$	elimination half-life
t_{12form}	half-life of formation
T_{last}	time of last measureable concentration
T_{max}	time of maximum plasma concentration
Vd	volume of distribution

10 List of Tables

Table 1: Overview of recommended PK parameters to investigate during drug development	6
Table 2: Data of HPLC-System	17
Table 3: Elution gradient profile.....	17
Table 4: Materials and Equipment	18
Table 5: Blood sampling time points of rats after iv CPD3 administration.....	40
Table 6: Blood sampling time points of rats after ip CPD3 administration.....	40
Table 7: Blood sampling time points of rats after iv CPD11 administration.....	41
Table 8: Blood sampling time points of rats after ip CPD11 administration.....	41
Table 9: Blood sampling time points of mouse after ip and sc CPD11 administration.....	42
Table 10: Preparation set up of different formulations for the EpiDerm™ in vitro model ...	44
Table 11: Experimental setup of in vitro EpiDerm™ model.....	46
Table 12: Experimental setup of in vivo guinea pigs model with CPD11.....	47
Table 13: Intra- and inter-day coefficients of variation (% CV), bias [%] and recovery [%] for the determination of CPD11 in PBS (n = 6)	53
Table 14: Intra- and inter-day coefficients of variation (% CV), bias [%] and recovery [%]	54
Table 15: Short-term (24 h) and long-term (72 h) stability of CPD11 in PBS and plasma...	55
Table 16: Regression parameters of the calibration curve of CPD11 in plasma	56
Table 17: Summary of the characteristics of CPD11 related test-compounds and HPLC parameters	57
Table 18: List of SeaLife compounds and marketed drugs. Physiochemical parameters and f_u were predicted using the ADMET Predictor. fPPB parameters determined from TRANSIL ^{XL} results (n = 6) are shown as the means with the SD.	59
Table 19: List of SeaLife compounds and marketed drugs with the f and f_u parameters for HSA and AGP predicted with the TRANSIL ^{XL} assay (n = 6). TRANSIL ^{XL} results are shown as the means with the SD.	61
Table 20: List of SeaLife compounds and marketed drugs with their V_d (L/kg), logMA, f_u [%] and P_{int} [cm/sec] parameters predicted with the ADMET Predictor and in TRANSIL ^{XL} assays. TRANSIL ^{XL} results (n = 6) are shown as the means with the SD.....	64
Table 21: Regression parameters of the calibration curve of CPD11 in incubation medium	66
Table 22: Stability of CPD11 in incubation medium.....	67
Table 23: Metabolic stability of CPD11 in human male hepatocytes [μ M]	69
Table 24: Metabolic stability of CPD11 in human male hepatocytes [%]	70

Table 25: Metabolic stability of CPD11 in human female hepatocytes [μM and %]	71
Table 26: Metabolic stability of CPD11 in rat hepatocytes [μM].....	74
Table 27: Metabolic stability of CPD11 in rat hepatocytes [%]	75
Table 28: Metabolic stability of CPD11 in monkey hepatocytes [μM and %].....	76
Table 29: PK calculations of CPD11 in hepatocytes experiments	79
Table 30: Regression parameters of the calibration curve of CPD22 in incubation medium	86
Table 31: Metabolic stability of CPD22 in human female hepatocytes [μM]	87
Table 32: Metabolic stability of CPD22 in monkey hepatocytes [μM]	89
Table 33: Metabolic stability of CPD22 in rat hepatocytes [μM].....	91
Table 34: PK calculations of transformation products; na: only three data points available.	94
Table 35: Regression parameters of the calibration curve of testosterone in incubation.....	98
Table 36: Metabolic stability of testosterone in human male hepatocytes [μM and %].....	99
Table 37: Metabolic stability of testosterone in human female hepatocytes [μM and %].....	99
Table 38: Metabolic stability of testosterone in rat hepatocytes [μM and %]	100
Table 39: Metabolic stability of testosterone in monkey hepatocytes [μM and %].....	100
Table 40: PK calculations of testosterone in hepatocytes experiments	103
Table 41: Regression parameters of the calibration curve of CPD3 in plasma.....	105
Table 42: Plasma concentrations [$\mu\text{g/mL}$] of CPD3 after iv administration	106
Table 43: Plasma concentrations [$\mu\text{g/mL}$] of CPD3 after ip administration	107
Table 44: Plasma concentrations [$\mu\text{g/mL}$] of CPD11 after iv administration in rats.....	112
Table 45: Plasma concentration [$\mu\text{g/mL}$] of CPD11 after ip administration in rats	113
Table 46: Plasma concentrations [$\mu\text{g/mL}$] of CPD11 after iv administration in mice.....	114
Table 47: Plasma concentrations [$\mu\text{g/mL}$] of CPD11 after ip administration in mice.....	115
Table 48: Plasma concentrations [$\mu\text{g/mL}$] of CPD11 after ip administration in mice.....	115
Table 49: NCA PK parameters of CPD3 in rats.....	120
Table 50: NCA PK parameters of CPD11 in rats and mice	121
Table 51: Regression parameters of the calibration curve of caffeine in PBS.....	123
Table 52: Regression parameters of the calibration curve of CPD11 in PBS	124
Table 53: Peak areas x 1000 and peak areas x 1000 accumulation of the different caffeine formulations	126
Table 54: Permeated proportions of caffeine in different formulations in $\mu\text{g/mL}$	127
Table 55: Overview of the CPD11 concentration [$\mu\text{g/mL}$] results in the in vitro EpiDerm™ model.....	130

11 List of Figures

Figure 1: a-h Chemical structures of investigated test-compounds (CPD3, CPD5, CPD6, CPD7, CPD10, CPD11, CPD13 and CPD17)	3
Figure 2: Drug discovery process	5
Figure 3: Skin structure [100]	12
Figure 4: VWR® HITACHI Chromaster HPLC-System	16
Figure 5: Illustration of the TRANSIL ^{XL} Kits assay plate [61]	23
Figure 6: Photograph of annotated tube units [61]	24
Figure 7: Workflow of TRANSIL ^{XL} Kit [61]	25
Figure 8: Certificate of cryopreserved human male hepatocytes.....	30
Figure 9: Certificate of cryopreserved human female hepatocytes	32
Figure 10: Certificate of cryopreserved rat (sprague-dawley) hepatocytes	33
Figure 11: Certificate of cryopreserved monkey (cynomolgus) hepatocytes	34
Figure 12: EpiDerm TM skin model devices [86]	44
Figure 13: Permeability configuration utilizing EpiDerm TM tissue model [86]	45
Figure 14: HPLC chromatograms of some CPD compounds diluted in ACN with a concentration of 10 µg/mL	50
Figure 15: a-e Representative HPLC chromatograms of CPD11 in, human pooled plasma 5.0 µg/mL (a), bovine liver tissue 5.0 µg/mL (b), cryopreserved human hepatocytes 25µM (c), PK mouse plasma 10 min after iv bolus injection (d) and PK rat plasma 10 min after iv bolus injection (e).	51
Figure 16: LOQ and LOD of CPD11 in PBS	52
Figure 17: Calibration curve of CPD11 in plasma.....	56
Figure 18: Calibration curve of CPD11 in incubation medium	65
Figure 19: Hepatocytes metabolic stability of CPD11 in human hepatocytes.....	73
Figure 20: Hepatocyte metabolic stability of CPD11 in rat and monkey hepatocytes	77
Figure 21: Metabolites and rearrangement products of CPD11 in human female hepatocytes at 10 µM.....	80
Figure 22: Metabolites and rearrangement products of CPD11 in human male hepatocytes at 10 µM.....	80
Figure 23: Metabolites and rearrangement products of CPD11 in human male hepatocytes at 25 µM.....	81
Figure 24: Metabolites and rearrangement products of CPD11 in rat hepatocytes at 10 µM	81

Figure 25: Metabolites and rearrangement products of CPD11 in rat hepatocytes at 25 μ M	81
Figure 26: Metabolites and rearrangement products of CPD11 in monkey hepatocytes at 10 μ M.....	82
Figure 27: 10 μ M CPD 11 spiked in rat hepatocytes and incubation medium	82
Figure 28: 10 μ M CPD11 spiked in incubation medium	83
Figure 29: Comparison of chromatograms of CPD11 in different hepatocytes models at a concentration of 10 μ M.....	84
Figure 30: Calibration curve of CPD22 in incubation medium	85
Figure 31: Esterases and oxidation from CPD22 to CPD11	87
Figure 32 Hepatocyte metabolic stability of CPD22 in human female hepatocytes.....	88
Figure 33: Hepatocytes metabolic stability of CPD22 in monkey hepatocytes.....	90
Figure 34: Concentration versus time curve of metabolic stability of CPD22 in rat hepatocytes	92
Figure 35: Chromatograms of metabolic stability of CPD22 in different hepatocytes after incubation 60 min. Incubation volume: 10 μ M.....	93
Figure 36: Human female hepatocytes spiked with 25 μ M CPD22.....	95
Figure 37: Rat hepatocytes spiked with 25 μ M CPD22.....	95
Figure 38: Monkey hepatocytes spiked with 25 μ M CPD22.....	96
Figure 39: Calibration curve of testosterone in incubation medium.....	97
Figure 40: Concentration versus time curves of metabolic stability of testosterone in human male and female hepatocytes.....	101
Figure 41: Concentration versus time curves of metabolic stability of testosterone in rat and monkey hepatocytes	101
Figure 42: Calibration curve of CPD3 in plasma.....	104
Figure 43: Plasma concentration [μ g/mL] versus time [min] curves of CPD3.....	108
Figure 44: Temporal concentration gradients of CPD11 in plasma of mouse 2 iv	109
Figure 45: Comparison between chromatograms of blank mouse plasma (black line) and plasma of mouse 2 iv (red line).....	110
Figure 46: Temporal concentration gradients of CPD11 in plasma of rat 3 iv	110
Figure 47: Plasma concentration [μ g/mL] versus time [min] curves of CPD11 in rats.....	116
Figure 48: Plasma concentration [μ g/mL] versus time [min] curves of CPD11 in mice.....	117
Figure 49: Plasma concentration [μ g/mL] versus time [min] curves of CPD11 in mice.....	118
Figure 50: Calibration curve of caffeine in PBS	122
Figure 51: Calibration curve of CPD11 in PBS	124

Figure 52: Chromatograms of caffeine in the EpiDerm™ skin model.....	125
Figure 53: Logarithmic presentation of caffeine accumulation results	127
Figure 54: Concentration versus time curves of caffeine in various formulations [µg/mL]	127
Figure 55: Chromatograms of blank samples	128
Figure 56: Chromatograms of CPD11 in EpiDerm™ model with different formulations ..	129
Figure 57: Chromatograms of CPD11 on perforated skin in the EpiDerm™ model	129
Figure 58: Chromatograms of negative control guinea pigs number 4 and 6 samples.....	131
Figure 59: Chromatograms of guinea pigs number 1-3 plasma samples.....	131
Figure 60: Correlation of f_u HSA and f_u AGP values	136
Figure 61: Comparison of the affinity of SeaLife compounds to intestinal and microsomal membranes, expressed as $\log MA_{int}$ (blue circles) and $\log MA_{micro}$ (green circles); red line: mean value.	137
Figure 62: Comparison of PPB [%] values obtained from ADMET Predictor software (blue circles) and TRANSIL ^{XL} (green circles); red line: mean value	138
Figure 63: Instability of 100 µM CPD11 in incubation medium.....	140
Figure 64: Instability of 25 µM CPD11 in incubation medium.....	140
Figure 65: Correlation of PK results of spiked CPD11 concentration with scaled CL_{met} , scaled CL_{int} and hepatic CL_{int} in human male hepatocytes	142
Figure 66: Chromatograms of metabolic stability of CPD22 in different hepatocytes species, incubation volume: 10 µM.....	143
Figure 67: Comparison of CPD11 chromatograms in mouse (left) and rat (right).....	145
Figure 68: Comparison of concentration versus time curves [µg/mL] in mice (left) and rats (right) after an iv bolus injection of CPD11	146

12 References

- [1] WHO Drug resistance. WHO http://www.who.int/drugresistance/global_action_plan/en/. Access: 05 August **2016**
- [2] Boucher HW, Talbot GH, Bradley JS, Edwards JE, Gilbert D, Rice LB, Scheld M, Spellberg B, Bartlett J. **2009**. *Bad bugs, no drugs: No ESCAPE! An update from the infectious diseases society of America*. Clin Infect Dis. 48(1):1-12.
- [3] Laxminarayan R, Duse A, Wattal C, Zaidi AKM, Wertheim HFL, Sumpradit N, Vlieghe E, Hara GL, Gould IM, Goossens H. **2013**. *Antibiotic resistance-the need for global solutions*. Lancet Infect. 13(12):1057-1098.
- [4] Strobel G and Daisy B. **2003**. *Bioprospecting for microbial endophytes and their natural products*. Microbiol. Mol. Biol. Rev. 67:491-502.
- [5] Lou J, Fu L, Peng Y and Zhou L. **2013**. *Metabolites from alternaria fungi and their bioactivities*. Molecules. 18:5891-5935.
- [6] Liu Y, Wray V, Abdel-Aziz MS, Wang C-Y, Lai D and Proksch P. **2014**. *Trimeric anthracenes from the endophytic fungus Stemphylium globuliferum*. J. Nat. Prod. 77:1734-1738.
- [7] Ondeyka J, Buevich AV, Williamson RT, Zink DL, Polishook JD, Occi J, Vicente F, Basilio A, Bills GF, Donald RGK, Phillips JW, Goetz MA and Singh SB. **2014**. *Isolation, structure elucidation, and biological activity of altersolanol P using Staphylococcus aureus fitness test based genome-wide screening*. J. Nat. Prod. 77:497-502.
- [8] Zheng CJ, Shao CL, Guo ZY, Chen JF, Deng DS, Yang KL, Chen YY, Fu XM, She ZG, Lin YC and Wang CY. **2012**. *Bioactive hydroanthraquinones and anthraquinone dimers from a soft coral-derived alternaria sp. fungus*. J. Nat. Prod. 75:189–197.
- [9] Klaiklay S, Rukachaisirikul V, Phongpaichit S, Pakawatchai C, Saithong S, Buatong J, Preedanon S and Sakayaroj J. **2012**. *Anthraquinone derivatives from the mangrove-derived fungus Phomopsis sp. PSU-MA214*. Phytochem Lett. 5:738-742.
- [10] Teiten M-H, Mack F, Debbab A, Aly AH, Dicato M, Proksch P and Diederich M. **2013**. *Anticancer effect of altersolanol A, a metabolite produced by the endophytic fungus*

stemphylium globuliferum, mediated by its pro-apoptotic and anti-invasive potential via the inhibition of NF- κ B activity. Bioorg. Med. Chem. 21:3850-3858.

[11] Pompeng P, Sommit D, Sriubolmas N, Ngamrojanavanich N, Matsubara K and Pudhom K. **2013**. Antiangiogenic effects of anthranoids from *alternaria* sp., an endophytic fungus in a thai medicinal plant *erythrina variegata*. Phytomedicine. 20:918-922.

[12] Mishra PD, Verekar SA, Deshmukh SK, Joshi KS, Fiebig HH and Kelter G. **2015**. Altersolanol A: a selective cytotoxic anthraquinone from a *phomopsis* sp. Lett. Appl. Microbiol. 60:387-391.

[13] Huang X, Sun X, Lin S, Xiao Z, Li H, Bo D and She Z. **2014**. Xylanthraquinone, a new anthraquinone from the fungus *Xylaria* sp. 2508 from the South China Sea. Natural Product Research. 28:111-114.

[14] Chen B, Shen Q, Zhu X and Lin Y. 2014. The anthraquinone derivatives from the fungus *Alternaria* sp. XZSBG-1 from the saline lake in Bange, Tibet, China. Molecules. 19:16529-16542.

[15] Debbab A, Aly AH, Edrada-Ebel R, Wray V, Müller WEG, Totzke F, Zirrgiebel U, Schächtele C, Kubbutat MHG, Lin WH, Mosaddak M, Hakiki A, Proksch P and Ebel R. **2009**. Bioactive metabolites from the endophytic fungus *stemphylium globuliferum* isolated from *mentha pulegium*. J. Nat. Prod. 72:626-631.

[16] Debbab A, Aly AH, Edrada-Ebel R, Wray V, Pretsch A, Pescitelli G, Kurtan T, Proksch P. **2012**. New anthracene derivatives – structure elucidation and antimicrobial activity. Eur. J. Org. Chem. Doi:10.1002/ejoc.201101442.

[17] Haraguchi H, Abo T, Fukuda A, Okamura N, Yagi A. **1996**. Mode of phytotoxic action of altersolanols. Phytochemistry 43:989-992.

[18] Haraguchi H, Abo T, Hashimoto K, Yagi A. **1992**. Action-mode of antimicrobial altersolanol A in *pseudomonas aeruginosa*. Biosci Biotechnol Biochem 56:1221–1224.

[19] Okamura N, Mimura K, Haraguchi H, Shingu K, Miyahara K, Yagi A. **1996**. altersolanol-related compounds from the culture liquid of *alternaria solani*. Phytochemistry 42:77-80.

[20] Steglich W, Fugmann B, Lang-Fugmann S. **1997**. *Roempp Lexikon Naturstoffe*. Georg Thieme Verlag, Stuttgart.

- [21] Kuck D, Caulfield T, Lyko F and Medina-Franco JL. **2010**. *Nanaomycin A selectively inhibits DNMT3B and reactivates silenced tumor suppressor genes in human cancer cells*. Mol. Cancer Ther. 9:3015-3023.
- [22] Nakashima T, Boonsongcheep P Toru Kimura, Iwatsuki M, Sato N, Nonaka K, Prathanturarug S, Takahashi Y and Omura S. **2015**. *New compounds, Nanaomycin F and G, discovered by physicochemical screening from a culture broth of Streptomyces rosa subsp. notoensis OS-3966*. J. Biosci. Bioeng. 120:596-600.
- [23] Pereira EM, de Barros Machado T, Correa I, Leal R, Jesus DM, de Almeida Damaso CR, Pinto AV, Giambiagi-deMarval M, Kuster RM, Netto dos Santos KR. **2006**. *Tabebuia avellaneda naphthoquinones: activity against methicillin-resistant staphylococcal strains, cytotoxic activity and in vivo dermal irritability analysis*. Ann Clin Microbiol Antimicrob 5:1-7.
- [24] Lin JH and Lu AYH. **1997**. *Role of pharmacokinetics and metabolism in drug discovery and development*. Pharmacol. Rev. 49(4):403-449.
- [25] Hughes JP, Rees S, Kalindjian SB and Philpott KL. **2011**. *Principles of early drug discovery*. Br. J. Pharmacol. 162(6):1239-1249.
- [26] Wang J and Urban L. 2004. *The impact of early ADME profiling on drug discovery and development strategy*. Drug Discovery World Fall 2004. 73-86.
- [27] Elbehri Aziz. **2005**. *Biopharmig and food system: examining the potential benefits and risks*. Ag. Bio. Forum. 8(1):18-25.
- [28] Kummar S, Kinders R, Rubinstein L, et al. **2007**. *Compressing drug development timelines in oncology using phase '0' trials*. Nat. Rev. Cancer. 7:131-139.
- [29] Ed. McCarthy MW, Kockler DR. **2009**. *Oxford American Handbook of Clinical Pharmacy*. Hobs M, McCarthy MW chapter 7: *Clinical trials*. Oxford University Press, Inc., New York. 115-120.
- [30] EMA European Medicines Agency.
http://www.ema.europa.eu/ema/index.jsp?curl=pages/regulation/general/general_content_000370.jsp 12.08.2016. Access: 12 August **2016**

- [31] European Medicines Agency. **21 July 2011**. *EMA/CHMP/EWP/192217/2009, Committee for Medicinal Products for Human Use (CHMP) Guideline on bioanalytical method validation*. 1-23.
- [32] Guidance for Industry: bioanalytical method validation. **May 2001**. *U.S. Department of Health and Human Services Food and Drug Administration Center for Drug Evaluation and Research (CDER). Center for Veterinary Medicine (CVM)*. 1-25.
- [33] Singh S and Bakshi M. 2000. *Guidance on conduct of stress tests to determine inherent stability of drugs*. Pharmaceutical Technology Online. 1-14.
- [34] Cox GS. **2008**. *Preclinical development Handbook, ADME and Biopharmaceutical Properties*. John Wiley & Sons, Inc., Hoboken, New Jersey. 211-223.
- [35] Kerns EH, Di L, Petusky S, Farris M, Ley R, Jupp P. **2004**. *Combined application of parallel artificial membrane permeability assay and Caco-2 permeability assays in drug discovery*. J. Pharm. Sci. 93:1440-1453.
- [36] Spruill WJ, Wade WE, DiPiro JT, Blouin RA, Pruemer JM. **2014**. *Concepts in clinical pharmacokinetics*. 6th ed., Bethesda, Maryland, USA: American Society of Health-System Pharmacists. 103-107.
- [37] Scheife RT. **1989**. *Protein binding: what does it mean?*. DICP 23(7-8 Suppl): 27-31.
- [38] Kerns EH, Di L. **2008**. *Drug-like properties: concepts, structure design and methods: from ADME to toxicity optimization*. Chapter 14: Plasma Protein Binding. 1st ed., Oxford, UK: Elsevier. 187-197.
- [39] Obach RS. **1999**. *Prediction of human clearance of twenty-nine drugs from hepatic microsomal intrinsic clearance data: an examination of in vitro half-life approach and nonspecific binding to microsomes*. Drug. Metab. Dispos. 27(11):1350-1359.
- [40] Obach RS. **1997**. *Nonspecific binding to microsomes: impact on scale-up of in vitro intrinsic clearance to hepatic clearance as assessed through examination of warfarin, imipramine, and propranolol*. Drug. Metab. Dispos. 25(12):1359-1369.
- [41] Berry LM, Roberts J, Be X, Zhao Z, Lin MHJ. **2009**. *Prediction of V_{ss} from in vitro tissue-binding studies*. Drug Metab. Dispos. 38:115-121.

- [42] Ballard P, Leahy DE, Rowland M. **2003**. *Prediction of in-vivo tissue distribution from in-vitro data. 3. Correlation between in-vitro and in-vivo tissue distribution of a homologous series of nine 5-n-alkyl-5-ethyl barbituric acids*. Pharm. Res. 20:864-872.
- [43] Ed. Cox GS. **2008**. *Preclinical development handbook, ADME and biopharmaceutical properties*. Rollas S chapter 23: *In vivo metabolism and preclinical drug development*. John Wiley & Sons, Hoboken, New Jersey. 829-851.
- [44] Ed. Greim H, Snyder R. **2008**. *Toxicology and risk assessment: A comprehensive introduction*. JTM Buters chapter 2.2A: *Phase I metabolism*. John Wiley & Sons, Chichester. 49-73.
- [45] Ed. Cox GS. **2008**. *Preclinical development handbook, ADME and biopharmaceutical properties*. Li AP: *In vitro evaluation of metabolic drug-drug interactions: scientific concept and practical considerations*. John Wiley & Sons, Inc., Hoboken, New Jersey. 853-877.
- [46] Zhanga D, Luob G, Dingc X, Lud C. **2012**. *Preclinical experimental models of drug metabolism and disposition in drug discovery and development*. Acta. Pharm. Sin. B. 2(6):549-561
- [47] Ed. Bonate PL, Howard D. **2004**. *Pharmacokinetics in drug development. Vol 2: regulatory and development paradigms*. Natarajan C, Rohatagi S. Chapter 6: *Role of preclinical pharmacokinetics in drug development*. American Association of Pharmaceutical Scientists, USA. 127-162.
- [48] Barre J, Urien S, Albengres E, Tillement JP. **1988**. *Plasma and tissue binding as determinants of drug body distribution. Possible applications to toxicological studies*. Xenobiotica. 18(1):15-20.
- [49] Kragh-Hansen U, Chuang VTG, Tagiri M. **2002**. *Practical aspects of the ligand-binding and enzymatic properties of human serum albumin*. Biol. Pharm. Bull. 25 (6): 695-704.
- [50] Bohnert T, Gan LS. **2013**. *Plasma protein binding: from discovery to development*. J. Pharm. Sci. 9: 2953-2994.
- [51] Peters T. **1996**. *All about albumin: Biochemistry, genetics, and medical applications. Chapter 5: Metabolism: Albumin in the body*. San Diego, CA: Academic Press. 188-249.
- [52] Quinlan GJ, Martin GS, Evans TW. **2005**. *Albumin: Biochemical properties and therapeutic potential*. Hepatology. 41: 1211-1219.

- [53] Fournier T, Medjoubi N, Porquet D. **2000**. *Alpha-1-acid glycoprotein*. Biochemica et Biophysica Acta. 1482 (1-2): 157-171.
- [54] Poulin P. *Drug distribution to human tissues: Prediction and examination of the basic assumption in in vivo pharmacokinetics–pharmacodynamics (PK/PD) research*. **2015**. J. Pharm. Sci. 104:2110-2118
- [55] Rowland M, Tozer TN. **1995**. *Clinical pharmacokinetics: Concepts and applications*. Williams and Wilkins. Philadelphia. 143-155.
- [56] Pacifici GM, Viani A. **1992**. *Methods of determining plasma and tissue binding of drugs*. Clin. Pharmacokinet. 23:449-468.
- [57] Barre J, Chamouard JM, Houin G, Tillement JP. **1985**. *Equilibrium dialysis, ultrafiltration, and ultracentrifugation compared for determining the plasma–protein-binding characteristics of valproic acid*. Clin. Chem. 31(1): 60-64.
- [58] Schuhmacher J, Buhner K, Witt-Laido A. **2000**. *Determination of the free fraction and relative free fraction of drugs strongly bound to plasma proteins*. J. Pharm. Sci. 89 (8): 1008-1021.
- [59] Sebillé B. *Methods of drug protein binding determinations*. **1990**. Fundam. Clin. Pharmacol. 4(2): 151-161.
- [60] Austin MP. **2002**. *Spatial prediction of species distribution: an interface between ecological theory and statistical modelling*. Ecological Modelling. 157:101-118.
- [61] User Guide Transil^{XL}. **2012**. AGP, HSA, PPB, Intestinal absorption and Microsomal binding kit. Sovicell. Germany.
- [62] Ed. Evans G. **2004**. *A handbook of bioanalysis and drug metabolism*. CRC Press LLC. Somers G, Mutch P, Woodrooffe A. *In vitro techniques to evaluate drug metabolism*. 244-250.
- [63] Ed. Proudlock R. **2016**. *Genetic toxicology testing: a laboratory manual*. Fellows M, Lloyd M chapter 5: *the mouse lymphoma TK assay*. Elsevier, UK. 139-160.
- [64] Nelson AC, Huang W, Moody DE. **2001**. *Variables in human liver microsome preparation: impact on the kinetics of l- α -acetylmethadol (LAAM) n-demethylation*. Drug Metab. Dispos. 29:319-325.

- [65] McGinnity DF, Soars MG, Urbanowcz RA, Riley RR. **2004.** *Evaluation of fresh and cryopreserved hepatocytes as in vitro drug metabolism tools for the prediction of metabolic clearance.* Drug. Metab. Dispos. 32:1247-1253.
- [66] Li AP. **1999.** *Overview; hepatocytes and cryopreservation - a personal historical perspective.* Chem.-Biol. Interact. 121:1-5.
- [67] Soars MG, Burchell B, Riley RJ. **2002.** *In vitro analysis of human drug glucuronidation and prediction of in vivo metabolic clearance.* The journal of pharmacology and experimental therapeutics. J. Pharm. Exp. Ther. 301(1):382-390.
- [68] Li AP. **2008.** *Human hepatocytes as an effective alternative experimental system for the evaluation of human drug properties: general concepts and assay procedures.* ALTEX. 25:33-42.
- [69] Ed. Benninghoff, Görttler. **1975.** *Lehrbuch der Anatomie des Menschen III.* Ferner H. *Nervensystem, Haut und Sinnesorgane.* Urban & Schwarzenberg. 447-451.
- [70] Silver FH, Siperko LM, Seehra GP. **2003.** *Mechanobiology of force transduction in dermal tissue.* Skin Research and Technology. 9(1): 3-23.
- [71] Ed. Goldsmith LA. **1991.** *Physiology, biochemistry, and molecular biology of the skin.* Odland GF: *Structure of the skin.* Oxford University Press.
- [72] Xu F, Lu T. **2011.** *Introduction of skin, biothermomechanics and thermal pain.* Chapter 2: *Skin structure and skin blood flow.* Science Press Beifing and Springer-Verlag Berlin. 7-17.
- [73] Schaefer H , Zesch A, Stüttgen G. **1982.** *Skin Permeability.* Springer Verlag Berlin Heidelberg. 541-551.
- [74] Bos JD, Meinardi MMHM. **2000.** *The 500 Dalton rule for the skin penetration of chemical compounds and drugs.* Exp. Dermatol. 9:165-169.
- [75] WHO Antimicrobial resistance. WHO.
<http://www.who.int/mediacentre/factsheets/fs194/en/>. Access: 11 June **2015.**
- [76] Van de Waterbeemd H, Smith DA, Jones BC. **2001.** *Lipophilicity in PK design: methyl, ethyl, futile.* J. Comput. Aid. Mol. Des. 15:273-286.

- [77] Smith DA, Jones BC, Walker DK. **1996.** *Design of drugs involving the concepts of drug metabolism and pharmacokinetics.* Med. Res. Rev. 16:279-301.
- [78] Dominik A, Steinhilber D, Wurglics M. **2013.** *Instrumentelle Analytik kompakt.* Wissenschaftliche Verlagsgesellschaft, Stuttgart. 229-250.
- [79] Gey MH. **2008.** *Instrumentelle Analytik und Bioanalytik.* Springer Verlag. 101-108.
- [80] Nürnberg E, Surmann P. **1991.** *Hagers Handbuch der pharmazeutischen Praxis: Methoden.* Springer Verlag. 431-438.
- [81] Shrivastava A, Gupta VB. **2011.** *Methods for the determination of limit of detection and limit of quantitation of the analytical methods.* Chronicles of Young Scientists. 2(1):21-25.
- [82] Rieth M. **2012.** *Pharmazeutische Mikrobiologie: Qualitätssicherung, Monitoring, Betriebshygiene.* 2012. Wiley-VCH Verlag GmbH & Co KGaA, Weinheim. 212.
- [83] Houston JB and Carlile DJ. **1997.** *Prediction of hepatic clearance from microsomes, hepatocytes, and liver slices.* Drug. Metab. Rev. 29(4):891-922.
- [84] Davies B, Morris T. **1993.** *Physiological Parameters in Laboratory Animals and Humans.* T. Pharm. Res. 10(7):1093-5.
- [85] Houston B. **1994.** *Utility of in vitro drug metabolism data in predicting in vivo metabolic clearance.* Biochem. Pharmacol. 47(9):1469-1479.
- [86] MatTek corporation, percutaneous absorption, for use with EpiDerm™ Skin Model, protocol.
- [87] Kratochwil NA, Huber W, Müller F, Kansy M, Gerber PR. **2002.** *Plasma protein binding of drugs: a new approach.* Biochem. Pharmacol. 64:1355-1374.
- [88] Heuberger J, Schmidt S, Derendorf H. **2013.** *When is protein binding important?.* J. Pharm. Sci. 102:3458-3467.
- [89] Russo A, Rossel R, Rolfo C. **2015.** *Targeted therapies for solid tumors.* Springer New York. 19-20.
- [90] Gee T, Ellis R, Marshall G, Andrews J, Ashby J, Wise R. **2001.** *Pharmacokinetics and tissue penetration of linezolid following multiple oral doses.* Antimicrob. Agents Chemother. 45:1843-1846.

- [91] Shibata Y, Takahashi H, Chiba M and Ishii Y. **2002**. *Prediction of hepatic clearance and availability by cryopreserved human hepatocytes: an application of serum incubation method*. Drug. Metab. Dispos. 30 (8) 892-896.
- [92] Griffin SJ and Houston JB. 2004. *Comparison of fresh and cryopreserved rat hepatocyte suspensions for the prediction of in vitro intrinsic clearance*. Drug. Metab. Dispos. 32(5):552-558.
- [93] Li AP, Lu C, Brent AJ, Pham C, Fackett A, Ruegg CE, Silber PM. **1999**. *Cryopreserved human hepatocytes: characterization of drug-metabolizing enzyme activities and applications in higher throughput screening assays for hepatotoxicity, metabolic stability, and drug – drug interaction potential*. Chem.-Biol. Interact.121:17-35.
- [94] Nishimuta H, Houston JB, Galetin A. **2014**. *Hepatic, intestinal, renal, and plasma hydrolysis of prodrugs on human, cynomolgus monkey, dog, and rat: implications for in vitro - in vivo extrapolation of clearance of prodrugs*. Drug. Metab. Dispos. 42(9):1522-31.
- [95] Ed. Schmidt H. 2007. *Pharmakologie und Toxikologie für Studium und Praxis*. Klotz U, Schwab M, Schmidt H, Chapter: *Pharmakokinetik*. Schattauer Verlag, Stuttgart New York. 20-45.
- [96] Trauer S, Patzelt A, Otberg N, Knorr F, Rozycki C, Balizs G, Büttemeyer R, Linscheid M, Liebsch M, Lademann J. **2009**. *Permeation of topically applied caffeine through human skin – a comparison of in vivo and in vitro data*. Br. J. Clin. Pharmacol. 68(2):181-186.
- [97] Sukkar E. **2013**. *Why are there so few antibiotics in the research and development pipeline?* The Pharmaceutical Journal. 291:520.
- [98] Leahy DE, Lynch J, Taylor DC. **1998**. *Mechanism of absorption of small molecules. Novel drug delivery and its therapeutic applications*. John Wiley & Sons. New York. 33-34.
- [99] Wan H. *What ADME test should be conducted for preclinical studies?*. **2013**. ADMET & DMPK. 1:19-28.
- [100] Structure of the skin
<http://www.slideshare.net/NamXal1/skin-and-its-appendages>. Access: 16 August 2016.

13 Curriculum Vitae

Personal Details:

Name	Mag. pharm. Nairi Baroian
Geburtsdatum	17.11.1987
Geburtsort	Vienna, Austria

Education:

06/2013-12/2016	Doctoral thesis at the University of Vienna, Division of Clinical Pharmacy and Diagnostics
05/2013	Austrian Pharmacist's Diploma (Diploma: authorized pharmacist)
9/2006-03/2012	Study of Pharmacy at the University of Vienna; Master thesis: "Pharmacokinetic and metabolism of erlotinib after single dose und multiple dose" (Division of Clinical Pharmacy and Diagnostics)
09/1998-06/2006	Highschool, Piaristengymnasium VIII, Vienna

Work Experience:

Since 10/2015	Clinical Research Associate at Celerion (former Assign), Vienna
Since 09/2013	Lecturer at the University of Vienna for the laboratory exercises: "Chemical Diagnostics and Clinical Pharmacy"
06/2013-10/2015	Pharmacist at Paulaner-Apotheke, Vienna
05/2012-05/2013	Pharmacist at Schlangen-Apotheke, Vienna
03/2013-05/2013	Internship at NewBridge Pharmaceuticals, Dubai
09/2010-03/2013	Tutor at the University of Vienna for the course: "Chemical Diagnostics and Clinical Pharmacy"
07/2009	Internship at Dubiotech, Dubai Biotechnology & Research Park, Dubai
07/2008-03/2013	Clinical Coordinator at Assign, Vienna (part time)

Training Courses:

09/2015	ICH E6 GCP Training, Vienna
09/2015	Participating in ECCO 2015, Vienna,
05/2015	Participating in 1 st International Cancer Cluster Salzburg Workshop and 11 th International CLL Workshop, Fuschl am See
11/2014	Participating in ADME, PK/TK and Drug Metabolism in Drug Discovery and Development, Berlin
01/2014	Participating in Evaluation of ADMET Drug Properties in Drug Discovery and Development, Brussels
11/2013	Participating in DESO Workshop 2013, "Methodik klinischer Prüfungen in der Onkologie", Vienna, Austria

Language Skills:

German: native

Armenian: bilingual

English: proficient

French: basic

Publications and Posters:

Kitzmüller M, Gruber A, Baroian Nairi, Sahmanovic-Hrgovcic A, Schönbichler C, Keplinger M, Czejka M. **2016**. Preclinical pharmacokinetics (PK) of new tyrosine kinase inhibitors (TKI): In vitro investigations versus in silico predictions. Conference Paper: CESAR Annual Meeting 2016.

Sahmanovic A, Buchner P, Lichtneckert M, Dittrich C, Farkouh A, Gruber A, Baroian N, Kitzmueller M, Czejka M. **2016**. Monitoring of erlotinib plasma concentrations after long time administration of 100 mg in advanced pancreatic cancer patients, P-139; Conference Paper Conference: ESMO 18th World Congress on Gastrointestinal Cancer, June 2016, Annals of Oncology 27 (Supplement 2): ii41.

Sahmanovic Hrgovcic A, Dittrich C, Kitzmüller M, Gruber A, Baroian N, Buchner P, Czejka M, Farkouh A. **2016**. Protonenpumpeninhibitoren - Potential für pharmakokinetische Wechselwirkungen mit peroral verabreichten Arzneistoffen am Beispiel von Erlotinib;

Conference Paper March 2016, Conference: 49. Wissenschaftliche Fortbildungswoche der Österreichischen Apothekerkammer, Schladming, Austria.

Buchner P, Sahmanovic A, Schreiber V, Baroian N, Dittrich C, Czejka M. **2015**. A simple method for comparing enzymatic capecitabine activation in various mono- and combination chemotherapies. Pharmacology. 95(1-2):29-31.